Density Matrix Embedding Theory

Foundations, Applications and Connection to Functional Theories

Dissertation zur Erlangung des Doktorgrades
an der Fakultät für Mathematik, Informatik und Naturwissenschaften,
Fachbereich Physik der Universität Hamburg

vorgelegt von
Teresa E. Reinhard
aus Sommersell

Hamburg 2018

GutachterInnen der Dissertation:	Prof. Dr. Angel Rubio Prof. Dr. Daniela Pfannkuche
Zusammensetzung der Prüfungskommission:	Prof. Dr. Angel Rubio Prof. Dr. Daniela Pfannkuche Prof. Dr. Henning Moritz Dr. Heiko Appel Prof. Dr. Michael Potthoff
Vorsitzender der Prüfungskommission:	Prof. Dr. Michael Potthoff
Eingereicht am:	20.12.2018
Tag der wissenschaftlichen Aussprache:	26.03.2019
Vorsitzender des Fach-Promotionsausschusses Physik:	Prof. Dr. Michael Potthoff
Leiter des Fachbereichs Physik:	Prof. Dr. Wolfgang Hansen
Dekan der Fakultät MIN:	Prof. Dr. Heinrich Graener

Preface

Summary

The Schrödinger equation describes the motion of the microscopic particles that constitute our world such as the electrons or atomic nuclei. Albeit being applicable to the smallest particle that we know of, it has observable consequences in the macroscopic world. It determines the conductivity of metals, it tells us which materials are magnetic and whether they show exotic behaviour such as super-conductivity.

Unfortunately, solving the Schrödinger equation directly for any piece of material that is visible for the human eye is practically impossible. Already a grain of sand contains 10^{23} (that is written out 10.000.000.000.000.000.000.000) electrons and atomic nuclei. This means that only specifying the initial positions of the particles requires to safe an incredible amount of data; a procedure which is unfeasible for any human or computer.

Due to the fundamental problem of applying quantum mechanics to practically relevant scenarios, a number of effective and approximate methods have been developed. In essence, they all try to reduce the *dimension* of the problem, i.e., the curse of the enormous amount of data required to simulate the Schrödinger equation.

In this thesis, we try to analyze and expand one of those methods called *Density Matrix Embedding Theory* (DMET). In a lot of physical systems, especially when considering solid states, we can already learn a lot about its physics when describing its properties on a small fragment of the whole system. In a system with interacting particles though, we cannot simply consider just a subsystem and describe its properties without taking into account its interactions with the rest of the system.

The basic idea of DMET is to divide the considered system into two parts called *impurity* and *environment*. The impurity is chosen to be so small that its wave function can be computed exactly. In the environment, only those degrees of freedom directly interacting with the impurity are considered and are included in our description. The physics on the environment itself is neglected.

In the following, we will explain in detail how this can be done specifically. In part I of this thesis, we will set the stage for the considered systems and present well-known and established methods to solve them. In the next part II, we will present DMET in great mathematical detail, which allows us to illustrate the advantages of DMET, but also some problems and drawbacks. We proceed by expanding DMET to the treatment of coupled electron-phonon system in part III and applying this new method to the Hubbard-Holstein model. Part of this work has been published in [53]. Finally, in part IV, we discuss some problems of DMET and, by combining DMET with functional theories, solve these problems. These insights, together with the extensive discussion of the DMET algorithm, will be published soon [59]. We illustrate this new method with an example system. This work will be published in paper [44] soon. We conclude this thesis by a summary and outlook (part V).

Zusammenfassung

Die Schrödingergleichung beschreibt die Bewegungen aller mikroskopischen Teilchen, wie zum Beispiel Elektronen, Atomkerne oder Licht-teilchen, die Photonen genannt werden und aus denen unsere Welt zusammengesetzt ist. Diese Teilchen sind zwar winzig klein, aber trotzdem beeinflussen sie Materialen auf eine Art, die wir in unserer makroskopischen Welt beobachten können. Mithilfe der Schrödingergleichung kann man zum Beispiel feststellen, ob ein Material magnetisch ist oder sogar exotische Eigenschaften, wie Supraleitfähigkeit besitzt.

Leider ist es aber trotzdem praktisch nicht möglich, Materialien die für uns sichtbar sind mit der exakten Schrödingergleichung zu beschreiben: Schon ein Sandkorn enthält 10^{23} (das sind ausgeschrieben 10.000.000.000.000.000.000.000) Elektronen und Atomkerne. Deshalb ist es nicht möglich, auch nur die Orte der einzelnen Teilchen auf einem Computer abzuspeichern, geschweige denn ihre Bewegungen und Wechselwirkungen zu berechnen.

Weil es aber für bestimmte Fragestellung (also zum Beispiel für die Frage: Ist dieses Material magnetisch?) notwendig ist, auch den Einfluss der mikroskopischen Teilchen zu berücksichtigen, beschäftigt sich ein großer Teil der *Vielteilchenquantenmechanik* damit, entweder die Schrödingergleichung approximativ und effizient zu lösen, oder die Elementalteilchen auf einem Umweg genau beschreiben zu können.

In dieser Doktorarbeit beschäftigen wir uns mit einer bestimmten Methode, um die Schrödingergleichung zu nähern und effektiv zu lösen. Die Methode, die hier genau unter die Lupe genommen wird, heißt *Density Matrix Embedding Theory*, abgekürzt DMET. Diese Methode nutzt aus, dass für viele Systeme, vor allem für Festkörper, oft ausreicht, wenn ein Teil des gesamten Systems genau beschrieben werden kann ohne die Physik des restlichen Systems kennen zu müssen. Auch um nur ein Subsystem zu beschreiben, muss man aber die Wechselwirkungen mit dem Rest des Systems berücksichtigen.

Die Grundidee von DMET ist dementsprechend, das System, welches bestimmt werden soll, in zwei Teile zu teilen: Ein Teil ist die *impurity*, also das Subsystem, welches genauer beschrieben werden soll, und der zweite Teil ist das *environment*, also der restliche Teil des Systems. Die *impurity* wird so klein gewählt, dass es möglich ist, für dieses Subsystem die Schrödingergleichung exakt zu lösen. Von dem *environment* werden nur die Anteile berücksichtigt, die direkt mit der *impurity* wechselwirken und der Rest wird vernachlässigt. Die Hauptaufgabe von DMET ist also, herauszufinden, welche Teile des *environments* eigentlich mit der *impurity* wechselwirken und welche anderen Teile vernachlässigt werden können.

In dieser Arbeit werden wir detailliert erklären, wie DMET genau funktioniert. Außerdem werden wir die Methode, die eigentlich für rein elektronische Systeme entwickelt wurde, erweitern, sodass auch gekoppelte Elektron-Phonon Systeme damit behandelt werden können.

List of publications

1) T. E. Reinhard, U. Mordovina, C. Hubig, J. S. Kretchmer, U. Schollwöck, H. Appel, M. A. Sentef, and A. Rubio, *Density-matrix embedding theory study of the one-dimensional Hubbard-Holstein model*, arXiv:1811.00048, submitted to the Journal of Chemical Theory and Computation

2) U. Mordovina[†], T. E. Reinhard[†], H. Appel, and A. Rubio, *Self-consistent density-functional embedding: a systematically improvable approach for density functionals*, submitted to the Journal of Chemical Theory and Computation

3) T. E. Reinhard, I. Theophilou, M. Ruggenthaler and A. Rubio *Foundations of Density Matrix Embedding Theory revisited: a Density Matrix Functional perspective*, in preparation

[†] Both authors contributed equally to this paper.

Contents

Part I

Introduction and foundations

Chapter 1

Setting the stage

This thesis is mainly concerned with extending and developing efficient and accurate methods to describe quantum many body systems at temperature zero. While the concepts are quite general, we will mainly deal with toy models from solid state physics such as the Hubbard model or its extension towards coupled electron-phonon systems, the Hubbard-Holstein model. These toy models play an important role in solid state physics, because although being the most simple approximation for the description of interacting quantum particles, they already show the complex behaviour of many body quantum mechanics. Thus, fundamental features of actual systems, such as quantum phase transitions, can be described qualitatively in terms of these minimalistic models.

Before we start with the technical details, however, we feel that it is worth the try to embed our theory in a larger theoretical framework: what does it actually mean to model nature? is there a good reason to use toy models? or, more specifically considering quantum mechanics: if the basics of quantum physics (which can be described in the Schrödinger equation) are known, why should one bother to study it further?

1.1 Describing and understanding nature

This thesis is about fundamental research in quantum physics. Fundamental research is driven by the curiosity to explain and understand how and why the world that surrounds us works.

This goal, being as simple as it is abstract, raises a lot of questions: What do we understand as *the world that surrounds us*? Are we, as human beings, able to describe it? How can we interpret the results of this description to formulate *the laws of nature*? Are there actually any *laws of nature*?

To speak already about *the world that surrounds us* is a misleading statement as it implicitly assumes that there is an objective world, which we can observe without influencing it. But already Heisenberg uncertainty principle tells us that this is impossible: observing a system changes it, information is physical [37] or, as Wheeler states: *It from bit* [69]. Additionally, our observation of nature is limited because our senses are limited. Thus it is not possible for anybody to grasp all aspects of one situation or system, let alone the whole world. Any attempt to formulate the laws of nature necessarily incorporates incomplete information about the given problem [26].

The goal to describe and understand all the whole world that surrounds us in one single model of this world is not possible to fulfill. Nonetheless, we can still try to approximately describe a part of the world that surrounds us and try to make sense of it. In order to do so we have to specify the specific part of the world, which is called the system, that we want to consider.

In physics, once a specific system is chosen, there are two different strategies towards understanding and describing it: experimental and theoretical physics. These two different approaches influence and complement each other on many different levels. Both approaches, have the goal to answer a specific question and to verify or falsify a theory.

In experimental physics, the answers to the questions are obtained by inferring from a finite amount of data relations and correlations in a reproducible manner. An experimental physicist has instruments with various knobs in her lab. She uses these instruments and knobs to prepare, transform and

measure a given *system*.

Opposed to this, the instruments of a theoretical physicist are mathematical theories build upon a given set of axioms and plausible approximations applied within a specific context. A theoretical *model* is exactly defined by the given set of approximations.

Although it is not possible from neither of the above mentioned approaches to *objectively* find the laws of physics, we hope that at the point where both descriptions of nature - from observation to models and from models to observation - yield the same result, our predictions and reasonings are not completely off. Theoretical models can be built from insights on how a certain system behaves in an experiment and all theoretical theories have to be verified by an experiment. Also, theoretical predictions can be used for posing leading questions to an experiment. On the one hand, often surprising results are found in experiments that lead to completely new theoretical models and hence, a new understanding of the world. Major examples, which have sparked a lot of research activity in many body quantum mechanics include the discovery of superfluidity [30], superconductivity [49] and the quantum hall effect [64], which then lead to the investigation of topology in theoretical physics. On the other hand, there also have been predictions of physics that later were tested and confirmed, such as the Aharonov-Bohm effect [12] or the description of topological states that lead to an understanding of exotic materials such as topological insulators, Chiral superconductors or Weyl semimetals [65].

Since the development of powerful computers the approaches in both, experimental and theoretical physics, have changed drastically: In experimental physics, computers are used to capture and process the data gained by the experiment. In this way, a lot more measurements can be performed and processed. In theoretical physics there are two different ways to take advantage of computers. Instead of solving formulas and equations exactly or approximately with pen and paper, we can also set up models and formulas which can be solved numerically on a computer. Another way to do numerical physics is to perform simulations of models on the computer which can yield additional and new insights about the implemented model and whether the model is capable to describe aspects of the real world.

This thesis can be assigned to the group of theoretical physics. More specifically, we will deal with *method development* in quantum many body physics. Method development is a branch of theoretical physics, where instead of testing the validity of a model by comparing to measurements, we try to find new ways to solve already existing models more efficiently. In this thesis, we specifically will try to find ways to solve models describing the ground state properties of quantum particles in a closed system at temperature zero. In doing so, on the one hand we try to expand our method to be able to treat more realistic settings. These might be able to describe experiments in more detail at some point. On the other hand, through the approximations we employ on a specific model, we hope to learn more about fundamental laws of nature.

The goal of this thesis is threefold:

1. To explain the different numerical techniques that have been developed to solve model systems in many body quantum mechanics. Specifically, we will concentrate on one technique that we hope to be able to brigde the model description of the world with the experimental description of the world.

2. To investigate a model system that describes some important aspects of nature, solve it and explain the implications that our results have for the understanding of physical procedures.

3. To expand this method in two novel ways: first, we will extend the method to be able to describe not only electronic systems, but also coupled electron-phonon systems. Second, we will consider the method itself and demonstrate a pathway towards the description of more realistic systems. We will show that this expansion performs well for a specific example.

1.2 The system and methods

An isolated quantum mechanical system or setup that is not influenced at all by the outside world, can be fully described by a complex object called the wave function Ψ of the system.

The wave function describes the quantum mechanical state of a system of elementary particles in

position space,

$$\Psi(\mathbf{r}_1, ..., \mathbf{r}_M), \tag{1.1}$$

where each particle i has a specific position in the three dimensional space $\mathbf{r}_i = (x_i, y_i, z_i)$. It can be abstractly written as $|\Psi\rangle$ and is the solution of the stationary, non-relativistic Schrödinger equation

$$\hat{H}|\Psi\rangle = E|\Psi\rangle, \tag{1.2}$$

where $\hat{H}$ is called Hamiltonian, the operator corresponding to the total energy E of the system. Unfortunately, the wave function is an object that grows in dimension exponentially with the number of particles in the system, so we cannot simply solve the Schrödinger equation for normal situations in nature, where usually a lot of particles need to be considered. In order to solve this dilemma, there are again two fundamentally different approaches (depicted schematically in figure 1.1).

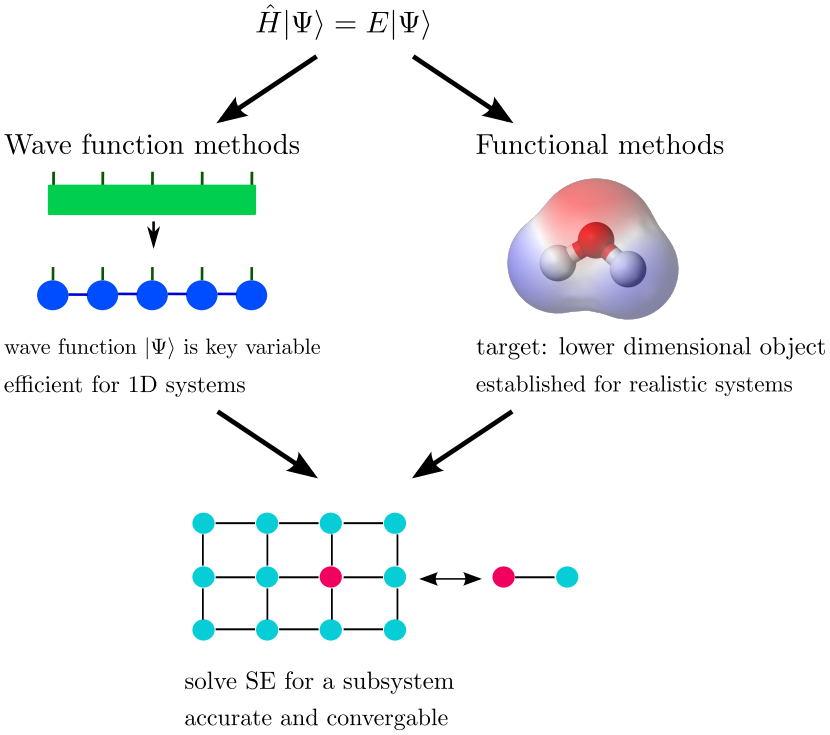

Figure 1.1: Sketch of some of the possible approaches to solve an isolated quantum system which is fully determined by the Schrödinger equation. We will elaborate on the precise meaning of the different pictures and methods in the next section(s).

Either, we can try to find an efficient representation of $|\Psi\rangle$ which makes it lower-dimensional and thus, solvable. There are a lot of methods trying to do so, the group of methods they form is called *wave function methods* (figure 1.1, left hand side). A completely different approach is to find different objects that are not the wave function and that can be described more easily. This group of methods is called *functional methods* (figure 1.1, right hand side).

There is a third approach that belongs to a group of methods in between the two groups explained before, the embedding methods (figure 1.1, bottom). Here, instead of computing the Schrödinger equation of the full system, which is very costly, we divide the system up into small parts, compute their respective Schrödinger equation and then patch the result back together. The trick here is to divide the system up such that, in every single patch, the interactions of the rest of the system with this patch is still included.

In this thesis we concentrate on a method belonging to the third group called *Density Matrix Embedding Theory* (DMET). We will explain and develop it in detail. Being in between functional methods and wave function methods, we hope that it can take advantage of the *best of both worlds* and can be further improved by insights from the other two groups of methods. The connection between the methods and our pathway throughout this thesis is depicted in figure 1.1.

Chapter 2

Wave function methods

2.1 Lattice wave function

When simulating model systems on the computer, we have to choose a finite basis set as a computer can only process quantized data. There are many different choices for basis sets with advantages and disadvantages such as k-space vectors, atomic orbitals or Gaussians. In this work, we choose to describe our model systems in terms of the discretized real space. This will prove to be advantageous for the development of the embedding method that is the focus of this thesis.

2.1.1 Particle states on the discretized lattice

In this thesis, we choose to describe our physical system on a discretized real space lattice where the total number of lattice sites is N. The particles that are in the system are then positioned on the lattice sites.

In quantum mechanics, there are two different groups of particles. The first group are fermions, which have a spin of half integer and the second group are bosons which have an integer spin. We additionally restrict ourselves to a non-relativistic setting. In this case, the only fermionic particles are electrons. Further, in this thesis we consider two different types of bosons: photons which describe electromagnetic interactions, and phonons, describing the lattice vibrations of a solid. In the following, we consider electrons as the only fermionic particle, and when mentioning bosons, we have in mind either photons or phonons.

In the most general setting, on each lattice site i, all possible configurations of the two groups of particles can co-exist. We call these possible configurations local electronic or bosonic states on lattice site i. The local electronic basis on site i is denoted with the abstract vector $|\nu_i\rangle$, while the bosonic local basis on site i is denoted by $|\tau_i\rangle$. Here, $|\nu_i\rangle$ and $|\tau_i\rangle$ span the local Hilbert spaces, $|\nu_i\rangle \in \mathcal{H}_{\text{el}}$, $|\tau_i\rangle \in \mathcal{H}_{\text{bos}}$.

Electronic states

The local electronic basis on lattice site i is determined by

$$|\nu_i\rangle = \begin{pmatrix} |\uparrow\downarrow\rangle \\ |\downarrow\rangle \\ |\uparrow\rangle \\ |0\rangle \end{pmatrix}_{\text{el}}, \tag{2.1}$$

which means that on each lattice site, we can find four different electronic configurations: either no particles, $|0\rangle$, a particle with spin up $|\uparrow\rangle$ or spin down $|\downarrow\rangle$ or two particles, one with spin up and one with spin down $|\uparrow\downarrow\rangle$. The local electronic wave function then yields the probability to find any of

these states

$$|\varphi_i\rangle = \varphi_{\nu_i}|\nu_i\rangle, \tag{2.2}$$

$$\varphi_{\nu_i} = \left(\varphi_{\uparrow\downarrow}\ \varphi_{\downarrow}\ \varphi_{\uparrow}\ \varphi_0\ \right)_{\text{el}}, \tag{2.3}$$

where φ_{ν_i} is a vector giving the probabilities a of finding the system in any of the possible states.

The reason that on each lattice site, there can only be found one single electron with a certain spin is called Pauli's exclusion principle. In order to understand that, we have to consider two lattice sites $1, 2$ with two local Hilbert spaces on them. The wave function of these two states is

$$|\varphi_{1,2}\rangle = \varphi_{\nu_1,\nu_2}|\nu_1\rangle \otimes |\nu_2\rangle, \tag{2.4}$$

where $\otimes$ is the tensor product between two different states and φ_{ν_1,ν_2} now denotes all possible combinations of configurations of the two states:

$$\varphi_{\nu_1,\nu_2} = \left\{\varphi_{0,0}, \varphi_{0,\uparrow}, .., \varphi_{0,\uparrow\downarrow}, \varphi_{\uparrow,0}, ...\varphi_{\uparrow\downarrow,\uparrow\downarrow}\right\}. \tag{2.5}$$

Electrons are indistinguishable particles, so the ordering of the states does not matter: $|\nu_1\rangle \otimes |\nu_2\rangle = |\nu_2\rangle \otimes |\nu_1\rangle$. Pauli's exclusion principle states that, upon interchange of two electronic particles, the wave function is anti-symmetric:

$$|\varphi_{1,2}\rangle = \varphi_{\nu_1,\nu_2}|\nu_1\rangle \otimes |\nu_2\rangle = -\varphi_{\nu_1,\nu_2}|\nu_2\rangle \otimes |\nu_1\rangle. \tag{2.6}$$

From this equality, one can follow that no two electrons can be in the same state on the same lattice site by considering a situation where two particles in the same state occupy the same lattice site

$$|\varphi_{1,1}\rangle = \varphi_{\nu_1,\nu_1}|\nu_1\rangle \otimes |\nu_1\rangle = -\varphi_{\nu_1,\nu_1}|\nu_1\rangle \otimes |\nu_1\rangle = 0, \tag{2.7}$$

which automatically yields 0.

Bosonic states

Analog to the electrons, we can set up a bosonic local basis on lattice site i as:

$$|\tau_i\rangle = \begin{pmatrix} |\infty\rangle \\ ... \\ |1\rangle \\ |0\rangle \end{pmatrix}_{\text{bos}}. \tag{2.8}$$

Different to the electrons, two bosons can have the same state at the same lattice site, leading to an infinite local Hilbert space (called Fock space) for the description of only one local bosonic state.

A bosonic wave function of site i again yields the probability to find the system in a certain state:

$$|\chi_i\rangle = \chi_{\tau_i}|\tau_i\rangle, \tag{2.9}$$

where χ_{τ_i} now is an infinite vector.

The wave function of two lattice sites τ_1 and τ_2 is then

$$|\chi_{1,2}\rangle = \chi_{\tau_1,\tau_2}|\tau_1\rangle \otimes |\tau_2\rangle. \tag{2.10}$$

Bosons are, like fermions indistinguishable particles $|\tau_1\rangle \otimes |\tau_2\rangle = |\tau_2\rangle \otimes |\tau_1\rangle$, but unlike the fermionic case, the bosonic wave function is symmetric upon interchange of a particle:

$$|\chi_{1,2}\rangle = \chi_{\tau_1,\tau_2}|\tau_1\rangle \otimes |\tau_2\rangle = \chi_{\tau_1,\tau_2}|\tau_2\rangle \otimes |\tau_1\rangle. \tag{2.11}$$

This is why, different from electrons, two bosons can be in the same state on the same lattice site.

2.1.2 The most general many body wave function in a lattice

Having defined what a local (electronic or bosonic) wave function is, we can now try to set up the most general many body wave function for our system.

A wave function $|\Psi\rangle$ describes the quantum mechanical state of a closed system (that is, a system that is not in any way influenced from anything outside of the system). The energy operator is the Hamiltonian $\hat{H}$ which describes all the dynamics and interactions of the particles in the system. This Hamiltonian can be generally written in the form

$$\hat{H} = \hat{T} + \hat{V} + \hat{W} \tag{2.12}$$

where $\hat{T}$ describes the kinetic energy in the system, $\hat{V}$ some arbitrary external potential and $\hat{W}$ the interactions of the particles in the system. When considering closed systems, all observables can be derived from the many body wave function $|\Psi\rangle$ which is the ground state of the eigenvalue problem

$$\hat{H}|\Psi\rangle = E|\Psi\rangle \tag{2.13}$$

called the Schrödinger equation.

Generalizing Eqns. (2.4) and (2.10), the wave function on all lattice sites of the discretized grid is represented as

$$|\Psi\rangle = \sum_{\nu_1}^{4} ... \sum_{\nu_N}^{4} \sum_{\tau_1}^{\infty} ... \sum_{\tau_N}^{\infty} \Psi_{\nu_1,...,\nu_N;\tau_1,...,\tau_N} |\nu_1\rangle \otimes ... \otimes |\nu_N\rangle \otimes |\tau_1\rangle \otimes ... \otimes |\tau_N\rangle. \tag{2.14}$$

Here, N is the total number of regarded lattice sites. The $|\nu_i\rangle$ are the fermionic and the $|\tau_i\rangle$ are the bosonic bases as have been defined before.

The full wave function Eq. (2.14) is defined on the Hilbert space which is build from the tensor product of all the (fermionic and bosonic) Hilbert spaces on the local sites

$$\mathcal{H}_N = \mathcal{H}_{\nu_1} \otimes \mathcal{H}_{\nu_2} \otimes ... \otimes \mathcal{H}_{\nu_N} \otimes \mathcal{H}_{\tau_1} \otimes \mathcal{H}_{\tau_2} \otimes ... \otimes \mathcal{H}_{\tau_N} \tag{2.15}$$

and has the dimension

$$\dim(\mathcal{H}_\mathrm{N}) = L^N \tag{2.16}$$

where $L = L_\mathrm{el} \cdot L_\mathrm{bos} = (4 \cdot L_\mathrm{bos})$ is the total amount of local basis states per lattice. Note that the wave function $|\Psi\rangle$ describes all possible configurations of fermionic and bosonic states without fixing either the electronic or the bosonic particle number. The Hilbert space $\mathcal{H}_N$, which contains all possible particle configurations is often called Fock space $\mathcal{F}$.

In this first part of the thesis, we will concentrate on the fermionic wave function, neglecting all bosonic degrees of freedom. In this setting, the wave function reads

$$|\Psi\rangle = \sum_{\nu_1}^{4} ... \sum_{\nu_N}^{4} \Psi_{\nu_1,...,\nu_N} |\nu_1\rangle ... |\nu_N\rangle. \tag{2.17}$$

and is defined on the fermionic Fock space

$$\mathcal{F}^\mathrm{ferm} = \mathcal{H}_N^\mathrm{ferm} = \mathcal{H}_{\nu_1} \otimes \mathcal{H}_{\nu_2} \otimes ... \otimes \mathcal{H}_{\nu_N}. \tag{2.18}$$

In this wave function Eq. (2.17) **all** possible combinations of **all** possible local basis sets are taken into account and the dimension of the wave function is 4^N. Note that this way of writing the wave function is strictly local, the $|\nu_i\rangle$ are only defined on lattice site i. While this might seem like an unnecessary complicated way of writing a wave function, we need this definition for the explanation of the tensor network method in section 2.2.

In order to describe an actual physical system, not all of the configurations $\{|\nu_1 \otimes \nu_2 \otimes ... \otimes \nu_N\rangle\}$ need to be taken into account. There are two main reasons for that:

> **A priori:** The fermionic wave function needs to obey Pauli's exclusion principle which means that all the wave functions not fulfilling this requirement need to be excluded. Additionally, the wave function will reflect certain symmetries corresponding to the chosen Hamiltonian. These symmetries arise through the conservation laws of the Hamiltonian.

A posteriori: In the wave function above, all particles on all lattice sites couple to each other, given by the coupling tensor $\Psi_{\nu_1,\nu_2,...,\nu_N;\tau_1,...,\tau_N}$. In a system with short range interactions though, a lot of the entries in the tensor are zero or very small and do not have to be considered. Specifically, the interaction strength between two particles often decreases rapidly with growing distance between the particles. With the Tensor Network Method, we can find a basis that only takes into account those elements of $\Psi_{\nu_1,\nu_2,...,\nu_N;\tau_1,...,\tau_N}$ that are not negligible.

2.1.3 Lattice wave function with creation operators

In a fermionic system, the wave function needs to be anti-symmetric, which means that certain combinations of Eq. (2.17) need to be excluded. One way to exclude those combinations from the beginning which has proven to be very clean and practical for the formulation of problems in Fock space, is to describe the wave function in terms of particle creation and annihilation operators [6, pp.7].

$$\begin{aligned} &\hat{c}_i^\dagger : \mathcal{F}^{\text{ferm}} \to \mathcal{F}^{\text{ferm}}; \\ &|\nu_1\rangle \otimes ... \otimes |\nu_i\rangle \otimes ... \otimes |\nu_N\rangle \to \sqrt{M+1}|\nu_1\rangle \otimes ... \otimes |\nu_i+1\rangle \otimes ... \otimes |\nu_N\rangle \\ &\hat{c}_i = \left(\hat{c}_i^\dagger\right)^\dagger \end{aligned} \tag{2.19}$$

going from a state of M particles to a state of $M+1$ particles in the system, which obey the anti-commutation relations

$$\left\{\hat{c}_i, \hat{c}_j^\dagger\right\} = \hat{c}_i \cdot \hat{c}_j^\dagger + \hat{c}_j^\dagger \cdot \hat{c}_i = \delta_{ij} \tag{2.20}$$

$$\left\{\hat{c}_i^\dagger, \hat{c}_j^\dagger\right\} = \{\hat{c}_i, \hat{c}_j\} = 0. \tag{2.21}$$

We further define $|0\rangle$ as the vacuum state, applying the particle annihilation operator to it yields the absolute 0:

$$\hat{c}_i|0\rangle_i = 0, \tag{2.22}$$

where $|0\rangle_i$ is the vacuum state on lattice site i. With these definitions we can then set up a general many body wave function that obeys Pauli's principle as

$$|\Psi\rangle = \sum_{i=1}^{4^N} \alpha_i |\Phi\rangle_i, \tag{2.23}$$

where $|\Phi\rangle$ is called a Slater determinant, which is a fully anti-symmetrized many body wave function with particle number M:

$$\begin{aligned} |\Phi\rangle &= \prod_{\mu=1}^{M} \sum_{i=1}^{N} \varphi_i^\mu \hat{c}_i^\dagger |0\rangle \\ &= \frac{1}{\sqrt{M}} \det \begin{vmatrix} \varphi_1^1 & ... & \varphi_1^M \\ ... & ... & ... \\ \varphi_N^1 & ... & \varphi_N^M \end{vmatrix} |\nu_1\rangle \otimes ... \otimes |\nu_\text{N}\rangle. \end{aligned} \tag{2.24}$$

Unlike the wave function defined in Eq. (2.17), the combinations which are excluded a posteriori due to Pauli's principle do not enter at all.

2.1.4 Exploiting symmetries

In many physical settings, a Hamiltonian with certain symmetries is chosen. These symmetries then leed to conservation laws such as particle number conservation, the conservation of the square of the total spin of the system $< \hat{S}^2 >$ or the conservation of the z-component of the total spin of the system $< \hat{S}_z >$. In this thesis we will analyze the Hubbard model, in which, for example, all three of the above mentioned conservation laws are fulfilled.

When it is known that the Hamiltonian obeys these laws, this can also be included in the wave function in order to simplify it. This is why, in most of the standard wave function methods such as Hartree Fock, Configuration Interaction, Coupled Cluster etc. the wave functions are set up on a basis set that is defined on a subset of Eq. (2.16) and only includes physically sensible configurations.

2.1.5 Wave function in the mean field approximation

System which do not consider particle interactions can be described by the mean field Hamiltonian

$$\hat{T} = \sum_{ij} t_{ij} \hat{c}_i^\dagger \hat{c}_j = \sum_{\alpha} \epsilon_\alpha \hat{a}_\alpha^\dagger \hat{a}_\alpha, \tag{2.25}$$

which only includes the kinetic energy term of the general Hamiltonian $\hat{H}$ from Eq.(2.12). Here,

$$\hat{a}_\alpha^\dagger : \mathcal{F} \to \mathcal{F}; \tag{2.26}$$
$$\frac{1}{\sqrt{M!}} \sum_{\sigma \in S_\mu} \text{sign}(\sigma) |\mu_{\sigma(1)}\rangle \otimes ... \otimes |\mu_{\sigma \text{M}}\rangle \to \frac{1}{\sqrt{(\text{M}+1)!}} \sum_{\sigma \in \text{S}_\mu} \text{sign}(\sigma) |\mu_{\sigma(1)}\rangle \otimes ... \otimes |\mu_{\sigma \text{M}}\rangle \otimes |\mu_{\sigma(\text{M}+1)}\rangle,$$
$$|\mu_\alpha\rangle = \hat{a}_\alpha^\dagger |0\rangle, \quad \hat{a}_\alpha = \left(\hat{a}_\alpha^\dagger\right)^\dagger$$

are particle creation and annihilation operator in the eigenbasis of the Hamiltonian $\hat{T}$. They obey the same relations (Eqns. (2.20,2.22)) as the creation and annihilation operators in the lattice basis. The wave function of Hamiltonian Eq (2.25) can then be written as

$$|\Phi\rangle = \hat{a}_1^\dagger ... \hat{a}_M^\dagger |0\rangle = \prod_{\mu=1}^{M} \hat{a}_\mu^\dagger |0\rangle. \tag{2.27}$$

$|\Psi\rangle$ is again a Slater determinant of M particles .

The connections between this eigenbasis of the Hamiltonian $\hat{a}_\mu^\dagger$ and the local lattice basis $\hat{c_i}^\dagger$ is given by

$$\hat{a}_\mu^\dagger |0\rangle = \sum_{i=1}^{N} \varphi_i^{(\mu)} \hat{c}_i^\dagger |0\rangle, \tag{2.28}$$

as defined in Eq.(2.24), yielding

$$|\Phi\rangle = \hat{a}_M^\dagger ... \hat{a}_1^\dagger |0\rangle = \prod_{\mu=1}^{M} \sum_{i=1}^{N} \varphi_i^\mu \hat{c}_i^\dagger |0\rangle \tag{2.29}$$

yielding the same form as Eq. (2.24). A Slater determinant has one possible (physically sensible) particle distribution and usually a specific $\hat{S}_z$ spin configuration of the many body wave function. It is per construction the exact ground state wave function of the Hamiltonian in Eq. (2.25).

There are methods, which, starting from the ground state of this mean field system, use perturbation theory to describe a general wave function belonging to an interacting system. These methods are extensively used in quantum chemistry. Depending on the degree of perturbation, they are called Configuration Interaction singles (CIS, perturbation theory of first order), Configuration Interaction doubles (CID, perturbation order of second order). A similar and very powerful technique is the Coupled Cluster method, where the interacting wave function is described with an exponential ansatz of a Slater determinant,

$$|\Psi\rangle = e^{\hat{T}} |\Phi\rangle. \tag{2.30}$$

Here, $\hat{T}$ is called the cluster operator and can be expanded, similar to the CI methods:

$$\hat{T} = \hat{T}_1 + \hat{T}_2 ..., \tag{2.31}$$

where $\hat{T}_1$ corresponds to all the single excitations in the system, $\hat{T}_2$ corresponds to all the double excitations in the system and so on.

These methods are very efficient for system whose wave function can be approximated well with one single Slater determinant; they fail when the interactions in the system become very large.

2.2 Tensor networks for one-dimensional systems

In this chapter, we will briefly explain the concept of the DMRG method, an efficient wave function method for the diagonalization of one-dimensional (lattice) systems in terms of Tensor Networks. While focusing on the one-dimensional lattice case here, the Tensor Network method can also be used to treat higher dimensional lattice systems. Additionally, expansions towards the treatment of quantum chemistry problems with continuous basis sets exist. We roughly follow the review by Schollwöck [55].

2.2.1 The wave function as a Matrix Product state

As mentioned before, not all elements of $\Psi_{\nu_1,\nu_2,\ldots,\nu_L}$ of the wave function Eq. (2.17) need to be taken into account: while this object contains all interactions of all particles with one other, for a lot of physical systems, many entries in $\Psi_{\nu_1,\nu_2,\ldots,\nu_L}$ are either zero or very small which means that correlation between the two particles coupled by those entries is zero or very small.

Correlation, in other words, can be understood as the dependence between two particles. In many physical system, the amount of correlation between two particles depends strongly on their distance between each other; often the correlation decreases exponentially with distance. This is for example valid for all gapped systems, while for metals, the correlation is usually very strong.

In other words, a lot of elements in the vector $\Psi_{\nu_1,\nu_2,\ldots,\nu_L}$ can be neglected because their absolute value is small and the observables of interest will still be rather close to their original values.

The goal of the Tensor Network Method now is to find a smart way to neglect those elements that are not important by neglecting those coupling elements between two sites that are small. In order to do so, we rearrange our wave function such that already in the form of the wave function, we can distinguish between the different local basis states and the indices connecting them. Instead of writing the wave function as one vector (which is a rank 1 tensor) of the dimension 4^L as defined in Eq. (2.14), we write it as a tensor of rank L, where each lattice site of the wave function contributes with one to the rank of this tensor as is depicted schematically in figure 2.1. In order to see how we then further

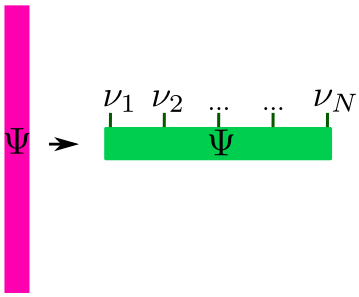

Figure 2.1: In the tensor network method, the wave function, which in many other methods can be represented as a vector of length 4^L is written as a tensor of rank L. The total dimensionality of this object does not change through this rewriting.

decompose this tensor, consider first a system with only two lattice sites 1 and 2. The wave function (which in the tensor network method can be understood as a rank 2 tensor, that is, a matrix) can be written as

$$|\Psi\rangle = \sum_{\nu_1}^{4}\sum_{\nu_2}^{4} \Psi_{\nu_1\nu_2}|\nu_1\rangle|\nu_2\rangle \tag{2.32}$$

where all physical information about this system is contained in the matrix Ψ_{ν_1,ν_2}. For a system with no correlation between those sites

$$\Psi_{\nu_1,\nu_2} \Rightarrow A_{\nu_1} A_{\nu_2} \tag{2.33}$$

can be written as the tensor product of two vectors of the dimension 4×1. Assuming correlation between the two sites we can write the wave function as:

$$\Psi_{\nu_1,\nu_2} = \sum_{m=1}^{4} A_{\nu_1,m} A^m_{\nu_2}. \tag{2.34}$$

The wave function can be re-written in terms of two matrices, where one dimension of the matrix is taking care of the local basis and the other dimension is the coupling from the first to the second site. We can generalize the way of writing the wave function in Eq. (2.34) to a wave function that is defined on L lattice sites. Then, for each lattice site we get a rank 3 tensor $A^{m_{i-1}}_{\nu_i m_i}$. Here, the index ν_i is accounting for the physical state the system has at lattice site i. For an electronic problem,

$$\nu_i = \begin{pmatrix} \uparrow\downarrow \\ \downarrow \\ \uparrow \\ 0 \end{pmatrix}_{\text{el}} \tag{2.35}$$

as before. The indices m_i and m_{i-1} on the other hand are so-called virtual indices; they account for the correlation of the considered physical state on lattice site i with the state on the lattice site before $(i-1)$. In this way, each lattice site is only directly coupled to the neighbouring lattice sites and we get a chain of tensors of rank 3, as is depicted in figure 2.2.

Although the Matrix Product State (MPS) form is only taking into account nearest neighbour interactions, we want to be able to describe all kinds of wave functions (more or less efficiently). This is why we have to be able to account for correlation between (in principle) all particle sites with each other. In the MPS formulation, long range correlation therefore has to be taken into account implicitly through the local bond indices, that is through the correlation between neighbouring particles. In order to explain this implicit coupling more clearly, we consider a wave function that is defined on four lattice sites and can be written in the MPS form as:

$$\Psi_{\nu_1,\nu_2,\nu_3,\nu_4} = \sum_{m_1=1}^{4} \sum_{m_2=1}^{4^2} \sum_{m_3=1}^{4} A_{\nu_1,m_1} A^{m_1}_{\nu_2,m_2} A^{m_2}_{\nu_3,m_3} A^{m_3}_{\nu_4}. \tag{2.36}$$

The coupling between the first lattice site ν_1 and the second lattice site ν_2 is, as, before: both lattice sites can be in 4 different physical states and combining all possible combinations of physical states yields a matrix $4 \times 4 = 16$ possible combinations. The situation changes when now considering the coupling between the second lattice site ν_2 and the third lattice site ν_3. Although locally, on each site we have four different possible configurations, the physical configuration of lattice site ν_2 is also influenced by the coupling with lattice site ν_1, yielding to a virtual index m_2 of maximally $4^2 = 16$ different configurations.

We can write any general wave function of L lattice sites as an MPS in this form:

$$\Psi_{\nu_1\nu_2\ldots\nu_N} = \sum_{m_1}^{4} \sum_{m_2}^{4^2} \ldots \sum_{m_{N/2}}^{4^{N/2}} \ldots \sum_{m_{N-1}}^{4} A_{\nu_1 m_1} A^{m_1}_{\nu_2 m_2} \ldots A^{m_{N/2-1}}_{\nu_{(N/2)} m_{(N/2)}} \ldots A^{m_{N-1}}_{\nu_N}. \tag{2.37}$$

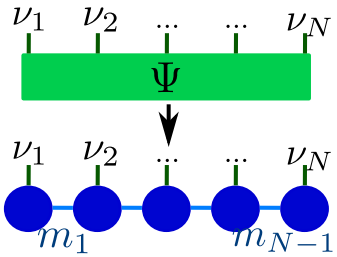

Figure 2.2: As a second step, in the Tensor Network notation, we decompose the tensor of rank N into N-tensors A_i of rank 3. Again, this decomposition is just a rewriting and does not change any physical properties of the model.

Then the virtual indices m_i (also called bond indices) indicate the correlation between the whole system to the left of the bond (ν_1 until ν_i) and the whole system to the right of the bond (ν_{i+1} until ν_N). The number of bond indices grow with each site: the sum over m_1 goes from 1 to four $\left(\sum_{m_1=1}^{4}\right)$, the sum over m_2 goes from one to 4^2 $\left(\sum_{m_2=1}^{4^2}\right)$ until the sum of $m_{N/2}$: $\left(\sum_{m_{N/2}=1}^{4^{N/2}}\right)$ in the middle of the chain. If the total amount of sites is odd, the sum over $m_{N/2-1}$ and $m_{N/2+1}$ is simply the same. From the middle of the chain on, the amount of bond indices again decrease until m_{N-1} which again

only goes from one to four $\left(\sum_{m_{N-1}=1}^{4}\right)$.
When re-writing the wave function from a vector to this rank N tensor, the total dimensionality, as before, is 4^N so nothing really is gained from the alternative expression. We call this representation of a wave function a Matrix Product state or MPS.

Singular value decomposition In order to make the explicit calculation of the MPS feasible for larger systems, some approximations must be made, specifically, the dimensionality of the bond indices must be reduced. As the amount of indices in each sum is 4^i, indicating the correlation of the system to the left of the bond (ν_1 until ν_i) and the system to the right of the bond (ν_{i+1} until ν_L), we hope that for systems with low correlation between its particles, some entries in the sums can be neglected. A measure for this gives the singular value decomposition. We will explain the singular value decomposition [33, pp. 564] by considering the MPS in Eq. (2.37) more closely. Specifically, we are interested in the coupling between two (arbitrary) elements of the MPS wave function that we can re-write in a new form:

$$\Psi_{\nu_i,\nu_{i+1}} \equiv \sum_{m_i=1}^{4^i} A_{\nu_i,m_i} A^{m_i}_{\nu_{i+1}} = \sum_{m_i=1}^{4^i} L_{\nu_i,m_i} \sigma_{m_i} R^{m_i}_{\nu_{i+1}}. \tag{2.38}$$

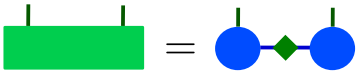

Figure 2.3: Singular value decomposition: When regarding two neighbouring sites, the correlation between the particles on the sites can be measured via the singular value decomposition. The matrix connecting site i and $i+1$ is diagonal; the entries are the singular values. Their amplitudes are a measure for the correlation between the particles in the system.

Here, $\sigma_1 \geq \sigma_2 ... \geq \sigma_m$ are the singular values of the two matrices and the procedure is depicted in the sketch 2.3. The matrices $L_{\nu_1,m}$ and $R^m_{\nu_2}$ are orthogonal matrices in the sense that

$$\sum_m L_{\nu_1,m} L^{m,\nu_2} = \delta_{\nu_1\nu_2}, \tag{2.39}$$

$$\sum_m R^m_{\nu_1} R^{\nu_2}_m = \delta_{\nu_1\nu_2}. \tag{2.40}$$

Our goal is to approximate the sum in Eq. (2.38) by only taking into account those addends belonging to singular values σ_i which are bigger than a certain value δ. The addends belonging to singular values below this threshold will be neglected, yielding a sum that goes over less indices, $m_\delta < 4^i$

$$\Psi_{\nu_i,\nu_{i+1}} = \sum_{m_i=1}^{m_\delta} L_{\nu_i,m_i} \sigma_{m_i} R^{m_i}_{\nu_{i+1}}. \tag{2.41}$$

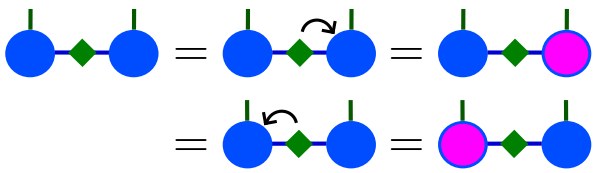

Figure 2.4: Gauge freedom of the MPS formulation: The MPS notation is not unique, but a certain gauge can be chosen, depending on whether the singular values are absorbed on the right hand side lattice or the left hand side lattice

The MPS written in Eq. (2.37) is not unique. This is due to the general gauge freedom in the formulation of many body quantum mechanics. Specifically, here the gauge freedom manifests itself in the auxiliary indices: we can absorb the singular values σ_{m_i} in Eq. (2.41)either to the right lattice site or to the left lattice site as is schematically depicted in figure 2.4

2.2.2 The Hamiltonian as a Matrix Product operator

In order to find the ground state MPS, we also need to write the Hamiltonian chosen to describe our physical system in a similar way as the MPS, namely, as a Matrix Product Operator (MPO), which is depicted in figure 2.5.

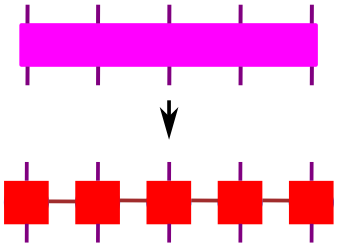

Figure 2.5: Similar to the decomposition of the wave function into a MPS, also an operator can be decomposed into a Matrix Product Operator (MPO). The difference here is that there are two physical indices (one in going, one outgoing) which then forms a chain of 4th order tensors.

Any operator acting on a Hilbert space of dimension $\dim(\mathcal{H}_{\mathrm{L}}) = \mathrm{N}^{\mathrm{L}}$ can be written as:

$$\hat{H} = \sum_{\nu_1,\mu_1}^{4} \sum_{\nu_2,\mu_2}^{4} ... \sum_{\nu_L,\mu_L}^{4} H^{\mu_1,\mu_2...\mu_L}_{\nu_1,\nu_2...\nu_L} |\nu_1\rangle|\nu_2\rangle...|\nu_L\rangle\langle\mu_1|\langle\mu_2|...\langle\mu_L|, \tag{2.42}$$

where $H^{\mu_1,\mu_2...\mu_L}_{\nu_1,\nu_2...\nu_L}$ is then a tensor of rank 2L. Similar to the tensor of rank L which describes the transition matrix $\Psi_{\nu_1...\nu_L}$ defining the wave function Eq. (2.37), this tensor can be decomposed into a chain of L tensors of rank 4 which is then called a Matrix Product Operator (MPO):

$$H^{\mu_1,\mu_2...\mu_L}_{\nu_1,\nu_2...\nu_L} = \sum_{w_1}^{4} \sum_{w_2}^{4^2} ... \sum_{w_{L/2}}^{4^{L/2}} ... \sum_{w_{L-1}}^{4} W^{\nu_1}_{\mu_1,w_1} W^{\nu_2,w_1}_{\mu_2,w_2} ... W^{\nu_{L/2},w_{L/2-1}}_{\mu_{L/2},w_{L/2}} ... W^{\nu_L,w_{L-1}}_{\mu_L}. \tag{2.43}$$

Here, the w_i again correspond to the correlation of the left part of the chain (going from 1 to i) with the right part of the chain (going from $i+1$ to L). Unlike an MPS though, we have two physical degrees of freedom per tensor: one dimension of the tensor (ν_i) corresponds to the physical state of the in going MPS and the other dimension of the tensor (μ_i) corresponds to the physical state of the MPS after applying the MPO onto in going MPS.

2.2.3 The variational principle in the Tensor Network method: Density Matrix Renormalization Group

We want to find the ground state MPS, that is, the MPS that minimizes:

$$\min_{\Psi} \left[\langle\Psi|\hat{H}|\Psi\rangle - E\langle\Psi|\Psi\rangle \right]. \tag{2.44}$$

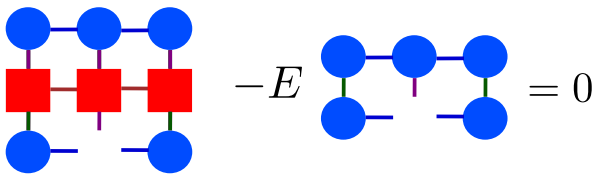

Figure 2.6: Energy minimization in the Density Matrix Renormalization group style: We optimize the whole MPS by only optimizing one single tensor (belonging to one lattice site) at a time. Due to the chosen gauge, this can be rewritten into an eigenvalue problem.

We do that by always only optimizing with respect to a single tensor of the MPS, belonging to a specific local site

$$\frac{\partial}{\partial\left(A^{m_i}_{\nu_{i+1}m_{i+1}}\right)} \left(\langle\Psi|\hat{H}|\Psi\rangle - E\langle\Psi|\Psi\rangle \right) = 0 \tag{2.45}$$

at a time and then sweeping through the whole system by performing this optimization for each site (figure 2.6). In order to find the global minimum of the MPS, several sweeps are usually necessary. This problem corresponds to a generalized eigenvalue problem which can be simplified to a normal eigenvalue problem by choosing a clever gauge as is depicted in figure 2.7.

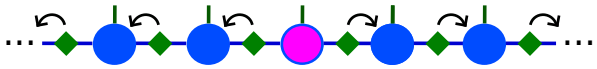

Figure 2.7: Sketch of the DMRG-gauge, where one site is chosen to not absorb any singular values. The sites to the right and to the left each absorb singular values, leaving them diagonal in the before mentioned fashion.

We decide that the specific site $i+1$ that is minimized will not absorb any singular values, whereas all sites to the left (site i until 1) will absorb the singular values coming from the right, and all sites to the right (sites $i+2$ until L) to always absorb the singular values coming from the left. This is the Density Matrix Renormalization Group (DMRG) form of writing a MPS.

Then, the calculation of the MPS wave function is very easy, as, due to their orthogonality, all sites but the one being minimized yield a unitary matrix, as is schematically depicted in figure 2.8.

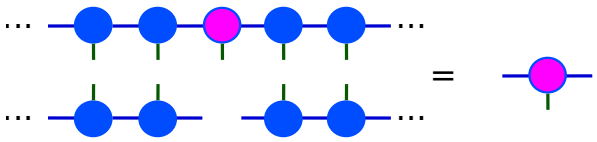

Figure 2.8: Using the gauge freedom of the MPS, the overlap of two states on the same lattice site is simply a unity matrix.

2.3 Summary

In this chapter, we have given an overview over different ways to formulate lattice wave functions. We presented various, commonly used and successful methods to solve those lattice wave functions. The different techniques can be divided into three groups:

- Exact solution of the wave function

  The Full-Configuration-Interaction method (which is also called Exact Diagonalization), diagonalizes the wave function of interest exactly. Being exact, it can be applied to any possible wave function. The disadvantage of this method is that its numerical costs grow exponentially with the number of considered particles. As such, it can only be used to solve the wave function of small systems with only a few particles in them.

- Wave function methods that have a Slater determinant as the starting point

  A lot of quantum chemistry methods, such as Coupled Cluster or Configuration-Interaction Singles or Doubles are very efficient methods starting from the mean field description of the system of interest and then doing efficient perturbation theory on this basis. They are very successful in describing systems that can be approximated well by one single Slater determinant, they fail when the there are strong interactions present.

- Tensor network methods in one dimension

  The Tensor Network method uses that a wave function on the lattice can be written in terms of local Hilbert spaces. Here, the wave function is split up into tensors of third order, describing only one lattice site; interactions between the sites are considered through a so-called virtual index. This method is effective for systems with short range interactions as in this case the correlation between two particles decreases drastically with their distance. With the Tensor Network method, locally strongly interacting particles can be described very well.

Chapter 3

Functional Methods

In the following chapter, we give an overview over existing functional methods and their advantages and drawbacks. This part of the thesis roughly follows an excellent talk, given by Klaas Giesbertz in the scope of the Young Researchers Meeting (YRM) in 2018 while adapting the presentation to lattice models. Part of this talk has been published in the book [52, pp.125].

3.1 Hierarchy of different functional methods

In order to describe the properties of any quantum mechanical system, instead of solving the Schrödinger equation directly (as has been presented in the previous section), one can also bypass this high dimensional problem and try to calculate the observables of interest directly.

An object that usually is of great interest in this context is the ground state energy E. From the Schrödinger equation, we know that this property is a functional of the wave function:

$$E[\Psi] = \langle \Psi | \hat{H} | \Psi \rangle. \tag{3.1}$$

The Hamiltonian is defined here as

$$\hat{H} = \hat{T} + \hat{V} + \hat{W} = \sum_{i,j,\sigma} t_{ij} \hat{c}^\dagger_{i,\sigma} \hat{c}_{j,\sigma} + \sum_i v_i^{\text{ext}} \hat{n}_{i\sigma} + \sum_{i,j,\sigma,\sigma'} w_{ij} \hat{c}^\dagger_{i\sigma} \hat{c}^\dagger_{j,\sigma'} \hat{c}_{i,\sigma} \hat{c}_{j\sigma'} \tag{3.2}$$

where $\hat{T}$ is the kinetic energy, $\hat{V}$ an arbitrary external potential and $\hat{W}$ is some two-particle interaction. $\hat{c}^\dagger_{i,\sigma}$ and $\hat{c}_{i,\sigma}$ are the creation and annihilation operators of an electron with spin σ on lattice site i, as defined in section 2.1.3. We further define the spin dependent density operator as $\hat{n}_{i\sigma} = \hat{c}^\dagger_{i,\sigma} \hat{c}_{i,\sigma}$.

Examining the total energy $\langle \Psi | \hat{H} | \Psi \rangle$, we see directly that it does not depend on the whole wave function, but can be formulated in terms of objects that have a lower dimension than $|\Psi\rangle$:

$$\langle \Psi | \hat{H} | \Psi \rangle = V[n] + T[\gamma] + W[\Gamma]. \tag{3.3}$$

Specifically, the external potential $V[n]$ is a functional of the density n_i:

$$V[n] = \langle \Psi | \hat{V} | \Psi \rangle = \sum_i \hat{n}_i v_i^{\text{ext}} \tag{3.4}$$

$$n_i = \sum_\sigma \hat{c}^\dagger_{i,\sigma} \hat{c}_{i,\sigma}. \tag{3.5}$$

The kinetic energy $T[\gamma]$ is a functional of the one particle reduced density matrix γ_{ij}:

$$T[\gamma] = \langle \Psi | \hat{T} | \Psi \rangle = \sum_{i,j} t_{ij} \gamma_{ij} \tag{3.6}$$

$$\gamma_{ij} = \sum_\sigma \hat{c}^\dagger_{i,\sigma} \hat{c}_{j,\sigma} \tag{3.7}$$

and the interaction energy $W[\gamma]$ is a functional of the two particle reduced density matrix Γ_{ijkl}:

$$W[\Gamma] = \sum_{ijkl} w_{ij}\Gamma_{ijkl} \tag{3.8}$$

$$\Gamma_{ijkl} = \sum_{\sigma,\sigma'} \hat{c}^\dagger_{k,\sigma}\hat{c}^\dagger_{l,\sigma'}\hat{c}_{j,\sigma}\hat{c}_{i,\sigma'} \tag{3.9}$$

3.1.1 Two particle reduced density matrix functional theory

From the definitions in Eqns. (3.4), (3.6) and (3.8), it follows that instead of trying to find the ground state wave function Ψ that fulfills

$$\hat{H}|\Psi\rangle = E|\Psi\rangle, \tag{3.10}$$

where E is the lowest energy of the regarded system, one can as well just find the two particle reduced density matrix (from now on called 2RDM), that contains also the information about the density and the one particle reduced density matrix.

$$\begin{aligned} E_0 &= \min_{|\Psi\rangle}\langle\Psi|\hat{H}|\Psi\rangle \\ &= \min_{\Gamma}\left(V[\Gamma] + T[\Gamma] + W[\Gamma]\right) && (3.11)\\ &= \min_{\Gamma} E[\Gamma] && (3.12)\end{aligned}$$

Unfortunately though, there is a condition that makes this process harder than it seems: We can only consider *physical* 2RDMs, that means, the Γ needs to belong to a certain wave function Ψ:

$$P \equiv \{\Gamma : \exists\Psi \to \Gamma\} \tag{3.13}$$

$$\min_{\Gamma\in P} E[\Gamma] = E_0. \tag{3.14}$$

The Γ that are in P are called the N-representable 2RDMs and it is very complicated to implement the conditions the 2RDMs need to fulfill in order to be N-representable numerically.

3.1.2 One particle reduced density matrix functional theory

Because the conditions the 2RDMS have to fulfill in order to represent a physical wave function are complicated, one can also decide to search for the functional of the one particle reduced density matrix (from now on called 1RDM) instead of trying to find the 2RDM functional.

Knowing the 1RDM functional, the external energy V and the kinetic energy T of the system can be described exactly, but the interaction part needs to be approximated:

$$\begin{aligned} E_0 &= \min_{\Psi}\langle\Psi|\hat{H}|\Psi\rangle \\ &= \min_{\gamma}\left(V[\gamma] + T[\gamma] + \min_{\Psi\to\gamma}\langle\Psi|\hat{W}|\Psi\rangle\right) && (3.15)\end{aligned}$$

In addition to having to approximate $W[|\Psi\rangle]$, also the 1RDMs do not automatically represent physical systems. Like in the case above, one needs to make sure that the 1RDM that is found to minimize the energy E_0 belongs to an actual wave function representing a physical system:

$$p \equiv \{\gamma : \exists\,\Psi \to \gamma\} \tag{3.16}$$

$$\min_{\gamma\in p} E[\gamma] + \min_{|\Psi\rangle\to\gamma}\langle\Psi|\hat{W}|\Psi\rangle = E_0. \tag{3.17}$$

The conditions the 1RDMs have to fulfill are not as many and less complicated then the conditions for the 2RDMs, which is why for some problems it is more sensible to choose this approach.

3.2 Density functional theory

In Density Functional Theory (DFT) [11, 7], we define the energy functional in terms of the density n which yields

$$\begin{aligned} E_0 &= \min_{\Psi} \langle \Psi | \hat{H} | \Psi \rangle \\ &= \min_{|\Psi\rangle \to n} \langle \Psi | \hat{H} | \Psi \rangle \\ &= \min_{n} \left(V[n] + \min_{\Psi \to n} \langle \Psi | \hat{T} + \hat{W} | \Psi \rangle \right) \end{aligned} \tag{3.18}$$

Here, only the potential energy functional as defined in Eq. (3.4) is found exactly while the functionals decribing the kinetic and the interaction energy of the system need to be approximated.

There are two advantages of DFT which makes it very successful and used in a lot of different fields: The first advantage is the small dimensionality of the density. The density is just a function of space $n(\mathbf{r})$ so its computation is much more feasible than the calculation of any other property such as the 1RDM or especially the 2RDM. The second big advantage of DFT is that every density which yields the correct number of particles belongs to a physically sensible wave function, i.e. all densities are ensemble N-representable which was shown by Hohenberg and Kohn in 1964 [23].

3.2.1 The Hohenberg Kohn theorem for non-degenerate ground states

The Hohenberg Kohn theorem for non-degenerate ground state[23] states, that there is a one-to-one correspondence between the local external potential of a given interacting system $\hat{V}$ and its wave function $|\Psi\rangle$, as well as there is a one to one correspondence between the wave function of this system and its ground state density $n(\mathbf{r})$:

$$\hat{V}(\mathbf{r}) \xleftrightarrow{1:1} |\Psi\rangle \xleftrightarrow{1:1} n(\mathbf{r}) \tag{3.19}$$

This means that all ground state quantities of a many-body system are determined by its ground state density. In other words, knowing the ground state density of a system and the belonging functionals, one can describe every (many body) property of the system.

$$|\Psi\rangle = |\Psi[n]\rangle \;\Rightarrow\; \langle \hat{O} \rangle = \langle \Psi | \hat{O} | \Psi \rangle = \langle \hat{O} \rangle [n] \tag{3.20}$$

3.2.2 Kohn Sham DFT

By itself, the Hohenberg-Kohn theorem is lacking practical applicability, as the exact properties of the many body system as functionals of the ground state density are in general unknown which means in other words, the term

$$F[n] = \min_{|\Psi\rangle \to n} \langle \Psi | \hat{T} + \hat{W} | \Psi \rangle \tag{3.21}$$

needs to be approximated. DFT has become such a highly successful method due to an additional insight, made by Kohn and Sham [36] that is schematically represented in figure 3.1.

The Hohenberg Kohn theorem states that any system is unambiguously defined by its density. Beside that, Kohn and Sham later showed that additionally, to each density $n(\mathbf{r})$, one can find one interacting system with belonging wave function Ψ and external potential $\hat{V}(\mathbf{r})$, but also one non-interacting system with a (different) belonging wave function Φ and a different external potential $\hat{V}_s(\mathbf{r})$.

While the interacting system is hard to solve, the non-interacting system can be solved more easily, but has the same density as the interacting system.

The non-interacting system can be described by a single Slater determinant which can effectively be solved by solving uncoupled one-body equations of motions. Thus, the density of the non-interacting system reads:

$$\sum_j \left(\hat{t}_{ij} + \hat{v}_j^S \right) \varphi_j^\mu = \varepsilon^\mu \varphi_i^\mu \tag{3.22}$$

$$n_i = \sum_\mu |\varphi_i^\mu|^2. \tag{3.23}$$

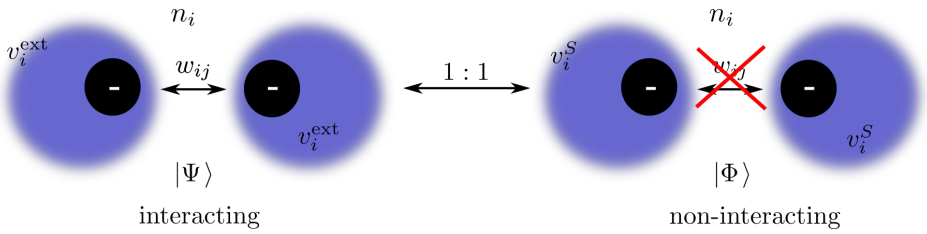

Figure 3.1: One-to-one correspondence between interacting and non-interacting system: A system consisting of interacting electrons w_{ij} and an external potential v_i^{ext} (left hand side), if fully determined by the many body wave function $|\Psi\rangle$, but also by its density n_i. There exists one and only one non-interacting system (right hand side), with the same density n_i, but a different Kohn-Sham potential that is defined as $v_{\text{S}}(r) = v_{\text{S}}[n(r), v_{\text{ext}}(\mathbf{r})]$. In the non-interacting case, the full system is determined by the Kohn-Sham potential.

In order for the interacting and the non-interacting system to have the same density, the external potential of the non-interacting system needs to include the terms accounting for the interaction and correlation in the non-interacting system:

$$v_i^S = v_i^{\text{ext}} - v_i^{\text{Hxc}}[n, v_i^{\text{ext}}](\mathbf{r}). \tag{3.24}$$

The second term in this equation accounts for the electrostatic potential created by the density n_i (Hartree term) and the term exchange and correlation interaction (exchange-correlation term), both. While the Hartree term is known, the exchange correlation term is in general not known and needs to be approximated.

In Kohn-Sham DFT, the term $v_i^S[n, v_i^{\text{ext}}]$ can be found self-consistently: An initial guess for the Kohn-Sham potential v_S is made, from which, with equations (3.22), the density n_i can be calculated. As the density enters directly in the Kohn-Sham potential (Eq. (3.24)), a new guess for v_i^S can be computed, yielding a new density and so on. Repeating this procedure until self-consistency gives an estimate for the (interacting) density.

Once the Kohn-Sham potential is known, also the density (of the non-interacting and the interacting system) is known. More importantly though, the energy functional of the interacting system can be approximated by the non-interacting system:

$$E[n] = T[n] + V[n] + W[n] \approx T_S[n] + \sum_i \hat{n}_i v_i^{\text{ext}} + E_{\text{Hxc}}[n]. \tag{3.25}$$

In Kohn-Sham DFT we have thus an explicit expression for the kinetic term $T[n]$. As this kinetic term in DFT is dominating (and usually also more error prone), this already helps improving the functional a lot.
The only term that needs approximation in Kohn Sham DFT is the exchange correlation term, which is part of the Hartree-exchange correlation which accounts for all interactions in the system:

$$E_{\text{Hxc}}[n] = F[n] - T_S[n] \tag{3.26}$$

$$v_i^{\text{Hxc}}[n] = -\frac{\delta E_{\text{Hxc}}[n]}{\delta\, n_i} \tag{3.27}$$

There are many different techniques and approximations to find the exchange-correlation potential $v_i^{\text{xc}}[n]$, the fundamental one being given by the Local Density Approximation (LDA), which can be expanded towards the inclusion of gradients (GGA). There are also a lot of hybrid functionals, which use parameters from other methods in order to fit the functional to experimental values [36, 51, 4, 5, 40].

3.3 Summary

In this chapter, we have given an overview over the hierarchy of different functional methods. We have explained that in order to avoid the computation of the wave function, we can instead formulate

the energy of a system in terms of its 2RDM, or, with approximations, in terms of its 1RDM or density. While the 1RDM and, even more so, the density are much less complex objects than the wave function, the challenge in functional methods consists in finding the functionals of the 1RDM or the density that determine the desired observables, such as the energy.

Part II

Density Matrix Embedding Theory

Chapter 4

Introduction: What is Density Matrix Embedding Theory?

So far, we have presented two possible ways to treat quantum mechanical (lattice) systems: One approach is to try to solve the Schrödinger equation

$$\hat{H}_{\mathrm{el}}|\Psi\rangle = E|\Psi\rangle, \tag{4.1}$$

$$\hat{H}_{\mathrm{el}} = \hat{T}_{\mathrm{el}} + \hat{U}_{\mathrm{el}} \tag{4.2}$$

for a given general electronic Hamiltonian directly by re-writing both the wave function as well as the Hamiltonian in an efficient way and making approximations to those quantities. One possible approach along these lines has been presented in section 2.2 as the tensor network method. Even though the tensor network methods give very accurate results and numerical costs to solve the Schrödinger equation is scaled down to polynomial growth with system size, it is still a fact that all wave function methods grow too fast with the size of the regarded system, making it hard to compute large systems.

Another approach to deal with quantum mechanical problems are functional methods, where instead of trying to solve the Schrödinger equation exactly, this minimization problem is written in terms of functionals which are given in terms of one-body Green's function, reduced density matrices or the density itself, respectively

$$\langle\Psi|\hat{H}|\Psi\rangle = V[n] + T[\gamma] + W[\Gamma]. \tag{4.3}$$

While these methods scale very well with growing system size, they have the disadvantage that all the physics is now hidden in functionals of the density, 1RDM or 2RDM and finding functionals of observables in terms of those properties can be a complicated task.

There is another possible approach to treat quantum many body systems, namely the embedding idea. When using an embedding method, instead of solving the Schrödinger equation for the whole system, a small subsystem is chosen, which is small enough to be solved efficiently. The various embedding techniques then differ in how the rest of the system is treated and how the connection between the embedded system and the full system is made.

We will consider one embedding approach, namely the Density Matrix Embedding Theory (DMET) which is depicted schematically in Figure 4.1. In DMET, additionally to computing the chosen subsystem, which is called impurity, also the interactions of the rest of the system with the impurity are included. In other words, in DMET, we divide the system into two disentangled parts: The so-called embedded system which consists of the impurity and the part of the system interacting with it, and the environment consisting of the part of the system not interacting with the impurity. The embedded system determines the physics of the impurity, including interactions with the rest of the system (and with that, also finite size effects and the influence of the boundaries). Since the embedded system is much smaller than the original system, it can be computed efficiently with an accurate wave function method.

In this thesis, we target lattice Hamiltonians, as explained in chapter 2.1. Thus, the following derivation will be shown for the lattice-site basis.

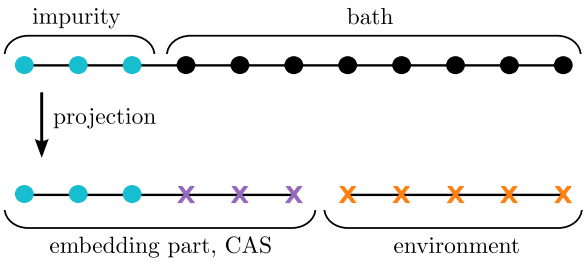

Figure 4.1: Basic idea of DMET: Instead of solving the full system with a wave function method, we split it up into an impurity (turquoise) and a bath part (black). While the impurity is treated explicitly and as accurately as possible, the bath part is split up into one part that interacts with the impurity (violet) and one part that does not interact with the impurity (orange). While the part not interacting with the impurity is discarded, the interacting part, together with the impurity region, is solved accurately with a wave function method. In order to separate the bath into the two parts, a projection from the lattice basis to a new basis is necessary.

The following part of this thesis is structured as follows: In chapter 5, we will derive the mathematical details of Density Matrix Embedding Theory. Then, in chapter 6, we will present the individual steps of the DMET procedure for a simple example. In the last chapter 7, we will give a recipe on how to practically implement this method and illustrate some subtleties and problems of the method.

Chapter 5

Mathematical derivation

In this chapter, we explain and derive in detail the Density Matrix Embedding Theory (DMET), which was introduced in 2012 by Knizia and Chan [34, 35]. Although loosely following a review article [70] of the group of Chan, we make an effort to describe each single step with all mathematical and technical details, including the treatment of a simple example, that can be found in chapter 6. This way, we are not only able to understand DMET thoroughly, but can also pin down possible pitfalls and suggest improvements.

The general idea of embedding methods is depicted in figure 5.1: We start from a system which is determined by the wave function Ψ (left hand side of figure 5.1). As Ψ is a very high-dimensional object, it cannot be computed in general. Instead, we choose a part of the system, which we call impurity (middle of figure 5.1, depicted in orange), that is fully determined by the wave function Ψ_{imp}. For many observables of interest, it is sufficient to describe only a small part of the whole system as accurately as possible. As the impurity interacts with the rest of the system though, it is not sufficient to just describe the wave function on the impurity; it is necessary to also describe the interactions of the rest of the system with the impurity. Thus, the goal of DMET is to describe the impurity region, including interaction of the rest of the system with it. In order to do that, but without having to compute the wave function Ψ of the full system, we find an effective system, determined by the wave function Ψ_{emb}, which we call embedded wave function. Ψ_{emb} is defined on a subspace of the Fock space describing the full problem. This subspace is optimized to describe the impurity region and the interaction of the rest of the system with the impurity as accurately as possible.

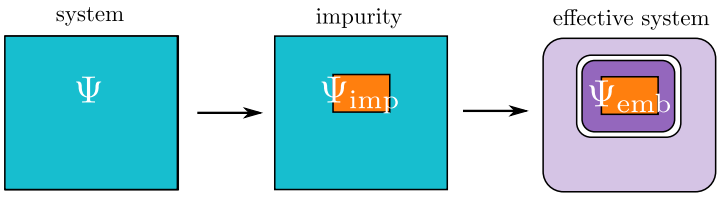

Figure 5.1: General idea of embedding methods: As the description of the wave function of the full system is oftentimes not feasible, a subsystem, called impurity is chosen. While keeping this impurity region as it is, the rest of the system is projected onto an optimal basis describing only the interactions of the system with the impurity. The effective system, containing the wave function of the impurity and part of the rest of the system can then be solved accurately. Graph is adapted from [44]

.

5.1 Exact embedding of the interacting system

In the tensor network method explained in section 2.2, the wave function is split up into L third-order tensors, where each of those tensors represents one lattice site. In DMET on the other hand, we are interested in splitting up the wave function into two different parts, one small part which is called impurity and one big part which is called bath. We are then only interested in the physics on the

impurity, which is influenced by the bath and try to treat the bath as inexpensive as possible while still considering all interactions and correlations between impurity and bath.

As explained in section 2.1.2, we can write a general wave function in the lattice basis as a vector of length 4^L:

$$|\Psi\rangle = \sum_{\nu_1}^{4}\sum_{\nu_2}^{4}...\sum_{\nu_L}^{4}\Psi_{\nu_1,\nu_2,...,\nu_L}|\nu_1\rangle|\nu_2\rangle...|\nu_L\rangle. \tag{5.1}$$

Choosing one part of the lattice that we call the impurity and the remaining part that we call the bath, we can split $|\Psi\rangle$ up into:

$$|A\rangle = \sum_{\nu_1=1}^{4}\sum_{\nu_2=1}^{4}...\sum_{\nu_{N_{\text{imp}}}=1}^{4}\Xi_{\nu_1,\nu_2...,\nu_{N_{\text{imp}}}}|\nu_1\rangle|\nu_2\rangle...|\nu_{N_{\text{imp}}}\rangle, \tag{5.2}$$

$$|B\rangle = \sum_{\nu_{N_{\text{imp}}+1}=1}^{4}...\sum_{\nu_N=1}^{4}\Upsilon_{\nu_{N_{\text{imp}}+1}...\nu_N}|\nu_{N_{\text{imp}}+1}\rangle...|\nu_N\rangle, \tag{5.3}$$

here $|A\rangle$ is only defined on a certain number of impurity lattice sites N_{imp}, and $|B\rangle$ is the rest of the system, namely the bath. As we treat a translational invariant system, we can always choose the impurity region to be at the beginning of the system, that is, at sites 1 to N_{imp}. We can then write again the full wave function as:

$$|\Psi\rangle = \sum_{i=1}^{4^{N_{\text{imp}}}}\sum_{j=1}^{4^{(N-N_{\text{imp}})}}\Psi_{ij}|A_i\rangle\otimes|B_j\rangle \tag{5.4}$$

in this equation, Ψ_{ij} is the connecting matrix between $|A_i\rangle$ and $|B_j\rangle$ and has the dimension $4^{N_{\text{imp}}} \times 4^{N-N_{\text{imp}}}$.

Similar to setting up of the wave function as a tensor network which we explained in section 2.2.1, we now use the Singular Value Decomposition (sometimes also called Schmidt Decomposition) of the matrix Ψ_{ij}. The Singular Value Decomposition is a mathematical relation [33, pp. 564] that is valid for arbitrary matrices and can be expressed as:

$$\Psi_{ij} = \sum_{\alpha}^{4^{N_{\text{imp}}}}U_{i\alpha}\lambda_\alpha V^\dagger_{\alpha j}. \tag{5.5}$$

Here, $U_{i\alpha}$ and $V^\dagger_{\alpha j}$ are orthogonal matrices and the λ_α are the so-called singular values of this decomposition. The dimension of α corresponds to the dimension of the smaller of the sub spaces. Plugging Eq. (5.5) into Eq. (5.4) then yields

$$\begin{aligned}
|\Psi\rangle &= \sum_{i=1}^{4^{N_{\text{imp}}}}\sum_{j=1}^{4^{(\text{N}-\text{N}_{\text{imp}})}}\sum_{\alpha=1}^{4^{N_{\text{imp}}}}U_{i\alpha}\lambda_\alpha V^\dagger_{\alpha j}|A_i\rangle\otimes|B_j\rangle, \\
&= \sum_{i=1}^{4^{N_{\text{imp}}}}\sum_{j=1}^{4^{(\text{N}-\text{N}_{\text{imp}})}}\sum_{\alpha=1}^{4^{N_{\text{imp}}}}\lambda_\alpha\underbrace{U_{i\alpha}|A_i\rangle}_{\equiv|\tilde{A}_\alpha\rangle}\otimes\underbrace{V^\dagger_{\alpha j}|B_j\rangle}_{|\tilde{B}_\alpha\rangle}, \\
&\equiv \sum_{\alpha=1}^{4^{N_{\text{imp}}}}\lambda_\alpha|\tilde{A}_\alpha\rangle\otimes|\tilde{B}_\alpha\rangle \equiv \sum_{\alpha=1}^{4^{N_{\text{imp}}}}\lambda_\alpha|\tilde{A}_\alpha\tilde{B}_\alpha\rangle.
\end{aligned} \tag{5.6}$$

By reorganizing the equation we see that this same wave function can be decomposed into the sum of the tensor product of two different sets of many body wave functions ($|\tilde{A}_\alpha\rangle$ and $|\tilde{B}_\alpha\rangle$) describing different parts of the system Ψ. The **number** of wave functions needed to completely describe both parts of the system is the same even if one part is much smaller than the other.

The dimension of the vectors though stays the same, being dim $= 4^{\text{N}_{\text{imp}}}$ for the $|\tilde{A}_\alpha\rangle$ and dim $= 4^{\text{N}-\text{N}_{\text{imp}}}$ for the $|\tilde{B}_\alpha\rangle$. While for the impurity region

$$|\tilde{A}_\alpha\rangle = \sum_{i}^{4^{N_{\text{imp}}}}U_{i\alpha}|A_i\rangle \tag{5.7}$$

the basis vectors have just been rotated (the number of basis vectors $|\tilde{A}_\alpha\rangle$ and $|A_i\rangle$ is the same), in the bath region

$$|\tilde{B}_\alpha\rangle = \sum_j^{4^{N-N_{\text{imp}}}} V^\dagger_{\alpha j}|B_j\rangle, \tag{5.8}$$

we find a completely new basis by linear combination of the original basis sets (the number of basis vectors $|\tilde{B}_\alpha\rangle$ is much smaller than the number of original basis vectors $|B_j\rangle$).

The full basis of the considered system, divided into two subsystems A and B is thus transformed such that the number of wave functions is the same as the number of wave functions it takes to describe system A.

5.1.1 The Projection derived from the interacting system

We use the re-written wave function Eq. (5.6) to define a projection $\hat{P}'$ that projects from the set of Eq. (5.4) to the new set found in Eq. (5.6):

$$\begin{aligned}\hat{P}' &= \sum_{\alpha=1}^{4^{N_{\text{imp}}}} |\tilde{A}_\alpha\tilde{B}_\alpha\rangle\langle\tilde{A}_\alpha\tilde{B}_\alpha|, \\ &= \sum_{\gamma=1}^{4^{N_{\text{imp}}}} \left(|\tilde{C}_\alpha\rangle\langle\tilde{C}_\alpha| + |\tilde{C}^*_\alpha\rangle\langle\tilde{C}^*_\alpha|\right),\end{aligned} \tag{5.9}$$

where we define

$$|\tilde{C}_\alpha\rangle + |\tilde{C}^*_\alpha\rangle = |\tilde{A}_\alpha\tilde{B}_\alpha\rangle \tag{5.10}$$

such that

$$|\tilde{C}_\alpha\rangle = |\tilde{A}_\alpha\rangle_{N_{\text{imp}}} \oplus |0\rangle_{N-N_{\text{imp}}} \tag{5.11}$$

$$|\tilde{C}^*_\alpha\rangle = |0\rangle_{N_{\text{imp}}} \oplus |\tilde{B}_\alpha\rangle_{N-N_{\text{imp}}}, \tag{5.12}$$

so that the $|\tilde{C}_\alpha\rangle$ just have values that are non-zero on the impurity although they are defined on the full system and the $|\tilde{C}^*_\alpha\rangle$ have just values other than zero on the environment.

Note that, although the number of wave functions $|\tilde{A}_\alpha\tilde{B}_\alpha\rangle$ is only 4^{imp}, they are still defined in the whole system, that these vectors have a length of 4^N.

We now define the wave function on the impurity $|\Psi_{\text{imp}}\rangle$, and the wave function on the environment $|\Psi\rangle_{\text{env}}$ as

$$|\Psi_{\text{imp}}\rangle \equiv \sum_{\alpha=1}^{4^{N_{\text{imp}}}} \lambda_\alpha|\tilde{A}_\alpha\rangle \in \mathcal{F}_{\text{imp}}, \tag{5.13}$$

$$\langle\nu_1,...\nu_{\text{imp}}|\Psi_{\text{imp}}\rangle = \sum_{\alpha=1}^{4^{N_{\text{imp}}}} \langle\nu_1,...\nu_{\text{imp}}|\tilde{A}_\alpha\rangle\lambda_\alpha \tag{5.14}$$

$$|\Psi_{\text{env}}\rangle \equiv \sum_{\alpha=1}^{4^{N_{\text{imp}}}} \lambda_\alpha|\tilde{B}_\alpha\rangle \in \mathcal{F}_{\text{env}}, \tag{5.15}$$

$$\langle\nu_{\text{imp}+1},...\nu_N|\Psi_{\text{env}}\rangle = \sum_{\alpha=1}^{4^{N_{\text{imp}}}} \langle\nu_{\text{imp}+1},...\nu_N|\tilde{B}_\alpha\rangle\lambda_\alpha, \tag{5.16}$$

where $\mathcal{F}_{\text{imp}}$ is the Fock space on N_{imp} lattice sites and $\mathcal{F}_{\text{env}}$ is the Fock space on $N - N_{\text{imp}}$ lattice sites.

Knowing that per construction the wave functions in the impurity are orthogonal to the wave functions in the environment, $\langle\tilde{A}_\alpha|\tilde{B}_\alpha\rangle = 0$ and that two different basis sets also form an orthogonal basis,

$\langle \tilde{A}_\alpha | \tilde{A}_\beta \rangle = \langle \tilde{B}_\alpha | \tilde{B}_\beta \rangle = 0$, $\alpha \neq \beta$ we can consider the overlap of these wave functions with the impurity and environment region:

$$\langle \Psi_{\text{imp}} | \tilde{A}_\alpha \tilde{B}_\alpha \rangle = \langle \Psi_{\text{imp}} | \tilde{C}_\alpha \rangle, \tag{5.17}$$

$$\langle \Psi_{\text{env}} | \tilde{A}_\alpha \tilde{B}_\alpha \rangle = \langle \Psi_{\text{env}} | \tilde{C}^*_\alpha \rangle, \tag{5.18}$$

We can then summarize the $|\tilde{C}_\alpha\rangle$ and $|\tilde{C}^*_\alpha\rangle$ in one index:

$$\begin{aligned} \hat{P}' &= \sum_{\gamma=1}^{4^{N_{\text{imp}}}} \left(|\tilde{C}_\alpha\rangle\langle\tilde{C}_\alpha| \; + \qquad |\tilde{C}^*_\alpha\rangle\langle\tilde{C}^*_\alpha| \right), \\ &= \sum_{\gamma=1}^{2\cdot 4^{N_{\text{imp}}}} |\tilde{C}_\gamma\rangle\langle\tilde{C}_\gamma| \qquad\qquad \tilde{C}_\alpha = \tilde{C}_\gamma \;\text{ for }\; \alpha = 1, ..., \mathrm{N_{imp}}, \gamma = 1, ...\mathrm{N_{imp}}, \\ &\qquad\qquad\qquad\qquad\qquad\qquad \tilde{C}^*_\alpha = \tilde{C}_\gamma \;\text{ for }\; \alpha = 1, ..., \mathrm{N_{imp}}, \gamma = \mathrm{N_{imp}} + 1, ...2 \cdot \mathrm{N_{imp}}. \end{aligned} \tag{5.19}$$

The $\tilde{C}_\gamma$ are not normalized and have the length $\|\tilde{C}_\gamma\|$.

We then define the projection $\hat{P}$ with the normalized $|C_\gamma\rangle = \tilde{C}_\gamma / \|\tilde{C}_\gamma\|$.

$$\hat{P} = |C_\gamma\rangle\langle C_\gamma| \tag{5.20}$$

As on the impurity, we have performed a unitary transformation the projection is a unitary matrix in the Fock space of the impurity:

$$\hat{P} = \mathbb{1}_{\mathfrak{F}_{N_{\text{imp}}}} + \sum_{\gamma=4^{N_{\text{imp}}}+1}^{2\cdot 4^{N_{\text{imp}}}} |C_\gamma\rangle\langle C_\gamma|. \tag{5.21}$$

$\hat{P}$ then projects into a subspace of the full Fock space that contains the exact wave function

$$\hat{P}|\Psi\rangle = |\Psi\rangle. \tag{5.22}$$

The projected Hamiltonian,

$$\hat{P}^\dagger H \hat{P} |\Psi\rangle = \hat{H}_{\text{emb}} |\Psi\rangle = \left(\hat{H}_{\text{imp}} + \hat{H}_{\text{imp-env}} + \hat{H}_{\text{env}} \right) |\Psi\rangle \tag{5.23}$$

has the same form as the original Hamiltonian $\hat{H}$ on the impurity but is defined on a much smaller Hilbert space than the latter:

$$\hat{H} : 4^{\mathrm{N}} \to 4^{\mathrm{N}}, \tag{5.24}$$

$$\hat{H}_{\text{emb}} : 2 \cdot 4^{N_{\text{imp}}} \to 2 \cdot 4^{N_{\text{imp}}}, \tag{5.25}$$

so that $\hat{H}_{\text{emb}}$ can be solved accurately by some wave function method.

By construction, the lowest eigenstate of $\hat{H}_{\text{emb}}$ is found by varying over the span of $\{|C\rangle_\gamma\}_{\gamma=1,..,2\cdot 4^{N_{\text{imp}}}}$:

$$\hat{P}^\dagger H \hat{P} |\Psi\rangle = \hat{P} H |\Psi\rangle = \hat{P} E |\Psi\rangle = E |\Psi\rangle. \tag{5.26}$$

With the help of the projection $\hat{P}$, we have thus found a way that makes it possible to solve a large interacting lattice problem efficiently.

Unfortunately though, in order to find the projection $\hat{P}$, the full wave function must be known. Thus, it is necessary to approximate the projection. One possible way to do so is to compute the projection from a non-interacting system instead.

Note that this derivation is valid generally and for all wave functions defined in Fock space $\mathcal{F}$. When treating electronic systems with this method, usually the particle number in the system is conserved by the Hamiltonian. In that case, both the wave function as well as the projection do not need to be defined on the full Fock space but only on the part of Fock space $\mathcal{F}|_M$ with the considered particle number M.

5.2 Embedding of the mean field system

As shown in the section before, in order to find the projection $\hat{P}$ for a given system, the many body wave functions needs to be known which is not in general possible. This is why, we approximate the many body wave function with a mean field description, which can be solved exactly. While for the standard DMET algorithm, this mean field description is always an approximation to the exact system, we will later discuss how this can be made exact with the use of ideas from functional theory. We then find the projection $\hat{P}^s$ corresponding to this mean field system which is defined by the Hamiltonian:

$$\hat{T} = \sum_{ij} t_{ij} \hat{c}_i^\dagger \hat{c}_j = \sum_{\alpha} \epsilon_\alpha \hat{a}_\alpha^\dagger \hat{a}_\alpha, \tag{5.27}$$

where

$$\begin{aligned} &\hat{c}_i^\dagger : \mathcal{F} \to \mathcal{F}; && (5.28)\\ &\quad |\nu_1\rangle \otimes ... \otimes |\nu_i\rangle ... \otimes |\nu_N\rangle \to \sqrt{N+1}|\nu_1\rangle \otimes ... \otimes |\nu_i + 1\rangle \otimes ... \otimes |\nu_N\rangle, \\ &\quad |\nu_i\rangle = \hat{c}_i^\dagger |0\rangle, && (5.29) \end{aligned}$$

is the particle creation and $\hat{c}_i = \left(\hat{c}_i^\dagger\right)^\dagger$ the particle annihilation operator in the local lattice-site basis and

$$\begin{aligned} &\hat{a}_\alpha^\dagger : \mathcal{F} \to \mathcal{F}; && (5.30)\\ &\quad \frac{1}{\sqrt{M!}} \sum_{\sigma \in S_\mu} \mathrm{sign}(\sigma) |\mu_{\sigma(1)}\rangle \otimes ... \otimes |\mu_{\sigma \mathrm{M}}\rangle \to \frac{1}{\sqrt{(\mathrm{M}+1)!}} \sum_{\sigma \in \mathrm{S}_\mu} \mathrm{sign}(\sigma) |\mu_{\sigma(1)}\rangle \otimes ... \otimes |\mu_{\sigma \mathrm{M}}\rangle, \\ &\quad |\mu_\alpha\rangle = \hat{a}_\alpha^\dagger |0\rangle, \end{aligned}$$

is the particle creation and $\hat{a}_\alpha = \left(\hat{a}_\alpha^\dagger\right)^\dagger$ the particle annihilation operator in the eigenbasis of the Hamiltonian $\hat{T}$. Here, S_μ are all possible permutations of μ.

The ground state of Hamiltonian $\hat{T}$ is a Slater determinant as defined in section 2.1.3 and can be written as

$$|\Phi\rangle = \hat{a}_M^\dagger ... \hat{a}_1^\dagger |0\rangle = \prod_{\mu=1}^{M} \hat{a}_\mu^\dagger |0\rangle. \tag{5.31}$$

Changing from the orbital basis to the local lattice basis is given by

$$\hat{a}_\mu^\dagger = \sum_{i=1}^{N} \varphi_i^{(\mu)} \hat{c}_i^\dagger, \tag{5.32}$$

$$|\Phi\rangle = \prod_{\mu}^{M} \hat{a}_\mu^\dagger |0\rangle = \prod_{\mu}^{M} \sum_{i=1}^{N} \varphi_i^{(\mu)} \hat{c}_i^\dagger |0\rangle. \tag{5.33}$$

The $\varphi_i^{(\mu)}$ are the overlap elements $\langle \mu | i \rangle$ between the site basis and the natural orbital basis, where

$$\mu : 1...M \tag{5.34}$$

$$i : 1...N. \tag{5.35}$$

Also, the $\varphi_i^{(\mu)}$ can be considered as a matrix of dimension $N \times M$.

5.2.1 Rewriting the exact embedding wave function

Dividing the Slater determinant of Eq. (5.33) into one part that is on the impurity and one part that is on the rest of the system, similar to the interacting case we can write:

$$|\Phi\rangle = \sum_{i=1}^{4^{N_{\mathrm{imp}}}} \sum_{j=1}^{4^{N-N_{\mathrm{imp}}}} \Phi_{ij} |A_i\rangle \otimes |B_j\rangle, \tag{5.36}$$

where

$$|A\rangle = |0\rangle_{\text{imp}} + \sum_{\nu=1}^{2N_{\text{imp}}} \prod_{\mu=1}^{\nu} \alpha_\mu \sum_{i=1}^{N_{\text{imp}}} \varphi_i^{(\mu)} \hat{c}_i^\dagger |0\rangle_{\text{imp}}, \tag{5.37}$$

$$|B\rangle = |0\rangle_{\text{env}} + \sum_{\nu=1}^{2N_{\text{imp}}} \prod_{\mu=1}^{\nu} \beta_\mu \sum_{i=N_{\text{imp}}+1}^{N} \varphi_i^{(\mu)} \hat{c}_i^\dagger |0\rangle_{\text{env}} \tag{5.38}$$

and $|0\rangle_{\text{imp}}$ and $|0\rangle_{\text{env}}$ is the vacuum of the impurity and environment subspace, respectively.

The particle number of the subsystems $|A\rangle$ and $|B\rangle$ are not known, that is, particles can go from one part to the other part. On the other hand, in a Slater determinant, the total particle number is fixed so that both subsystems need to add up to the correct particle number.

In the following, instead of doing the Schmidt decomposition as shown in the interacting case, we proceed slightly different by using that the mean field system is described by only one Slater determinant instead of by a sum of Slater determinants which would be the case in the interacting system.

5.2.2 Singular value decomposition

In contrast to the many body wave function, which can only be described by a sum of Slater determinants, our mean field wave function is fully determined by the overlap elements $\langle \mu | i \rangle = \varphi_i^\mu$ which were defined in Eq. (5.33). This is why we can simply rotate the single particle orbitals which build the Slater determinant in order to find an optimized basis. This optimized basis should be built such that it splits the system into one part only describing the impurity and one part only describing the rest of the system, as has been done in the interacting case.

Because of this, instead of performing a Schmidt decomposition on the matrix Φ_{ij}, as in the interacting case, we consider the overlap elements $\langle \mu | i \rangle = \varphi_i^\mu$ directly. They give us the norm that each orbital μ has on site i. In general, all of the elements $\langle \mu | i \rangle$ will be non-zero as all orbitals will have a certain occupation on each lattice site. These M vectors of length N can also be considered as a $N \times M$ matrix. In other words: in order to describe the wave function on the impurity region, all M orbitals need to be considered although we know that actually, only maximally $2N_{\text{imp}}$ particles can be on the impurity due to Pauli's principle.

As in the interacting case, we want to find a basis that describes the wave function on the impurity and the wave function on the environment separately. The minimal amount of basis functions needed to describe the impurity wave function is $2N_{\text{imp}}$ in the following.

We consider the sub-matrix of φ that includes the part that is defined only on the impurity sites:

$$\tilde{\varphi}_j^\nu, \text{ where j : 1..N}_{\text{imp}}; \ \nu : \text{1..M}. \tag{5.39}$$

In order to find a minimal basis set describing the impurity wave function, we rotate the matrix $\tilde{\varphi}$ (which means in other words, changing the occupied single-particle basis of the wave function) such that not all, but only a few of the orbitals still have an overlap with the impurity. In other words, we do a Singular value decomposition [33, pp. 564] of this $N_{\text{imp}} \times M$ matrix

$$\tilde{\varphi}_j^\nu = \sum_{i=1}^{N_{\text{imp}}} \sum_{\alpha=1}^{M} U_{ji} \sigma_i^\alpha V^{\alpha\nu\dagger}, \tag{5.40}$$

which re-orders all orbitals with respect to their overlap on the impurity. Here, $\mathbf{U}$ (size: $N_{\text{imp}} \times N_{\text{imp}}$) and $\mathbf{V}$ (size: $M \times M$) are both orthonormal matrices. σ_i^α is a $N_{\text{imp}} \times M$ matrix of the form

$$\sigma = \begin{pmatrix} \sigma_1 & 0 & 0 & 0 & 0 & ... & 0 \\ 0 & \sigma_2 & 0 & 0 & 0 & ... & 0 \\ 0 & 0 & \sigma_3 & 0 & 0 & ... & 0 \\ ... & ... & ... & ... & ... & ... & ... \\ 0 & ... & 0 & \sigma_{N_{\text{imp}}} & 0 & ... & 0 \end{pmatrix}. \tag{5.41}$$

The Matrix V rotates the orbitals into a new basis where only the first N_{imp} orbitals have overlap with the impurity sites.

5.2.3 Basis transformation

Again, we go from the eigenbasis of the Hamiltonian into a new basis, in which the wave function takes a more complex form. We do this by inserting the rotation matrix from before as $V_{\mu'\alpha}V_{\alpha\mu} = \mathbb{1}$

$$\begin{aligned} |\Phi\rangle &= \prod_{\mu=1}^{M} \hat{a}_\mu^\dagger |0\rangle & &= \prod_{\mu=1}^{M}\sum_{\mu'}^{M} \delta_{\mu\mu'}\hat{a}_{\mu'}^\dagger |0\rangle, \\ &= \prod_{\mu=1}^{M}\sum_{\mu'}^{M}\sum_{\alpha}^{M} V_{\mu\alpha}V_{\alpha\mu'}\hat{a}_{\mu'}^\dagger |0\rangle & &= \prod_{\mu=1}^{M}\sum_{\alpha}^{M} V_{\mu\alpha}\hat{b}_{\alpha}^\dagger |0\rangle. \end{aligned} \tag{5.42}$$

In the lattice-site representation, we can write the new creation operators as:

$$\hat{b}_\alpha^\dagger = \sum_{i=1}^{N} \xi_i^\alpha \hat{c}_i^\dagger, \tag{5.43}$$

with

$$V_{\mu\alpha}\xi_i^\alpha = \varphi_i^\mu \rightarrow \xi_i^\alpha = \varphi_i^\mu V_\mu^\alpha. \tag{5.44}$$

Only the first N_{imp} orbitals have a non vanishing contribution on the impurity sites while the rest of the elements $\xi_i^\alpha|_{i<N_{\text{imp}}}$ is zero.

Investigating the new occupied basis set more carefully, we additionally see that it can again be written as one single Slater determinant

$$\begin{aligned} |\Phi\rangle &= \prod_{\mu=1}^{M}\sum_{\alpha}^{M} V_{\mu\alpha}\hat{b}_\alpha^\dagger |0\rangle, \\ &= \det(\mathrm{V}) \prod_{\alpha=1}^{\mathrm{M}} \hat{\mathrm{b}}_\alpha^\dagger |0\rangle. \end{aligned} \tag{5.45}$$

We can see this by considering the definition of a Determinant [33, p.299]

$$\det(V) = \sum_{\sigma\in S_\mu} \mathrm{sign}(\sigma) \prod_{\mu=1}^{\mathrm{M}} \mathrm{V}_{\mu\sigma(\mu)}, \tag{5.46}$$

$$= \sum_{\sigma\in S_\mu} \left(\prod_{\mu=1}^{M} V_{\mu\sigma(\mu)}\right) \mathrm{sign}\left(\hat{\mathrm{b}}_{\sigma(1)}^\dagger ... \hat{\mathrm{b}}_{\sigma(\mathrm{M})}^\dagger\right),$$

$$= \prod_{\mu=1}^{M} V_{11}...V_{MM} \cdot \underbrace{\mathrm{sign}\left(\hat{\mathrm{b}}_1^\dagger ... \hat{\mathrm{b}}_{\mathrm{M}}^\dagger\right)}_{+1} + ..., \tag{5.47}$$

where S_μ are all possible permutations of μ and in the last line of Eq. (5.47), we have only written down one possible of all permutations. Additionally, as V is an orthonormal matrix, its determinant is one [33, p.308] so that we can write:

$$|\Phi\rangle = \prod_{\alpha=1}^{M} \hat{b}_\alpha^\dagger |0\rangle. \tag{5.48}$$

In this new occupied basis though, differently from the other basis set, per definition the last $M - N_{\text{imp}}$ orbitals do not have a contribution on the first N_{imp} lattice sites

$$|\Phi\rangle = \hat{b}_1^\dagger ... \hat{b}_{N\text{imp}}^\dagger |0\rangle_{N_{\text{imp}}} \otimes \hat{b}_{N_{\text{imp}}+1}^\dagger ... \hat{b}_M^\dagger |0\rangle_{\text{bath}}. \tag{5.49}$$

Note that here, although the operators $\hat{b}_{\mathrm{N_{imp}}+1}^\dagger ... \hat{b}_M^\dagger$ do not act on the impurity space, the $\hat{b}_1^\dagger ... \hat{b}_{\text{imp}}^\dagger$ act on the full space, $|0\rangle_{N_{\text{imp}}} \otimes |0\rangle_{\text{bath}} = |0\rangle$.

5.2.4 Splitting up between impurity and environment

Here, we re-write the wave function as a sum of wave functions where parts contain contributions only on the impurity $|A^s_\alpha\rangle$ and others only contain contributions on the rest of the system $|B^s_\alpha\rangle$. In order to do so, we split up the first N_{imp} creation operators:

$$\hat{b}^\dagger_\alpha = \hat{b}^\dagger_{N_{\text{imp}},\alpha} + \hat{b}^\dagger_{\text{env},\alpha}, \quad \alpha : 1...N_{\text{imp}}, \tag{5.50}$$

so that

$$\hat{b}^\dagger_{N_{\text{imp}},\alpha} \equiv \sum_{i=1}^{N_{\text{imp}}} \xi^\alpha_i \hat{c}^\dagger_i, \tag{5.51}$$

$$\hat{b}^\dagger_{\text{env},\alpha} \equiv \sum_{i=N_{\text{imp}}+1}^{\text{N}} \xi^\alpha_i \hat{c}^\dagger_i. \tag{5.52}$$

The remaining $M - N_{\text{imp}}$ creation operators

$$\hat{b}^\dagger_\alpha \;\; \alpha : N_{\text{imp}} + 1...\text{M} \tag{5.53}$$

do not have any contribution on the impurity lattice sites anyway.

The whole wave function can then be rewritten as:

$$\begin{aligned}
|\Phi\rangle &= \prod_{\alpha=1}^{N_{\text{imp}}} \left(\hat{b}^\dagger_{N_{\text{imp}},\alpha} + \hat{b}^\dagger_{\text{env},\alpha}\right) \otimes \prod_{\alpha=N_{\text{imp}}+1}^{M} \hat{b}^\dagger_\alpha |0\rangle, \\
&= \prod_{\alpha=1}^{N_{\text{imp}}} \hat{b}^\dagger_{N_{\text{imp}},\alpha} |0\rangle_{N_{\text{imp}}} \otimes \prod_{\alpha=1}^{N_{\text{imp}}} \hat{b}^\dagger_{\text{env},\alpha} \otimes \prod_{\alpha=N_{\text{imp}}+1}^{M} \hat{b}^\dagger_\alpha |0\rangle_{\text{env}}, \\
&= \sum_{\alpha=1}^{4^{N_{\text{imp}}}} |\tilde{A}^s_\alpha\rangle \otimes |\tilde{B}^s_\alpha\rangle = \sum_{\alpha=1}^{4^{N_{\text{imp}}}} |\tilde{A}^s_\alpha \tilde{B}^s_\alpha\rangle.
\end{aligned} \tag{5.54}$$

Note that although there is no pre-factor in the sum of equation 5.54, because we built up the wave function in terms of creation operators, Pauli's principle is still fulfilled even without an additional explicit anti-symmetrization.

5.2.5 The projection derived from the mean field system

Analogously to the interacting system, we define the projection of the mean field system as:

$$\begin{aligned}
\hat{P}'^s &= \sum_{\alpha=1}^{4^{N_{\text{imp}}}} |\tilde{A}^s_\alpha \tilde{B}^s_\alpha\rangle\langle\tilde{A}^s_\alpha \tilde{B}^s_\alpha| \\
&= \sum_{\alpha=1}^{4^{N_{\text{imp}}}} \left(|\tilde{C}^s_\alpha\rangle\langle\tilde{C}^s_\alpha| + |\tilde{C}^{s*}_\alpha\rangle\langle\tilde{C}^{s*}_\alpha|\right), \\
&= \sum_{\gamma=1}^{2\cdot 4^{N_{\text{imp}}}} |\tilde{C}^s_\gamma\rangle\langle\tilde{C}^s_\gamma|, \\
&= \sum_{\gamma=1}^{2\cdot 4^{N_{\text{imp}}}} \|\tilde{C}^s_\gamma\| |\tilde{C}^s_\gamma\rangle\langle\tilde{C}^s_\gamma|.
\end{aligned} \tag{5.55}$$

Here, we split the basis functions $|\tilde{A}^s_\alpha \tilde{B}^s_\alpha\rangle$ into those containing only contributions on the impurity $|\tilde{C}^s_\alpha\rangle$ and those containing only contributions on the environment $|\tilde{C}^{s*}_\alpha\rangle$ similar to the interacting case.

Again normalizing yields

$$\hat{P}^s = \sum_{\gamma=1}^{2\cdot 4^{N_{\text{imp}}}} |C^s_\gamma\rangle\langle C^s_\gamma|. \tag{5.56}$$

In contrast to the interacting case, we only rotated the single-particle orbitals from the basis $\hat{a}_\mu^\dagger$ to the basis $\hat{b}_\alpha^\dagger$. This means that the non-interacting projection $\hat{P}^s$ is not only $\mathbb{1}$ on the impurity, but on the whole system:

$$\hat{P}^s = \sum_{\gamma=1}^{2\cdot 4^{N_{\mathrm{imp}}}} |C_\gamma^s\rangle\langle C_\gamma^s| = \mathbb{1}, \tag{5.57}$$

so effectively, we have done nothing.

Projecting the Hamiltonian $\hat{T}$ thus just yields the same Hamiltonian again

$$\hat{P}^{s\dagger}\hat{T}\hat{P}^s = \hat{T}_{\mathrm{emb}} = \hat{T}. \tag{5.58}$$

The projection from the interacting system $\hat{P}$ and of the non-interacting system $\hat{P}^s$ are derived directly from the belonging (interacting or non-interacting) wave functions and, in general, are not the same:

$$\hat{P} \neq \hat{P}^s \tag{5.59}$$

5.2.6 Practical approximating for the projection

So far, we have not made any assumptions. While the projection $\hat{P}$ describes the full wave function accurately, the projection $\hat{P}^s$ describes the Slater determinant of the mean field system (which is itself an approximation to the full system) accurately. However we also have not gained any practical insights as the projection of the interacting system cannot be calculated in practice. We have to make approximations in order to find a projection that is directly applicable to the interacting problem.

As stated in the introduction, in the DMET method we are only interested in the physics on the impurity of the considered system. Often, the properties of the impurity region are sufficient to describe many properties of the full system (this will discussed in more detail in section 10.1.1). The properties on the impurity are nonetheless influenced by the interactions and correlations between the impurity and the rest of the system.

The property that includes all knowledge about the system on the impurity is the wave function, restricted to the impurity $|\Psi_{\mathrm{imp}}\rangle$, as defined in Eq. (5.13). As we are only interested in $|\Psi_{\mathrm{imp}}\rangle$, we will now try to find a projector that only reproduces the wave function on the impurity, while the rest of the system does not have to be reproduced.

Considering again the mean field wave function

$$|\Phi\rangle = \hat{b}_1^\dagger \otimes ... \otimes \hat{b}_{N_{\mathrm{imp}}}^\dagger \otimes \hat{b}_{N_{\mathrm{imp}}+1}^\dagger \otimes ... \otimes \hat{b}_M^\dagger |0\rangle, \tag{5.60}$$

we realize that all creation operators $\hat{b}_{N_{\mathrm{imp}}+1}^\dagger$ to $\hat{b}_M^\dagger$ do not influence the impurity in any way. A reduced wave function that exactly reproduces the impurity region can be defined as:

$$|\Phi'\rangle = \hat{b}_1^\dagger \otimes ... \otimes \hat{b}_{N_{\mathrm{imp}}}^\dagger |0\rangle, \tag{5.61}$$

$$|\Phi'_{\mathrm{imp}}\rangle = \sum_{\alpha=1}^{4^{N_{\mathrm{imp}}}} |\tilde{A}_\alpha^s\rangle, \tag{5.62}$$

$$\langle\Phi'_{\mathrm{imp}}|\Phi_{\mathrm{imp}}\rangle = 1. \tag{5.63}$$

Note that this is not possible for the interacting wave function which can be written as a sum of Slater determinants only:

$$|\Psi\rangle = \sum_{n=1}^{\aleph} c_n |\Phi_n\rangle, \tag{5.64}$$

where

$$\aleph = \frac{N!}{(\frac{1}{2}N + M)!(\frac{1}{2}N - M)!} \tag{5.65}$$

is the binomial coefficient for spin systems [17].

Because an interacting wave function cannot be written in terms of one single Slater determinant but only as a sum of many Slater determinants, irrespective on how we rotate the creation operators of the wave function, all $\hat{b}^\dagger_\alpha$ will have contributions on the impurity.

Going back to the mean field wave function, we can split up the wave function into one part that is only defined on the impurity sites N_{imp} and one part that is only defined on the environment N_{env}:

$$\begin{aligned}|\Phi'\rangle &= \hat{b}^\dagger_1 \otimes ... \otimes \hat{b}^\dagger_{N_{\text{imp}}}|0\rangle, \\ &= \left(\hat{b}^\dagger_{N_{\text{imp}},1} + \hat{b}^\dagger_{\text{env},1}\right) \otimes ... \otimes \left(\hat{b}^\dagger_{N_{\text{imp}},N_{\text{imp}}} \hat{b}^\dagger_{N_{\text{env}},N_{\text{imp}}}\right)|0\rangle, \\ &= \sum_{\alpha=1}^{4^{N_{\text{imp}}}} |\tilde{A}^s_\alpha\rangle \otimes |\tilde{B}^{s'}_\alpha\rangle, \end{aligned} \tag{5.66}$$

similar to before (Eq. (5.54)). With this new, reduced mean field wave function we define the projection similar as before (Eqns. (5.55) to (5.56)) as

$$\hat{P}^s_{\text{red}} \equiv \sum_{\gamma=1}^{2\cdot 4^{N_{\text{imp}}}} |C^{s'}_\gamma\rangle\langle C^{s'}_\gamma|. \tag{5.67}$$

Applying the projection $\hat{P}^s_{\text{red}}$ to the full mean field wave function now does not yield the same wave function but the reduced wave function that is though the same as the exact one on the impurity:

$$\hat{P}^s_{\text{red}}|\Phi\rangle = |\tilde{\Phi}\rangle, \tag{5.68}$$

$$\langle N_{\text{imp}}|\Phi\rangle = \langle N_{\text{imp}}|\tilde{\Phi}\rangle. \tag{5.69}$$

Projecting the Hamiltonian $\hat{T}$ yields:

$$\hat{P}^{s\dagger}_{\text{red}}\hat{T}\hat{P}^s_{\text{red}} = \hat{T}_{\text{emb}} = \hat{T}_{N_{\text{imp}}} + \hat{T}_{N_{\text{imp}}-env} + \hat{T}_{N_{\text{env}}}. \tag{5.70}$$

Again, the, embedded Hamiltonian is the same on the impurity as the original Hamiltonian, $\hat{T}_{N_{\text{imp}}} = \hat{T}|_{N_{\text{imp}}}$.

When diagonalizing the embedded Hamiltonian we see that the lowest eigenstate $|\tilde{\Phi}\rangle$ of the Hamiltonian has to be in the span of the projection, $\left\{|C\rangle^{s'}_\gamma\right\}_{\gamma=1,..,2\cdot 4^{N_{\text{imp}}}}$. But from this, we cannot follow that $|\tilde{\Phi}\rangle$ is in the span of the approximated wave function $|\Phi'\rangle$ which we used to build the projection. Differently stated, we can diagonalize the embedding Hamiltonian and find its lowest eigenstate

$$\hat{H}_{\text{emb}}|\tilde{\Phi}\rangle = E|\tilde{\Phi}\rangle, \tag{5.71}$$

but is is not clear that this eigenstate is the same as the original wave function $|\Phi'\rangle$ used to find the embedding Hamiltonian. In order for the projection to be useful, the two wave functions must be the same.

In order to relate the two wave functions $|\Phi'\rangle$ and $|\tilde{\Phi}\rangle$, we consider more carefully what the projection applied to the mean field Hamiltonian looks like:

$$\hat{T} = \sum_{ij}^{N} \hat{t}_{ij}\hat{c}^\dagger_i\hat{c}_j, \tag{5.72}$$

$$\hat{T}_{\text{emb}} = \hat{P}^{s\dagger}_{\text{red}}\hat{T}\hat{P}^s_{\text{red}} = \sum_{a,b}^{2N_{\text{imp}}} \hat{t}_{ab}\hat{b}^\dagger_a\hat{b}_b. \tag{5.73}$$

Note that $\hat{t}_{ab}$ is of a completely different form and dimension as the original Hamiltonian $\hat{t}_{ij}$. We observe that, as the mean field Hamiltonian is just a sum of single-particle Hamiltonians, so can the projection $\hat{P}^s_{\text{red}}$ be understood as a sum of single-particle projections:

$$\hat{t} \to \hat{p}^{\dagger s}_{\text{red}}\hat{t}\hat{p}^s_{red} = \hat{t}_{\text{emb}}. \tag{5.74}$$

In the following, we will consider the much simpler single-particle problem to show that the lowest eigenstate of the embedded Hamiltonian is related to the wave function the projection was built from.

5.2.7 The projection operator in the single-particle picture

The solution of the single-particle Hamiltonian $\hat{t}$ is given as:

$$\sum_{j=1}^{N} \hat{t}_{ij}\varphi_j^\mu = \epsilon^\mu \varphi_i^\mu, \tag{5.75}$$

where the φ_i^μ are the single-particle orbitals and the ϵ^μ the corresponding single-particle energies. The elements φ_i^μ are exactly the same as the overlap elements of Eq. (5.32) in section 5.2. They consist of N vectors of length M, if N is the total number of lattice sites and M the total particle number in the system, but we can also consider all elements together as a matrix:

$$\underline{\underline{\varphi}} = \begin{pmatrix} \varphi_1^1 & \dots & \varphi_1^M \\ \dots & \dots & \dots \\ \varphi_N^1 & \dots & \varphi_N^M \end{pmatrix}. \tag{5.76}$$

Similar to the approach before, we rotate the matrix so that only the first N_{imp} orbitals have a contribution on the first N_{imp} lattice sites:

$$\underline{\underline{\varphi}} \xrightarrow{\text{rotate}} \underline{\underline{\xi}} = \begin{pmatrix} \xi_1^1 & \dots & \xi_1^{N_{\text{imp}}} & 0 & \dots & 0 \\ \dots & \dots & \dots & \dots & \dots & \dots \\ \dots & \dots & \dots & \xi_{N_{N_{\text{imp}}+1}}^{N_{\text{imp}}+1} & \dots & \xi_{N_{N_{\text{imp}}+1}}^{M} \\ \xi_N^1 & \dots & \xi_N^{N_{\text{imp}}} & \xi_N^{N_{\text{imp}}+1} & \dots & \xi_N^M \end{pmatrix}. \tag{5.77}$$

In order to get the approximate projection, we neglect all elements without overlap on the impurity, $\xi_i^\alpha \geq \xi_i^{N_{\text{imp}}+1}$, yielding the matrix:

$$\underline{\underline{\xi'}} = \begin{pmatrix} \xi_1^1 & \dots & \xi_1^{N_{\text{imp}}} \\ \dots & \dots & \dots \\ \dots & \dots & \dots \\ \xi_N^1 & \dots & \xi_N^{N_{\text{imp}}} \end{pmatrix}. \tag{5.78}$$

We split up the orbitals $|\xi^\alpha\rangle$ into one set containing the impurity lattice sites, $|\xi_{N_{\text{imp}}}^\alpha\rangle$ and one set containing the environment lattice sites $|\xi_{N_{\text{env}}}^\alpha\rangle$, so that

$$|\xi^\alpha\rangle = |\xi_{N_{\text{imp}}}^\alpha\rangle + |\xi_{N_{\text{env}}}^\alpha\rangle. \tag{5.79}$$

Additionally, we renormalize both basis sets,

$$|\tilde{\xi}_{N_{\text{imp}}}^\alpha\rangle = \frac{1}{\|\xi_{N_{\text{imp}}}^\alpha\|}|\xi_{N_{\text{imp}}}^\alpha\rangle, \tag{5.80}$$

$$|\tilde{\xi}_{N_{\text{env}}}^\alpha\rangle = \frac{1}{1-\|\xi_{N_{\text{imp}}}^\alpha\|}|\xi_{N_{\text{env}}}^\alpha\rangle, \tag{5.81}$$

so that both sets individually are orthonormalized:

$$\langle\tilde{\xi}_{N_{\text{imp}}}^\alpha|\tilde{\xi}_{N_{\text{env}}}^\beta\rangle = 0, \tag{5.82}$$

$$\langle\tilde{\xi}_{N_{\text{imp}}}^\alpha|\tilde{\xi}_{\text{en}}^{N_{\text{imp}}}\rangle = \langle\tilde{\xi}_{N_{\text{env}}}^\alpha|\tilde{\xi}_{N_{\text{env}}}^\beta\rangle = \delta_{\alpha\beta} \;\; \forall\alpha,\beta, \;\; \forall\alpha,\beta. \tag{5.83}$$

We now have a set of N_{imp} orbitals $|\tilde{\xi}_{N_{\text{imp}}}^\alpha\rangle$ that are defined on all N lattice sites but that are always zero for lattice sites $i \geq N_{\text{imp}}+1$ and a set of N_{imp} orbitals $|\tilde{\xi}_{N_{\text{env}}}^\alpha\rangle$ that are defined on all N lattice sites but that are always zero for lattice sites $i \leq N_{\text{imp}}$. We can put them together such that

$$|\tilde{\xi}^\alpha\rangle = |\tilde{\xi}_{N_{\text{imp}}}^\alpha\rangle \;\text{ for }\; \alpha = 1,...\text{N}_{\text{imp}}, \tag{5.84}$$

$$|\tilde{\xi}^\alpha\rangle = |\tilde{\xi}_{N_{\text{env}}}^\alpha\rangle \;\text{ for }\; \alpha = \text{N}_{\text{imp}}+1,...2\text{N}_{\text{imp}}, \tag{5.85}$$

We build the projection from the $|\tilde{\xi}^\alpha\rangle$:

$$\hat{p} = \sum_{\alpha=1}^{2N_{\text{imp}}} |\tilde{\xi}^\alpha\rangle\langle\tilde{\xi}^\alpha|. \tag{5.86}$$

5.2.8 Projection of the single-particle Hamiltonian

Projecting the single-particle Hamiltonian $\hat{t}$ yields:

$$\begin{aligned}
\hat{t}_{\mathrm{emb}} =& \hat{p}^\dagger \hat{t} \hat{p} \\
=& \sum_{\alpha,\beta=1}^{2N_{\mathrm{imp}}} |\tilde{\xi}^\alpha\rangle\langle\tilde{\xi}^\alpha|\hat{t}|\tilde{\xi}^\beta\rangle\langle\tilde{\xi}^\beta| \\
=& \sum_{\alpha,\beta=1}^{N_{\mathrm{imp}}} |\tilde{\xi}^\alpha_{N_{\mathrm{imp}}}\rangle\langle\tilde{\xi}^\alpha_{N_{\mathrm{imp}}}|\hat{t}|\tilde{\xi}^\beta_{N_{\mathrm{imp}}}\rangle\langle\tilde{\xi}^\beta_{N_{\mathrm{imp}}}| \\
&+ \sum_{\alpha=1}^{N_{\mathrm{imp}}} \sum_{\beta=N_{\mathrm{imp}}+1}^{2N_{\mathrm{imp}}} |\tilde{\xi}^\alpha_{N_{\mathrm{imp}}}\rangle\langle\tilde{\xi}^\alpha_{N_{\mathrm{imp}}}|\hat{t}|\tilde{\xi}^\beta_{N_{\mathrm{env}}}\rangle\langle\tilde{\xi}^\beta_{N_{\mathrm{env}}}| + h.c. \\
&+ \sum_{\alpha,\beta=N_{\mathrm{imp}}+1}^{2N_{\mathrm{imp}}} |\tilde{\xi}^\alpha_{N_{\mathrm{env}}}\rangle\langle\tilde{\xi}^\alpha_{N_{\mathrm{env}}}|\hat{t}|\tilde{\xi}^\beta_{N_{\mathrm{env}}}\rangle\langle\tilde{\xi}^\beta_{N_{\mathrm{env}}}|.
\end{aligned} \tag{5.87}$$

We can now consider all terms of Eq. (5.87) separately. The embedding Hamiltonian on the impurity can be re-written as:

$$\begin{aligned}
\hat{t}^{N_{\mathrm{imp}}}_{\mathrm{emb}} &= \sum_{\alpha,\beta=1}^{N_{\mathrm{imp}}} |\tilde{\xi}^\alpha_{N_{\mathrm{imp}}}\rangle\langle\tilde{\xi}^\alpha_{N_{\mathrm{imp}}}|\hat{t}|\tilde{\xi}^\beta_{N_{\mathrm{imp}}}\rangle\langle\tilde{\xi}^\beta_{N_{\mathrm{imp}}}| \\
&= \sum_{\alpha,\beta=1}^{N_{\mathrm{imp}}} \sum_{i,i',j,j'=1}^{N_{\mathrm{imp}}} |i'\rangle\langle i'|\tilde{\xi}^\alpha_{N_{\mathrm{imp}}}\rangle\langle\tilde{\xi}^\alpha_{N_{\mathrm{imp}}}|i\rangle\langle i|\hat{t}|j\rangle\langle j|\tilde{\xi}^\beta_{N_{\mathrm{imp}}}\rangle\langle\tilde{\xi}^\beta_{N_{\mathrm{imp}}}|j'\rangle\langle j'| \\
&= \sum_{i,j=1}^{N_{\mathrm{imp}}} |i\rangle\hat{t}_{ij}\langle j|,
\end{aligned} \tag{5.88}$$

where we inserted unitary matrices $\sum_{i=1}^{N_{\mathrm{imp}}} |i\rangle\langle i|$ and used that both the lattice-site basis vectors $|i\rangle$ as well as the new basis vectors $|\xi^\alpha_{N_{\mathrm{imp}}}\rangle$ form a full, orthonormalized basis set of the impurity region, so that

$$\sum_{\alpha=1}^{N_{\mathrm{imp}}} \langle i|\xi^\alpha_{N_{\mathrm{imp}}}\rangle\langle\xi^\alpha_{N_{\mathrm{imp}}}|j\rangle = \delta_{ij} \tag{5.89}$$

holds. Considering the mixing terms between impurity and environment: we can apply this trick only once:

$$\begin{aligned}
\hat{t}^{N_{\mathrm{imp}}-env}_{\mathrm{emb}} &= \sum_{\alpha=1}^{N_{\mathrm{imp}}} \sum_{\beta=N_{\mathrm{imp}}+1}^{2N_{\mathrm{imp}}} |\tilde{\xi}^\alpha_{N_{\mathrm{imp}}}\rangle\langle\tilde{\xi}^\alpha_{N_{\mathrm{imp}}}|\hat{t}|\tilde{\xi}^\beta_{N_{\mathrm{env}}}\rangle\langle\tilde{\xi}^\beta_{N_{\mathrm{env}}}| + h.c. \\
&= \sum_{\alpha=1}^{N_{\mathrm{imp}}} \sum_{i,i'=1}^{N_{\mathrm{imp}}} \sum_{\beta=N_{\mathrm{imp}}+1}^{2N_{\mathrm{imp}}} |i'\rangle\langle i'|\tilde{\xi}^\alpha_{N_{\mathrm{imp}}}\rangle\langle\tilde{\xi}^\alpha_{N_{\mathrm{imp}}}|i\rangle\langle i|\hat{t}|\tilde{\xi}^\beta_{N_{\mathrm{env}}}\rangle\langle\tilde{\xi}^\beta_{N_{\mathrm{env}}}| + h.c. \\
&= \sum_{i=1}^{N_{\mathrm{imp}}} \sum_{\beta=N_{\mathrm{imp}}+1}^{2N_{\mathrm{imp}}} |i\rangle\hat{t}_{i\beta}\langle\tilde{\xi}^\beta_{N_{\mathrm{env}}}| + h.c.
\end{aligned} \tag{5.90}$$

The embedding Hamiltonian then reads

$$\hat{t}_{\mathrm{emb}} = \begin{pmatrix} \hat{t}_{ij} & \hat{t}_{i\mathfrak{b}} \\ \hat{t}_{\mathfrak{a}j} & \hat{t}_{\mathfrak{a}\mathfrak{b}} \end{pmatrix}. \tag{5.91}$$

5.2.9 The connection between the effective single particle embedding and the original Hamiltonian

In the following, we want to show the connection between the wave functions $\tilde{\xi}^i$ that we used to define the projection $\hat{p}$ with and the eigenfunctions of the projected Hamiltonian $\hat{t}_{\mathrm{emb}}$.

The single-particle Hamiltonian $\hat{t}$ acts on the Hilbert space that spans all single-particle orbitals:

$$\mathcal{H} = \mathrm{span}\{\varphi_1 ... \varphi_{\mathrm{M}} ... \varphi_{\mathrm{N}}\}. \tag{5.92}$$

Restricted to a specific particle number $M \leq N$, we only have to consider a subset of this Hilbert space,

$$\begin{aligned}
\mathcal{H}^M &= \mathrm{span}\{\varphi_1 ... \varphi_{\mathrm{M}/2}\} = \mathrm{span}\{\xi_1 ... \xi_{\mathrm{M}/2}\} \\
&\equiv \begin{pmatrix}
\xi_1^1 & ... & \xi_1^{N_{\mathrm{imp}}} & 0 & ... & 0 \\
... & ... & ... & ... & ... & ... \\
\xi_{N_{\mathrm{imp}}}^1 & ... & \xi_{N_{\mathrm{imp}}}^{N_{\mathrm{imp}}} & 0 & ... & 0 \\
\xi_{N_{\mathrm{imp}}+1}^1 & ... & \xi_{N_{\mathrm{imp}}+1}^{N_{\mathrm{imp}}} & \xi_{N_{\mathrm{imp}}+1}^{N_{\mathrm{imp}}+1} & ... & \xi_{N_{\mathrm{imp}}+1}^M \\
... & ... & ... & ... & ... & ... \\
\xi_{\mathrm{N}}^1 & ... & \xi_N^{N_{\mathrm{imp}}} & \xi_N^{N_{\mathrm{imp}}+1} & ... & \xi_N^M
\end{pmatrix}
\end{aligned} \tag{5.93}$$

$$\mathcal{H}^M \subset \mathcal{H}. \tag{5.94}$$

The orbitals belonging to higher particle numbers than M are orthogonal to the ξ^i orbitals describing the first $N_{N_{\mathrm{imp}}}$ orbitals,

$$\varphi_k \perp \xi_i, \;\; k \in M+1, ...N, i \in 1, ..., M. \tag{5.95}$$

As the ξ^i are orthogonal to each other,

$$\left(\xi^i\right)^T \xi^{N_{\mathrm{imp}}+1} = 0, \;\; i, : 1, ...N_{\mathrm{imp}}, \tag{5.96}$$

also the split up and renormalized orbitals $\tilde{\xi}^i$ are orthogonal to all ξ^k, for $k > N_{\mathrm{imp}}$

$$\tilde{\xi}^i \perp \xi^k, \;\; i = 1, ..., 2N_{\mathrm{imp}} \tag{5.97}$$

which means that also their spans are orthogonal to each other:

$$\mathrm{span}\left\{\tilde{\xi}^{\mathrm{i}}\right\}_{\mathrm{i}\in 1,..,2\mathrm{N_{imp}}} \perp \mathrm{span}\left\{\xi^{\mathrm{k}}\right\}_{\mathrm{k}\in(\mathrm{N_{imp}}+1,...,\mathrm{M})}. \tag{5.98}$$

On the other hand, the span containing the renormalized orbitals $\tilde{\xi}^i$ and the $\xi^{N_{\mathrm{imp}}+1}$ contains the span of the original single-particle orbitals on the impurity

$$\mathrm{span}\left\{\tilde{\xi}^1, ..., \tilde{\xi}^{2\mathrm{N_{imp}}}\right\} \supset \mathrm{span}\left\{\xi^1, .., \xi^{\mathrm{N_{imp}}}\right\}. \tag{5.99}$$

From the above two statements, we can conclude that the span of the renormalized orbitals can be decomposed into

$$\mathrm{span}\left\{\tilde{\xi}^1, ..., \tilde{\xi}^{2\mathrm{N_{imp}}}\right\} = \mathrm{span}\left\{\xi^1, ..., \xi^{\mathrm{N_{imp}}}\right\} \cup \left\{\lambda^{\mathrm{k}} \perp \varphi^1, .., \varphi^{\mathrm{M}}\right\} \tag{5.100}$$

where $\lambda^k = \sum_{i=M+1}^{N} c^i \varphi^i$ and $\mathrm{span}\left\{\xi^1, ..., \xi^{\mathrm{N_{imp}}}\right\} \subset \mathrm{span}\left\{\varphi^1, .., \varphi^{\mathrm{M}}\right\}$.

Now we consider the Hilbert spaces of the minimization problem of the projected Hamiltonian. The wave function of the original one-body problem is defined on the full Hilbert space, $\mathcal{H}$. We can rewrite

$$\min_{\chi\in\mathcal{H}} \langle\chi|\hat{p}^\dagger \hat{t} \hat{p}|\chi\rangle = \min_{\chi\in\mathcal{H}} \langle\hat{p}\chi|\hat{t}|\hat{p}\chi\rangle = \min_{\chi\in\mathrm{span}\left\{\tilde{\xi}^{\mathrm{i}}_{1..2\mathrm{N_{imp}}}\right\}} \langle\chi|\hat{t}|\chi\rangle = \tilde{\epsilon}_1. \tag{5.101}$$

The $\tilde{\epsilon}_1$ is the solution to the minimization problem

$$\tilde{\epsilon}^1 \tilde{\varphi}_a^1 = \sum_{b=1}^{2N_{\mathrm{imp}}} \hat{t}_{ab}^{\mathrm{emb}} \tilde{\varphi}_b^1, \tag{5.102}$$

$$\begin{aligned}
\tilde{\varphi}^1 &= \sum_{k=1}^{2N_{\mathrm{imp}}} c_k \tilde{\xi}^k, \;\; \sum_{k=1}^{2N_{\mathrm{imp}}} |c_k|^2 = 1 \\
&= \sum_{k=1}^{2N_{\mathrm{imp}}} c'_k \xi^k
\end{aligned} \tag{5.103}$$

Since the lowest energies are reached for those $\tilde{\varphi}^i$ that are constructed of only contributions contained in

$$\text{span}\left\{\varphi^1, ...\varphi^{\text{M}}\right\} \supset \text{span}\left\{\xi^1, ..\xi^{\text{N}_{\text{imp}}}\right\}, \tag{5.104}$$

we can conclude that for the lowest N_{imp} eigenstates $\tilde{\varphi}^i$,

$$\text{span}\left\{\tilde{\varphi}^1, ..., \tilde{\varphi}^{\text{N}_{\text{imp}}}\right\} = \text{span}\left\{\xi^1, ..., \xi^{\text{N}_{\text{imp}}}\right\}. \tag{5.105}$$

We can further conclude that although the single-particle wave functions used to create the projection with and the solutions of the eigenvalue problem of the projected Hamiltonian are not the same, their spans are the same and so are the 1RDMs on the impurity belonging to those single-particle wave functions:

$$\sum_{k=1}^{N_{\text{imp}}} \tilde{\varphi}_i^k \tilde{\varphi}_j^k = \sum_{k=1}^{N_{\text{imp}}} \xi_i^k \xi_j^k = \sum_{k=1}^{M} \varphi_i^k \varphi_j^k, \quad ij : 1, ..., N_{\text{imp}} \tag{5.106}$$

5.2.10 The connection between many body embedding and the original Hamiltonian

The Slater determinants that can be built from the two spans

$$\text{span}\left\{\xi^1, ..., \xi^{\text{N}_{\text{imp}}}\right\}, \tag{5.107}$$

$$\text{span}\left\{\tilde{\varphi}^1, ..., \tilde{\varphi}^{\text{N}_{\text{imp}}}\right\} \tag{5.108}$$

are

$$|\tilde{\Phi}\rangle = \tilde{b}_1^\dagger ... \tilde{b}_{N_{\text{imp}}}^\dagger |0\rangle \equiv \det\left\{\tilde{\varphi}^1, ..., \tilde{\varphi}^{N_{\text{imp}}}\right\} \tag{5.109}$$

$$|\Phi'\rangle = b_1^\dagger ... b_{N_{\text{imp}}}^\dagger |0\rangle \equiv \det\left\{\xi^1, ..., \xi^{N_{\text{imp}}}\right\}. \tag{5.110}$$

We now want to show that, if the spans from which the Slater determinants are built, also the Slater determinants must be the same,

$$\text{span}\left\{\xi^1, ..., \xi^{\text{N}_{\text{imp}}}\right\} = \text{span}\left\{\tilde{\varphi}^1, ..., \tilde{\varphi}^{\text{N}_{\text{imp}}}\right\} \overset{?}{\rightarrow} |\tilde{\Phi}\rangle = |\Phi'\rangle. \tag{5.111}$$

This can be realized in two different ways:

One way is to again consider the procedure that lead us to the reduced projection $\hat{P}^s_{\text{red}}$: we showed the occupied single-particle orbital basis of which the Slater determinant is built up can be rotated in arbitrarily and still yield a Slater determinant:

$$|\Phi\rangle = \det\left\{\varphi^1, ...\varphi^{\text{M}}\right\} \overset{\text{rotate}}{\rightarrow} \det\left\{\xi^1, ...\xi^{\text{M}}\right\} = |\Phi\rangle \tag{5.112}$$

where we can use the same argument as in Eqns. (5.46) to (5.47).

Another way of realizing that two Slater determinants which are defined on the same span of single-particle orbitals must be the same follows the proof in [58], which states that a Slater determinant is uniquely determined by its 1RDM. As the 1RDM is uniquely defined by the span of single particle orbitals, also the Slater determinant must be uniquely defined by its span.

5.3 Applying the reduced projection operator to the full Hamiltonian

We have found a projection $\hat{P}^s_{\text{red}}$ and proved that for a mean field system, the projection of the Hamiltonian $\hat{T}$ does not change the wave function $|\Phi_{\text{imp}}\rangle$ on the impurity region.

In a next step, we assume that this projection can be used to project the full interacting Hamiltonian

$$\hat{H} = \hat{T} + \hat{U}, \tag{5.113}$$

where $\hat{T}$ is the one-body hopping term from before and $\hat{U}$ is the two-body interaction term $\hat{U} \propto \hat{c}^\dagger_{i\sigma}\hat{c}^\dagger_{j\sigma}\hat{c}_{i\sigma}\hat{c}_{j\sigma}$. We project the two parts of the Hamiltonian separately, where $\hat{T}$ will be projected

$$\hat{T}_{\text{emb}} = \hat{P}^{s\dagger}_{\text{red}}\hat{T}\hat{P}^{s}_{\text{red}}. \tag{5.114}$$

The interaction part of the Hamiltonian is projected analoguosly by rotating each operator in the Hamiltonian once;

$$\sum_i \hat{P}^{s\dagger}_{\text{red},\alpha\text{i}}\hat{c}^\dagger_{i\sigma} = \hat{b}^\dagger_{\alpha\sigma,\text{emb}} \tag{5.115}$$

$$\sum_i \hat{c}_{i\sigma}\hat{P}^{s}_{\text{red,i}\alpha} = \hat{b}_{\alpha\sigma,\text{emb}} \tag{5.116}$$

$$\rightarrow \hat{U}_{\text{emb}} = \hat{P}^{s\dagger}_{\text{red}}\hat{P}^{s\dagger}_{\text{red}}\hat{U}\hat{P}^{s}_{\text{red}}\hat{P}^{s}_{\text{red}}. \tag{5.117}$$

In the non-interacting case, the Hamiltonian is projected onto the *active space* of the impurity, defined such that it fully defines the wave function on the impurity region, but not the wave function in the rest of the system. In other words, in the mean field system, although we do not consider all orbitals, we do consider all orbitals with an overlap over the impurity.

When applying the same projection to the interacting system, we thereby assume that the same orbitals as in the non-interacting case determine the wave function on the impurity. This is not correct and it depends on the interaction strength whether this is a good or a bad approximation. For large interaction strengths, we do not expect the approximation to be good. This is why we have to improve the initial guess of the projection, that is, we have to choose the set of single-particle orbitals that determine the basis of the wave function on the impurity more carefully. This can be done by the following procedure, which is also schematically presented in figure 7.1

5.4 Improving the projection through a self consistent scheme

In order to improve the projection, we want to optimize the set of orbitals chosen to describe the wave function on the impurity. Differently stated, we want a mean field system whose one-body properties look as similar to the one-body properties of the interacting system as possible, which means that their 1RDMs should be as similar as possible.

In order to achieve this goal, we self-consistently add a non-local potential $\hat{W}$ to the mean field system which we use to get the projection from:

$$\hat{T}' = \hat{T} + \hat{W} = -t\sum_{i\sigma}\hat{c}^\dagger_{i\sigma}\hat{c}_{i+1\sigma} + \sum_{i,j\sigma} w_{ij}\hat{c}^\dagger_{i\sigma}\hat{c}_{j\sigma} \tag{5.118}$$

The non-local potential is optimized such that the difference between 1RDMs of the (projected) interacting system and the (projected) non-interacting system is minimized:

$$\min\left|\sum_{i,j\in\text{emb}}\left\langle\Psi_{\text{emb}}|c^\dagger_i c_j|\Psi_{\text{emb}}\right\rangle - \left\langle\Phi_{\text{emb}}|c^\dagger_i c_j|\Phi_{\text{emb}}\right\rangle\right|, \tag{5.119}$$

where

$$|\Psi_{\text{emb}}\rangle = \hat{P}^{s\dagger}_{\text{red}}|\Psi\rangle, \tag{5.120}$$

$$|\Phi_{\text{emb}}\rangle = \hat{P}^{s\dagger}_{\text{red}}|\Phi\rangle, \tag{5.121}$$

are the projected interacting and mean field wave functions.

Practically, we choose the non-local potential to be zero in the first guess. Then the projection is gained from $\hat{T}'$ and the embedding Hamiltonian is calculated. This small Hamiltonian can be diagonalized accurately; we calculate its 1RDM. Equivalently, we also project $\hat{T}'$ to the new basis and calculate the 1RDM likewise.

The difference between the two 1RDMs (as written in Eq. (5.119)) is then minimized with a simple Downhill-Simplex method [46], that is known to be robust, leading to a guess for the non-local potential and a new projection Hamiltonian $\hat{T}'$. A new projection is gained, leading to a different Hamiltonian and the procedure is repeated until the projection Hamiltonian yields a 1RDM that is as close as possible to the 1RDM of the interacting system.

5.5 Observables

After the converged DMET calculation, we have obtained two different wave functions:

- The interacting wave function of the embedded system, that is, a wave function that is in a basis which we know how to interpret on the impurity but not on the environment.
- The non-interacting wave function of the whole system that is obtained from a Hamiltonian with a non-local potential. Here, the non-local potential of this mean field system is optimized to reproduce as well as possible the one-body properties of the interacting system.

With these two ingredients, a variety of physical observables such as the density, the double occupancy or the energy of the system can be obtained.

5.5.1 Local properties

Local observables or properties that are non-local, but restricted to the impurity, can be calculated straightforwardly by simply taking the expectation value with the interacting wave function of the embedded system.

The strictly local observables which we will calculate within this thesis are the density $\langle \hat{n}_i \rangle = \langle \hat{c}_i^\dagger \hat{c}_i \rangle$, the double occupancy $\langle \hat{n}_{i\uparrow} \hat{n}_{i\downarrow} \rangle$ and the kinetic energy density $\langle K_i \rangle = 2t_{i,i+1} \langle \hat{c}_i^\dagger \hat{c}_{i+1} \rangle$

The non-local property that is restricted to the impurity we will compute is the density deviation between neighbouring sites $\langle \hat{n}_i \rangle - \langle \hat{n}_{i+1} \rangle$.

5.5.2 Global ground state properties

Generally, in order to calculate any global observable $\left\langle \hat{O} \right\rangle$, the full wave function $|\Psi\rangle$ of the system needs to be known,

$$O = \langle \Psi | \hat{O} | \Psi \rangle. \tag{5.122}$$

As in the DMET algorithm we do not compute the full wave function, but only the wave function on impurity subsystems, we approximate the global observable by calculating the wanted property on each impurity individually and then summing up over all impurities

$$O \approx \sum_{N_{\text{imp}} \in \mathrm{N}} O_{N_{\text{imp}}}. \tag{5.123}$$

In a translational invariant system we can additionally use that the observable will have the same value on each subsystem so we compute the observable once on the impurity and then multiply with the total amount of fragments in the system.

The global observable in the subsystem is calculated by taking the partial trace over the impurity of the embedded system,

$$O = \mathrm{Tr}_{\mathrm{N_{imp}}} \left(\hat{\rho}_{\text{emb}} \hat{\mathrm{H}}_{\text{emb}} \right), \tag{5.124}$$

where $\hat{\rho}_{\text{emb}}$ is the density matrix of the embedded system that can be computed from the wave function. In this thesis, we will compute the energy per site with this method.

Because in DMET, we do not have an expression for the full wave function of the system, some observables cannot be computed. In fact, all properties that measure long range correlation such as the static structure factor or correlation functions are out of reach.

5.6 Summary

In this chapter, we derived the mathematical foundations of Density Matrix Embedding Theory. While the theory itself was invented by Chan and collaborators, in their papers, the derivation of the

algorithms is implicit and very brief. Here, we explicitly showed each step that leads to the DMET algorithm in its most general form which cannot, up to this point, be found in literature.

Before giving a practical guide on how to implement the DMET algorithm, we will now make an attempt to make the abstract steps clearer. We do this by showing different ways to understand the concepts of DMET (in terms of wave functions or in terms of 1RDMS), for a specific and simple example. This makes it possible to understand the complexity of the DMET procedure from different perspectives.

Chapter 6

Examplification of the DMET procedure

In order to understand each of the sometimes abstract steps of the derivation in the previous chapter, we now consider an example system of three spinless particles on five sites. With the help of this example, we frame and quantify the approximations performed in the previous chapter. This way, we hope to shed light on the different subtleties of the DMET algorithm from this, be able to critically review this method. We indicate the analogies to reference [70] for each step.

6.1 Fock space wave function in the mean field approximation

We start by considering our example mean field system, from which we want to obtain the approximate wave function, as was explained in general in section 5.2. The mean field system consists of 3 spinless particles on 5 lattice sites, its Hamiltonian $\hat{T}$ has the same form as defined in Eq. (2.25)

$$\hat{T} = \sum_{ij}^{5} \hat{t}_{ij} \hat{c}_i^\dagger \hat{c}_j, \tag{6.1}$$

where the single particle Hamiltonian $\hat{t}$ is defined as

$$\hat{t} = \begin{pmatrix} 0 & -1 & 0 & 0 & 0 \\ -1 & 0 & -1 & 0 & 0 \\ 0 & -1 & 0 & -1 & 0 \\ 0 & 0 & -1 & 0 & -1 \\ 0 & 0 & 0 & -1 & 0 \end{pmatrix} \tag{6.2}$$

The ground state wave function of $\hat{T}$ is a Slater determinant that can be written as [70, Eq. 3]:

$$|\Phi\rangle = \prod_{\mu=1}^{3} \hat{a}_\mu^\dagger |0\rangle = \hat{a}_1^\dagger \hat{a}_2^\dagger \hat{a}_3^\dagger |\mathrm{vac}\rangle_5. \tag{6.3}$$

Here, by $|\mathrm{vac}\rangle_\mathrm{N}$ we denote the vacuum state on any N lattice sites,

$$|\mathrm{vac}\rangle_\mathrm{N} = \underbrace{|0\rangle \otimes ... \otimes |0\rangle}_{\text{times N}}. \tag{6.4}$$

Equivalently, we can also write $|\Phi\rangle$ in a local lattice basis, where it takes the form

$$|\Phi\rangle = \prod_{\mu=1}^{3} \sum_{i=1}^{5} \varphi_i^{(\mu)} \hat{c}_i^\dagger |\mathrm{vac}\rangle_5 = \prod_{\mu=1}^{3} \sum_{\mathrm{i}=1}^{5} \Phi_{\mathrm{i}\mu} \hat{\mathrm{c}}_\mathrm{i}^\dagger |\mathrm{vac}\rangle_5. \tag{6.5}$$

Here, $\varphi_i^{(\mu)} = \Phi_{i\mu}$ are the overlap elements between the two different bases; in other words $\varphi_i^{(\mu)}$ gives the norm that orbital μ has on site i [70, Eq. 4]. All overlap elements together form the matrix:

$$\mathbf{\Phi} = \begin{pmatrix} \varphi_1^1 & \varphi_1^2 & \varphi_1^3 \\ \varphi_2^1 & \varphi_2^2 & \varphi_2^3 \\ \varphi_3^1 & \varphi_3^2 & \varphi_3^3 \\ \varphi_4^1 & \varphi_4^2 & \varphi_4^3 \\ \varphi_5^1 & \varphi_5^2 & \varphi_5^3 \end{pmatrix}. \tag{6.6}$$

Equivalently to the previous chapter, we now want to split up the full wave function. We want to obtain an embedded system, consisting of the impurity and the interactions between impurity and the rest of the system. The remaining part of the system (which does not interact with the impurity) can then be neglected. We find this embedded system by rotating the matrix $\mathbf{\Phi}$.

In order to find this rotation, we choose an example for $\mathbf{\Phi}$ with orthonormalized orbitals. Specifically, we take the three lowest eigenfunctions of the hopping Hamiltonian $\hat{t}$ and normalize them. This yields

$$\mathbf{\Phi} = \begin{pmatrix} \frac{1}{\sqrt{12}} & -0.5 & \frac{1}{\sqrt{3}} \\ \frac{1}{2} & -0.5 & 0 \\ \frac{2}{\sqrt{12}} & 0 & -\frac{1}{\sqrt{3}} \\ \frac{1}{2} & -0.5 & 0 \\ \frac{1}{\sqrt{12}} & 0.5 & \frac{1}{\sqrt{3}} \end{pmatrix}. \tag{6.7}$$

We will from now on show all single steps with this example wave function.

6.1.1 Finding the rotation for the mean field wave function

We choose the impurity of the system to comprise in total two sites and all orbitals. This yields an overlap matrix for the impurity that is defined as

$$\Phi_{j\nu} = \begin{pmatrix} \frac{1}{\sqrt{12}} & -0.5 & \frac{1}{\sqrt{3}} \\ \frac{1}{2} & -0.5 & 0 \end{pmatrix}, \tag{6.8}$$

where we consider all orbitals, restricted to the impurity region. In this basis, all orbitals ν have an overlap over all impurity lattice sites j. A system defined on two lattice sites (and spinless particles) can be fully described by in total two orbitals though, as this is the maximum number of particles that can be found on the impurity region. We want to optimize the orbitals such that only two of them have an overlap with the impurity.

In order to do so, with the help of Mathematica we perform a Singular value decomposition on that part of the matrix:

$$\Phi_{j\nu} = \sum_{i=1}^{2} \sum_{\mu=1}^{3} U_{ji} \Sigma_{i\mu} V^{\dagger}_{\mu\nu}. \tag{6.9}$$

Here $\mathbf{U}$ (size: 2×2) and $\mathbf{V}$ (size: 3×3) are both orthonormal matrices and Σ_{kl} is a 2×3 matrix with only 2 entries ≥ 0 on the diagonal [70, Eq. 5].

From Mathematica, we get the explicit matrices as

$$U = \begin{pmatrix} -0.776775 & -0.629778 \\ -0.629778 & 0.776775 \end{pmatrix} \tag{6.10}$$

$$\Sigma = \begin{pmatrix} 0.993167 & 0. & 0. \\ 0. & 0.424602 & 0. \end{pmatrix} \tag{6.11}$$

$$V = \begin{pmatrix} -0.542834 & 0.486541 & -0.68455 \\ 0.708115 & -0.173099 & -0.68455 \\ -0.451557 & -0.856338 & -0.250563 \end{pmatrix}. \tag{6.12}$$

The matrix V is now the sought-after rotation matrix, which rotates the orbitals into a new basis. In this new basis, only the first two orbitals have overlap with the first two impurity sites.

6.1.2 Basis transformation

We insert the rotation matrix V in ground state wave function of the Hamiltonian $\hat{t}$, taking advantage of the relation [70, Eq. 6, first part]:

$$V_{\mu' \mathfrak{a}} V_{\mathfrak{a}\mu} = \mathbb{1}. \tag{6.13}$$

The Slater determinant can then be written as

$$\begin{aligned} |\Phi\rangle = \prod_{\mu=1}^{3} \hat{a}_\mu^\dagger |\mathrm{vac}\rangle_5 &= \prod_{\mu=1}^{3} \sum_{\mu'}^{3} \delta_{\mu\mu'} \hat{a}_{\mu'}^\dagger |\mathrm{vac}\rangle_5 \\ = \prod_{\mu=1}^{3} \sum_{\mu'}^{3} \sum_{\mathfrak{a}}^{3} V_{\mu\mathfrak{a}} V_{\mathfrak{a}\mu'} \hat{a}_{\mu'}^\dagger |\mathrm{vac}\rangle_5 &= \prod_{\mu=1}^{3} \sum_{\mathfrak{a}}^{3} V_{\mu\mathfrak{a}} \hat{b}_{\mathfrak{a}}^\dagger |\mathrm{vac}\rangle_5. \end{aligned} \tag{6.14}$$

Considering the lattice-site representation of the new operator:

$$\hat{b}_{\mathfrak{a}}^\dagger = \sum_{i=1}^{5} \Xi_{\mathfrak{a}i} \hat{c}_i^\dagger, \tag{6.15}$$

we get the overlap matrix in this new basis representation as [70, Eq. 6, second part]

$$V_{\mu\mathfrak{a}} \Xi_{\mathfrak{a}i} = \Phi_{i\mu} \rightarrow \Xi_{\mathfrak{a}i} = \Phi_{i\mu} V_{\mu\mathfrak{a}} \tag{6.16}$$

$$\begin{aligned} \boldsymbol{\Xi} = \boldsymbol{\Phi} \cdot \mathbf{V} &= \begin{pmatrix} \frac{1}{\sqrt{12}} & -0.5 & \frac{1}{\sqrt{3}} \\ \sqrt{\frac{3}{12}} & -0.5 & 0 \\ \frac{2}{\sqrt{12}} & 0 & -\frac{1}{\sqrt{3}} \\ \sqrt{\frac{3}{12}} & -0.5 & 0 \\ \frac{1}{\sqrt{12}} & 0.5 & \frac{1}{\sqrt{3}} \end{pmatrix} \cdot \begin{pmatrix} -0.542834 & 0.486541 & -0.68455 \\ 0.708115 & -0.173099 & -0.68455 \\ -0.451557 & -0.856338 & -0.250563 \end{pmatrix} \\ &= \begin{pmatrix} 0.771467 & -0.267405 & 0. \\ 0.625475 & 0.32982 & 0. \\ 0.052699 & 0.775311 & 0.250563 \\ -0.0826406 & 0.156721 & 0.68455 \\ 0.0633515 & -0.440504 & 0.68455 \end{pmatrix}. \end{aligned} \tag{6.17}$$

We observe that in this basis, we achieved our goal: on the first two sites, only the first two orbitals have entries and the third orbital has a contribution of zero.

We now investigate the new basis set more carefully [70, Eq. 9] and see that we can simplify it to a

new Slater determinant form:

$$
\begin{aligned}
|\Phi\rangle &= \prod_{\mu=1}^{3}\sum_{\mathfrak{a}}^{3} V_{\mu\mathfrak{a}}\hat{b}_{\mathfrak{a}}^{\dagger}|\mathrm{vac}\rangle_5 \\
&= [\,\left(V_{11}\hat{b}_1^{\dagger}+V_{12}\hat{b}_2^{\dagger}+V_{13}\hat{b}_3^{\dagger}\right) \\
&\quad +\left(V_{21}\hat{b}_1^{\dagger}+V_{22}\hat{b}_2^{\dagger}+V_{23}\hat{b}_3^{\dagger}\right) \\
&\quad +\left(V_{31}\hat{b}_1^{\dagger}+V_{32}\hat{b}_2^{\dagger}+V_{33}\hat{b}_3^{\dagger}\right)\,]\,|\mathrm{vac}\rangle_5 \\
&= [\,V_{11}V_{22}V_{33}\hat{b}_1^{\dagger}\hat{b}_2^{\dagger}\hat{b}_3^{\dagger}-V_{11}V_{23}V_{32}\hat{b}_1^{\dagger}\hat{b}_2^{\dagger}\hat{b}_3^{\dagger} \\
&\quad -V_{12}V_{21}V_{33}\hat{b}_1^{\dagger}\hat{b}_2^{\dagger}\hat{b}_3^{\dagger}+V_{12}V_{23}V_{31}\hat{b}_1^{\dagger}\hat{b}_2^{\dagger}\hat{b}_3^{\dagger} \\
&\quad +V_{13}V_{21}V_{32}\hat{b}_1^{\dagger}\hat{b}_2^{\dagger}\hat{b}_3^{\dagger}-V_{13}V_{22}V_{31}\hat{b}_1^{\dagger}\hat{b}_2^{\dagger}\hat{b}_3^{\dagger}\,]\,|\mathrm{vac}\rangle_5 \\
&= [\,\left(V_{11}V_{22}-V_{12}V_{21}\right)\hat{b}_1^{\dagger}\hat{b}_2^{\dagger}\cdot V_{33}\hat{b}_3^{\dagger} \\
&\quad +\left(V_{21}V_{32}-V_{22}V_{31}\right)\hat{b}_1^{\dagger}\hat{b}_2^{\dagger}\cdot V_{13}\hat{b}_3^{\dagger} \\
&\quad +\left(V_{12}V_{31}-V_{11}V_{32}\right)\hat{b}_1^{\dagger}\hat{b}_2^{\dagger}\cdot V_{23}\hat{b}_3^{\dagger}\,]\,|\mathrm{vac}\rangle_5 \\
&= \det(\mathrm{V})\hat{\mathrm{b}}_1^{\dagger}\hat{\mathrm{b}}_2^{\dagger}\hat{\mathrm{b}}_3^{\dagger}|\mathrm{vac}\rangle_5 \\
&= \det(\mathrm{V})\left(\hat{\mathrm{b}}_1^{\dagger}\hat{\mathrm{b}}_2^{\dagger}|\mathrm{vac}\rangle_2\otimes\hat{\mathrm{b}}_3^{\dagger}|\mathrm{vac}\rangle_{3-5}\right) \\
&= \det(\mathrm{V})\left(\prod_{\mathfrak{a}=1}^{2}\hat{\mathrm{b}}_{\mathfrak{a}}^{\dagger}|\mathrm{vac}\rangle_2\otimes\hat{\mathrm{b}}_3^{\dagger}|\mathrm{vac}\rangle_{3-5}\right) \\
&= \left(\prod_{\mathfrak{a}=1}^{2}\hat{\mathrm{b}}_{\mathfrak{a}}^{\dagger}|\mathrm{vac}\rangle_2\otimes\hat{\mathrm{b}}_3^{\dagger}|\mathrm{vac}\rangle_{3-5}\right),
\end{aligned}
\tag{6.18}
$$

where we used that the Slater determinant of an orthonormal matrix is one.

$$
\det(V)=1. \tag{6.19}
$$

The last operator $\hat{b}_3^{\dagger}$ has no contribution on the impurity lattice sites (that is, on the first two sites). As this is the case, we can now split up the wave function into one part that is defined on the impurity and a remaining part that is defined on the rest of the system

6.1.3 Splitting up between impurity and environment

Splitting up between impurity lattice sites and the environment lattice sites yields

$$
\hat{b}_{\mathfrak{a}}^{\dagger}=\underbrace{\sum_{i=1}^{2}\sum_{\mu=1}^{3}V_{\mathfrak{a}\mu}\Phi_{\mu i}\hat{c}_i^{\dagger}}_{\hat{b}_{\mathrm{imp},\mathfrak{a}}^{\dagger}}+\underbrace{\sum_{i=3}^{5}\sum_{\mu=1}^{3}V_{\mathfrak{a}\mu}\Phi_{\mu i}\hat{c}_i^{\dagger}}_{\hat{b}_{N_{\mathrm{env}},\mathfrak{a}}^{\dagger}}. \tag{6.20}
$$

The whole wave function can be rewritten in terms of these split-up creation operators as

$$
\begin{aligned}
|\Phi\rangle &= \left[\left(\hat{b}_{\mathrm{imp},1}^{\dagger}+\hat{b}_{N_{\mathrm{env}},1}^{\dagger}\right)\left(\hat{b}_{\mathrm{imp},2}^{\dagger}+\hat{b}_{N_{\mathrm{env}},2}^{\dagger}\right)\hat{b}_3^{\dagger}\right]|\mathrm{vac}\rangle_5 \\
&= \left[\left(\hat{b}_{\mathrm{imp},1}^{\dagger}\hat{b}_{\mathrm{imp},2}^{\dagger}+\hat{b}_{\mathrm{imp},1}^{\dagger}\hat{b}_{N_{\mathrm{env}},2}^{\dagger}+\hat{b}_{\mathrm{imp},2}^{\dagger}\hat{b}_{N_{\mathrm{env}},1}^{\dagger}+\hat{b}_{N_{\mathrm{env}},1}^{\dagger}\hat{b}_{N_{\mathrm{env}},2}^{\dagger}\right)\hat{b}_3^{\dagger}\right]|\mathrm{vac}\rangle_5
\end{aligned}
\tag{6.21}
$$

We have now achieved the goal we stated in the beginning: solely by rotating the matrix $\mathbf{\Phi}$, we have split up the wave function into one part that contains the impurity and the interaction of the impurity with the rest of the system and another part that does not interact with the impurity.

From this wave function, we want to define the approximate projection. In order to explicitly see the implications for the projection does, we now consider the single-particle picture and specifically, the one-particle reduced density matrix (1RDM) in the single particle picture.

6.2 The 1RDM

Generally, the 1RDM of the mean field system can be written in the new basis as

$$\begin{aligned}\gamma_{ij} = \langle\Phi|\hat{c}_i^\dagger \hat{c}_j|\Phi\rangle &= \sum_{\mu=1}^{3}\langle\varphi^\mu|\hat{c}_i^\dagger\hat{c}_j|\varphi^\mu\rangle &= \sum_{\mu=1}^{3}\varphi_i^\mu\varphi_j^\mu \\ = \sum_{\mu=1}^{3}\sum_{\mu'=1}^{3}\sum_{\mathfrak{a}=1}^{3}\varphi_i^\mu V_{\mu\mathfrak{a}}V_{\mathfrak{a}\mu'}\varphi_j^{\mu'} &= \sum_{\mathfrak{a}=1}^{3}\left(\sum_{\mu=1}^{3}\varphi_i^\mu V_{\mu\mathfrak{a}}\right)\left(\sum_{\mu'=1}^{3}\varphi_i^{\mu'}V_{\mu'\mathfrak{a}}\right) &= \sum_{\mathfrak{a}=1}^{3}\Xi_{i\mathfrak{a}}\Xi_{\mathfrak{a}j} \qquad (6.22)\end{aligned}$$

Knowing the structure of the matrix $\boldsymbol{\Xi}$:

$$\Xi_{ia} = \begin{pmatrix} \xi_{11}^{\text{imp}} & \xi_{21}^{\text{imp}} & 0 \\ \xi_{21}^{\text{imp}} & \xi_{22}^{\text{imp}} & 0 \\ \xi_{31} & \xi_{23} & \xi_{33} \\ \xi_{41} & \xi_{24} & \xi_{34} \\ \xi_{51} & \xi_{25} & \xi_{35} \end{pmatrix}, \qquad (6.23)$$

we can explicitly write down the 1RDM in terms of the single particle orbitals $\xi_{\mu i}$:

$$\gamma = \begin{pmatrix} (\xi_{11}^{\text{imp}})^2 + (\xi_{12}^{\text{imp}})^2 & \xi_{11}^{\text{imp}}\xi_{21}^{\text{imp}} + \xi_{12}^{\text{imp}}\xi_{22}^{\text{imp}} & \xi_{11}^{\text{imp}}\xi_{31} + \xi_{12}^{\text{imp}}\xi_{32} & \xi_{11}^{\text{imp}}\xi_{41} + \xi_{12}^{\text{imp}}\xi_{42} & \xi_{11}^{\text{imp}}\xi_{51} + \xi_{12}^{\text{imp}}\xi_{52} \\ \xi_{11}^{\text{imp}}\xi_{21}^{\text{imp}} + \xi_{12}^{\text{imp}}\xi_{22}^{\text{imp}} & (\xi_{21}^{\text{imp}})^2 + (\xi_{22}^{\text{imp}})^2 & \xi_{21}^{\text{imp}}\xi_{31} + \xi_{22}^{\text{imp}}\xi_{32} & \xi_{21}^{\text{imp}}\xi_{41} + \xi_{22}^{\text{imp}}\xi_{42} & \xi_{21}^{\text{imp}}\xi_{51} + \xi_{22}^{\text{imp}}\xi_{52} \\ \xi_{11}^{\text{imp}}\xi_{31} + \xi_{12}^{\text{imp}}\xi_{32} & \xi_{21}^{\text{imp}}\xi_{31} + \xi_{22}^{\text{imp}}\xi_{32} & \xi_{31}^2 + \xi_{32}^2 + \xi_{33}^2 & \xi_{31}\xi_{41} + \xi_{32}\xi_{42} + \xi_{33}\xi_{43} & \xi_{31}\xi_{51} + \xi_{32}\xi_{52} + \xi_{33}\xi_{53} \\ \xi_{11}^{\text{imp}}\xi_{41} + \xi_{12}^{\text{imp}}\xi_{42} & \xi_{21}^{\text{imp}}\xi_{41} + \xi_{22}^{\text{imp}}\xi_{42} & \xi_{31}\xi_{41} + \xi_{32}\xi_{42} + \xi_{33}\xi_{43} & \xi_{41}^2 + \xi_{42}^2 + \xi_{43}^2 & \xi_{41}\xi_{51} + \xi_{42}\xi_{52} + \xi_{43}\xi_{53} \\ \xi_{11}^{\text{imp}}\xi_{51} + \xi_{12}^{\text{imp}}\xi_{52} & \xi_{21}^{\text{imp}}\xi_{51} + \xi_{22}^{\text{imp}}\xi_{52} & \xi_{31}\xi_{51} + \xi_{32}\xi_{52} + \xi_{33}\xi_{53} & \xi_{41}\xi_{51} + \xi_{42}\xi_{52} + \xi_{43}\xi_{53} & \xi_{51}^2 + \xi_{52}^2 + \xi_{53}^2 \end{pmatrix}$$

The first two lattice sites are still defined as the impurity. Considering this part of the 1RDM more explicitly and going back to the original basis, we observe:

$$\begin{aligned}\gamma_{ij}^{\text{imp}} &= \sum_{\mathfrak{a}=1}^{2}\Xi_{i\mathfrak{a}}\Xi_{\mathfrak{a}j} \\ &= \sum_{\mathfrak{a}=1}^{2}\sum_{\mu=1}^{3}\sum_{\mu'=1}^{3}\varphi_i^\mu V_{\mu\mathfrak{a}}V_{\mathfrak{a}\mu'}\varphi_j^{\mu'} \\ &= \sum_{\mu=1}^{3}\varphi_i^\mu\varphi_j^\mu. \qquad (6.24)\end{aligned}$$

This means that impurity region does not change upon the basis transformation.

Considering the elements of the 1RDM on the rest of the system, we can the eigenfunctions of the 1RDM on the environment:

$$\gamma_{ij}^{\text{env}}\phi_j^\epsilon = \lambda_\epsilon\phi_i^\epsilon, \qquad (6.25)$$

$$\begin{aligned}\gamma_{ij}^{\text{env}} &= \sum_{\epsilon=1}^{3}\phi_i^\epsilon\phi_j^\epsilon\lambda_\epsilon^2 \\ &= \sum_{\epsilon=1}^{2}\phi_i^\epsilon\phi_j^\epsilon\lambda_\epsilon^2 + \xi_i^3\xi_j^3 \\ &\text{with } 0 \le \lambda_\epsilon \le 1. \qquad (6.26)\end{aligned}$$

Where we used that the third single particle orbital ξ^3 does not have any contribution on the impurity, it must be fully determined by the environment 1RDM.

We can then split up the 1RDM on the environment into one part interacting with the impurity and

one part not interacting with the impurity:

$$\begin{aligned}\gamma_{ij}^{\text{env}} &= \gamma_{ij}^{\text{emb}}[\xi_{i1},\xi_{i2}] + \gamma_{ij}^{\text{bath}}[\xi_{i3}] \\ &= \begin{pmatrix} \xi_{31}^2+\xi_{32}^2+\xi_{33}^2 & \xi_{31}\xi_{41}+\xi_{32}\xi_{42}+\xi_{33}\xi_{43} & \xi_{31}\xi_{51}+\xi_{32}\xi_{52}+\xi_{33}\xi_{53} \\ \xi_{31}\xi_{41}+\xi_{32}\xi_{42}+\xi_{33}\xi_{43} & \xi_{41}^2+\xi_{42}^2+\xi_{43}^2 & \xi_{41}\xi_{51}+\xi_{42}\xi_{52}+\xi_{43}\xi_{53} \\ \xi_{31}\xi_{51}+\xi_{32}\xi_{52}+\xi_{33}\xi_{53} & \xi_{41}\xi_{51}+\xi_{42}\xi_{52}+\xi_{43}\xi_{53} & \xi_{51}^2+\xi_{52}^2+\xi_{53}^2 \end{pmatrix} \\ &= \begin{pmatrix} \xi_{31}^2+\xi_{32}^2 & \xi_{31}\xi_{41}+\xi_{32}\xi_{42} & \xi_{31}\xi_{51}+\xi_{32}\xi_{52} \\ \xi_{31}\xi_{41}+\xi_{32}\xi_{42} & \xi_{41}^2+\xi_{42}^2 & \xi_{41}\xi_{51}+\xi_{42}\xi_{52} \\ \xi_{31}\xi_{51}+\xi_{32}\xi_{52} & \xi_{41}\xi_{51}+\xi_{42}\xi_{52} & \xi_{51}^2+\xi_{52}^2 \end{pmatrix} + \begin{pmatrix} \xi_{33}^2 & \xi_{33}\xi_{43} & \xi_{33}\xi_{53} \\ \xi_{33}\xi_{43} & \xi_{43}^2 & \xi_{43}\xi_{53} \\ \xi_{33}\xi_{53} & \xi_{43}\xi_{53} & \xi_{53}^2 \end{pmatrix}\end{aligned} \tag{6.27}$$

.

Written less explicitly, the 1RDM is defined as

$$\gamma_{ij} = \sum_{\mathfrak{a}=1}^{3} \xi_i^{\mathfrak{a}}\xi_j^{\mathfrak{a}} = \sum_{\mathfrak{a}=1}^{3} \langle i|\xi^{\mathfrak{a}}\rangle\langle\xi^{\mathfrak{a}}|j\rangle. \tag{6.28}$$

We can split up each single particle orbital into one part that is defined on the impurity and one part that is defined on the environment and then rewrite the 1RDM as

$$\xi_i^{\mathfrak{a}} = \xi_{\text{imp,i}}^{\mathfrak{a}} + \xi_{N_{\text{env}},i}^{\mathfrak{a}} \tag{6.29}$$

$$\begin{aligned}\gamma_{ij} &= \sum_{\mathfrak{a}=1}^{3} \left(\xi_{\text{imp,i}}^{\mathfrak{a}} + \xi_{N_{\text{env}},i}^{\mathfrak{a}}\right)\left(\xi_{\text{imp,j}}^{\mathfrak{a}} + \xi_{N_{\text{env}},j}^{\mathfrak{a}}\right) \\ &= \sum_{\mathfrak{a}=1}^{2} \xi_{\text{imp,i}}^{\mathfrak{a}}\xi_{\text{imp,j}}^{\mathfrak{a}} + \sum_{\mathfrak{a}=1}^{3} \xi_{N_{\text{env}},i}^{\mathfrak{a}}\xi_{\text{imp,j}}^{\mathfrak{a}} + \sum_{\mathfrak{a}=1}^{3} \xi_{\text{imp,i}}^{\mathfrak{a}}\xi_{N_{\text{env}},j}^{\mathfrak{a}} + \sum_{\mathfrak{a}=1}^{3} \xi_{N_{\text{env}},i}^{\mathfrak{a}}\xi_{N_{\text{env}},j}^{\mathfrak{a}}.\end{aligned} \tag{6.30}$$

The first term in Eq. (6.30) is defined just the impurity, where we know that the 1RDM has not changed upon the basis transformation

$$\gamma_{ij}^{\text{imp}} = \sum_{\mathfrak{a}=1}^{2} \xi_{\text{imp,i}}^{\mathfrak{a}}\xi_{\text{imp,j}}^{\mathfrak{a}} = \sum_{\mu=1}^{3} \varphi_{\text{imp,i}}^{\mu}\varphi_{\text{imp,j}}^{\mu}. \tag{6.31}$$

Note that while in the first expression the sum over $\mathfrak{a}$ only includes the first two orbitals, it includes all three orbitals in the original representation, i.e., the sum over μ goes over all three orbitals.

Considering the last term in Eq. (6.29) which only includes environment lattice sites, we can further decompose it into:

$$\gamma_{ij}^{N_{\text{env}}} = \sum_{\mathfrak{a}=1}^{3} \xi_{N_{\text{env}},i}^{\mathfrak{a}}\xi_{N_{\text{env}},j}^{\mathfrak{a}} = \sum_{\mathfrak{a}=1}^{2} \xi_{N_{\text{env}},i}^{\mathfrak{a}}\xi_{N_{\text{env}},j}^{\mathfrak{a}} + \xi_i^3\xi_j^3 \tag{6.32}$$

Then, we can write the full 1RDM as:

$$\gamma_{ij} = \underbrace{\sum_{\mu=1}^{3} \varphi_{\text{imp,i}}^{\mu}\varphi_{\text{imp,j}}^{\mu}}_{\text{imp}} + \underbrace{\sum_{\mathfrak{a}=1}^{2} \xi_{N_{\text{env}},i}^{\mathfrak{a}}\xi_{N_{\text{env}},j}^{\mathfrak{a}}}_{\text{emb}} + \underbrace{\sum_{\mathfrak{a}=1}^{3} \xi_{N_{\text{env}},i}^{\mathfrak{a}}\xi_{\text{imp,j}}^{\mathfrak{a}}}_{\text{mix}} + \underbrace{\sum_{\mathfrak{a}=1}^{3} \xi_{\text{imp,i}}^{\mathfrak{a}}\xi_{N_{\text{env}},j}^{\mathfrak{a}}}_{\text{mix}} + \underbrace{\xi_i^3\xi_j^3}_{\text{bath}} \tag{6.33}$$

The first two terms are only determined by the first two orbitals in the new basis ξ_i^1 and ξ_i^2 and at the same time fully determine those two orbitals:

$$\begin{aligned}\gamma_{ij}^{\text{imp-emb}} &= \underbrace{\sum_{\mu=1}^{3} \varphi_{\text{imp,i}}^{\mu}\varphi_{\text{imp,j}}^{\mu}}_{\text{imp}} + \underbrace{\sum_{\mathfrak{a}=1}^{2} \xi_{N_{\text{env}},i}^{\mathfrak{a}}\xi_{N_{\text{env}},j}^{\mathfrak{a}}}_{\text{emb}} \\ &= \sum_{\mathfrak{a}=1}^{2} \xi_i^{\mathfrak{a}}\xi_j^{\mathfrak{a}} \\ &= \begin{pmatrix} \gamma_{11} & \gamma_{12} & 0 & 0 & 0 \\ \gamma_{21} & \gamma_{22} & 0 & 0 & 0 \\ 0 & 0 & \xi_{31}^2+\xi_{32}^2 & \xi_{31}\xi_{41}+\xi_{32}\xi_{42} & \xi_{31}\xi_{51}+\xi_{32}\xi_{52} \\ 0 & 0 & \xi_{31}\xi_{41}+\xi_{32}\xi_{42} & \xi_{41}^2+\xi_{42}^2 & \xi_{41}\xi_{51}+\xi_{42}\xi_{52} \\ 0 & 0 & \xi_{31}\xi_{51}+\xi_{32}\xi_{52} & \xi_{41}\xi_{51}+\xi_{42}\xi_{52} & \xi_{51}^2+\xi_{52}^2 \end{pmatrix}\end{aligned} \tag{6.34}$$

This leads to the conclusion that in the single particle picture, the 1RDM on the impurity and all interactions of the rest of the system with the impurity can be determined by two orbitals ξ^1 and ξ^2. Just describing properties on the impurity, the third orbital ξ^3 can be neglected. We want to find the projection that does exactly this.

6.3 Building the projection

From above defined single particle orbitals, we want to build a projection that does not change the one-particle properties of the hopping Hamiltonian $\hat{t}$ on the impurity.

We define the projection in the single particle picture as

$$\hat{p} \equiv \sum_{\mathfrak{a}=1}^{2} |\xi_{\mathfrak{a}}\rangle\langle\xi_{\mathfrak{a}}|. \tag{6.35}$$

Projection of the single particle Hamiltonian then yields

$$\hat{p}^\dagger \hat{t} \hat{p} = \sum_{\mathfrak{a}'\mathfrak{a}=1}^{2} |\xi_{\mathfrak{a}'}\rangle\langle\xi_{\mathfrak{a}'}|\hat{t}|\xi_{\mathfrak{a}}\rangle\langle\xi_{\mathfrak{a}}|. \tag{6.36}$$

Note that here, we only consider the first two orbitals ξ^1 and ξ^2 while the third orbital is neglected.

In order to take a closer look at the new form of the Hamiltonian, we again separate the single-particle orbitals into those parts defined on the impurity and those parts defined on the embedded system, $|\xi_{\mathfrak{a}'}\rangle = |\xi^{\mathrm{imp}}_{\mathfrak{a}'}\rangle + |\xi^{\mathrm{emb}}_{\mathfrak{a}'}\rangle$:

$$\begin{aligned}
\hat{p}^\dagger \hat{t} \hat{p} = &\sum_{\mathfrak{a}'\mathfrak{a}=1}^{2} |\xi^{\mathrm{imp}}_{\mathfrak{a}'}\rangle\langle\xi^{\mathrm{imp}}_{\mathfrak{a}'}|\hat{t}|\xi^{\mathrm{imp}}_{\mathfrak{a}}\rangle\langle\xi^{\mathrm{imp}}_{\mathfrak{a}}| \\
&+ \sum_{\mathfrak{a}'\mathfrak{a}=1}^{2} |\xi^{\mathrm{imp}}_{\mathfrak{a}'}\rangle\langle\xi^{\mathrm{imp}}_{\mathfrak{a}'}|\hat{t}|\xi^{\mathrm{emb}}_{\mathfrak{a}}\rangle\langle\xi^{\mathrm{emb}}_{\mathfrak{a}}| + c.c. \\
&+ \sum_{\mathfrak{a}'\mathfrak{a}=1}^{2} |\xi^{\mathrm{emb}}_{\mathfrak{a}'}\rangle\langle\xi^{\mathrm{emb}}_{\mathfrak{a}'}|\hat{t}|\xi^{\mathrm{emb}}_{\mathfrak{a}}\rangle\langle\xi^{\mathrm{emb}}_{\mathfrak{a}}|
\end{aligned} \tag{6.37}$$

We now consider the parts of the projection separately. The first part contains only orbitals defined on the impurity. Here, we can go back to the original basis set as:

$$\begin{aligned}
\hat{p}^\dagger_{\mathrm{imp}} \hat{t} \hat{p}_{\mathrm{imp}} &= \sum_{\mathfrak{a}'\mathfrak{a}=1}^{2} |\xi^{\mathrm{imp}}_{\mathfrak{a}'}\rangle\langle\xi^{\mathrm{imp}}_{\mathfrak{a}'}|\hat{t}|\xi^{\mathrm{imp}}_{\mathfrak{a}}\rangle\langle\xi^{\mathrm{imp}}_{\mathfrak{a}}| \\
&= \sum_{\mathfrak{a}'\mathfrak{a}=1}^{2} \hat{t}_{\mathfrak{a}'\mathfrak{a}} |\xi^{\mathrm{imp}}_{\mathfrak{a}'}\rangle\langle\xi^{\mathrm{imp}}_{\mathfrak{a}}| \\
&= \sum_{\mu'\mu=1}^{3} \hat{t}_{\mu'\mu} |\varphi^{\mathrm{imp}}_{\mu'}\rangle\langle\varphi^{\mathrm{imp}}_{\mu}| \\
&= \sum_{\mu'\mu=1}^{3} \sum_{i,j=1}^{2} |\varphi^{\mathrm{imp}}_{\mu'}\rangle\langle\varphi^{\mathrm{imp}}_{\mu'}|i\rangle\langle i|\hat{t}|j\rangle\langle j|\varphi^{\mathrm{imp}}_{\mu'}\rangle\langle\varphi^{\mathrm{imp}}_{\mu'}| \\
&= \sum_{i,j=1}^{2} \underbrace{\left(\sum_{\mu'=1}^{3} |\varphi^{\mathrm{imp}}_{\mu'}\rangle\langle\varphi^{\mathrm{imp}}_{\mu'}|i\rangle \right)}_{\langle \mathbb{1}_{\mathrm{sub}}|i\rangle} \hat{t}_{ij} \underbrace{\left(\sum_{\mu=1}^{3} \langle j|\varphi^{\mathrm{imp}}_{\mu'}\rangle\langle\varphi^{\mathrm{imp}}_{\mu'}| \right)}_{\langle j|\mathbb{1}_{\mathrm{sub}}\rangle} \\
&= \sum_{i,j=1}^{2} \hat{t}_{ij} |i\rangle\langle j|
\end{aligned} \tag{6.38}$$

The mixing term considers the overlap of the impurity orbitals with the embedding orbitals. The impurity orbitals are also rotated back to the original basis:

$$\begin{aligned}\hat{p}^\dagger_{\text{mix}}\hat{t}\hat{p}_{\text{mix}} &= \sum_{\mathfrak{a}'\mathfrak{a}=1}^{2} \hat{t}_{\mathfrak{a}'\mathfrak{a}}|\xi^{\text{imp}}_{\mathfrak{a}'}\rangle\langle\xi^{\text{emb}}_{\mathfrak{a}}| + c.c. \\ &= \sum_{\mu'=1}^{3}\sum_{\mathfrak{a}=1}^{2} \hat{t}_{\mu'\mathfrak{a}}|\xi^{\text{imp}}_{\mu'}\rangle\langle\xi^{\text{emb}}_{\mathfrak{a}}| + c.c. \\ &= \sum_{i=1}^{2}\sum_{\mathfrak{a}=1}^{2} \hat{t}_{i\mathfrak{a}}|i\rangle\langle\xi^{\text{emb}}_{\mathfrak{a}}| + c.c. \end{aligned} \tag{6.39}$$

With that, leaving the environment part of the Hamiltonian as it is, the full hopping matrix $\hat{t}$, after the projection reads:

$$\hat{t}_{\text{emb}} = \begin{pmatrix} \hat{t}_{ij} & \hat{t}_{i\mathfrak{b}} \\ \hat{t}_{\mathfrak{a}j} & \hat{t}_{\mathfrak{a}\mathfrak{b}} \end{pmatrix}. \tag{6.40}$$

The embedding Hamiltonian $\hat{t}_{\text{emb}}$ has the same form as the original Hamiltonian on the impurity, while the rest of it has changed. Also, while before the dimension of $\hat{t}$ was 5×5, it is now 4×4 in the new basis set as we have neglected the third orbital ξ^3.

6.4 Two different ways to obtain the same projection

In the previous section, we have defined the projection in the single particle picture, motivated by what we found for the 1RDM in the single particle picture. As a remaining step, we want to explicitly calculate this projection. The projection is determined by the single particle orbitals $\xi^{\mathfrak{a}}$. Those can be obtained either directly from the wave function in the new basis or through the 1RDM of the system. This is why, there are also two different ways to obtain the projection. For our explicit example, we will demonstrate that both approaches yield the same result.

- Explicitly through the wave function of the mean field problem

  This is the intuitive way to obtain the projection: we can compute the mean field wave function in terms of the single particle orbitals. Rotating the orbitals, we only choose those with an overlap over the impurity to build the projection.

- Through the 1RDM

  This is what is practically done as the 1RDM is a much more handy object than the wave function, even in the mean field system. Although less intuitive, we will show that we obtain the same projection by considering the 1RDM of the mean field system.

Diagonalizing the hopping Hamiltonian $\hat{t}$ with hopping $t=-1$:

$$\begin{pmatrix} 0 & -1 & 0 & 0 & 0 \\ -1 & 0 & -1 & 0 & 0 \\ 0 & -1 & 0 & -1 & 0 \\ 0 & 0 & -1 & 0 & -1 \\ 0 & 0 & 0 & -1 & 0 \end{pmatrix} \tag{6.41}$$

yields the eigenvalues $\{-\sqrt{3},\sqrt{3},-1,1,0\}$ with eigenvectors (written as columns of a matrix here):

$$\begin{pmatrix} \frac{1}{\sqrt{12}} & \frac{1}{\sqrt{12}} & -0.5 & -0.5 & \frac{1}{\sqrt{3}} \\ 0.5 & -0.5 & -0.5 & 0.5 & 0 \\ \frac{1}{\sqrt{6}} & \frac{1}{\sqrt{6}} & 0 & 0 & -\frac{1}{\sqrt{3}} \\ 0.5 & -0.5 & 0.5 & -0.5 & 0 \\ \frac{1}{\sqrt{12}} & \frac{1}{\sqrt{12}} & 0.5 & 0.5 & \frac{1}{\sqrt{3}} \end{pmatrix} \tag{6.42}$$

The ground state wave function of the problem in the many particle picture (determined by the mean field Hamiltonian $\hat{T}$) is then a Slater determinant built from the three orbitals with the lowest eigenvalues,

$$|\Phi\rangle = \prod_{\mu=1}^{3} \sum_{i=1}^{5} \Phi_{i\mu} \hat{c}_i^\dagger |\mathrm{vac}\rangle_5, \tag{6.43}$$

where

$$\mathbf{\Phi} = \begin{pmatrix} \frac{1}{\sqrt{12}} & -0.5 & \frac{1}{\sqrt{3}} \\ 0.5 & -0.5 & 0 \\ \frac{1}{\sqrt{6}} & 0 & -\frac{1}{\sqrt{3}} \\ 0.5 & 0.5 & 0 \\ \frac{1}{\sqrt{12}} & 0.5 & \frac{1}{\sqrt{3}} \end{pmatrix}. \tag{6.44}$$

The 1RDM belonging to this wave function is then defined as

$$\begin{aligned} \gamma_{\mathrm{full}} &= \sum_{\mu=1}^{3} |\varphi_i^\mu\rangle\langle\varphi_j^\mu| \\ &= \begin{pmatrix} 0.666667 & 0.394338 & -0.166667 & 0.394338 & 0.166667 \\ 0.394338 & 0.5 & 0.288675 & 0.5 & -0.105662 \\ -0.166667 & 0.288675 & 0.666667 & 0.288675 & -0.166667 \\ 0.394338 & 0.5 & 0.288675 & 0.5 & -0.105662 \\ 0.166667 & -0.105662 & -0.166667 & -0.105662 & 0.666667 \end{pmatrix} \end{aligned} \tag{6.45}$$

The goal of DMET is now to find an embedding Hamiltonian

$$\hat{p}^\dagger \hat{t} \hat{p} = \hat{t}_{\mathrm{emb}} \tag{6.46}$$

whose eigenvectors yield the same 1RDM on the impurity as γ_{full} from the previous equation. There are two different ways to find the projection $\hat{p}$: directly from the wave function or through the 1RDM.

6.4.1 Defining the projection directly from the wave function

In the above derivation, we find a basis set $\hat{b}_\mathfrak{a}^\dagger$, in which only two basis function have an overlap with the first two impurity sites in the lattice representation:

$$\hat{b}_\mathfrak{a}^\dagger = \sum_{i=1}^{5} \Xi_{\mathfrak{a}i} \hat{c}_i^\dagger, \tag{6.47}$$

with

$$\mathbf{\Xi} = \begin{pmatrix} 0.771467 & -0.267405 & 0. \\ 0.625475 & 0.32982 & 0. \\ 0.052699 & 0.775311 & 0.250563 \\ -0.0826406 & 0.156721 & 0.68455 \\ 0.0633515 & -0.440504 & 0.68455 \end{pmatrix}. \tag{6.48}$$

As the third orbital does not have any overlap with the impurity, we do not need it in order to describe the wave function on the impurity (that is, on the first two lattice sites). Additionally, we derived in Eq. (6.24) that the 1RDM on the impurity is not changed by the projection. As in the non-interacting case, the natural orbitals and the eigenstates of the hopping Hamiltonian are the same this means that also the wave function on the impurity does not change with the projection.

Stated otherwise: The projection is a unit matrix on the impurity and consists of the (re-normalized)

first two orbitals in the environment:

$$\hat{p} = \begin{pmatrix} 1 & 0 & 0 & 0 & 0 \\ 0 & 1 & 0 & 0 & 0 \\ 0 & 0 & 0.052699/\sqrt{c_1} & -0.0826406/\sqrt{c_1} & 0.0633515/\sqrt{c_1} \\ 0 & 0 & 0.775311/\sqrt{c_2} & 0.156721/\sqrt{c_2} & -0.440504/\sqrt{c_2} \end{pmatrix} \tag{6.49}$$
$$= \begin{pmatrix} 1 & 0 & 0 & 0 & 0 \\ 0 & 1 & 0 & 0 & 0 \\ 0 & 0 & 0.451557 & -0.708115 & 0.542834 \\ 0 & 0 & 0.856338 & 0.173099 & -0.486541 \end{pmatrix},$$

where

$$c_1 = 0.052699^2 + 0.0826406^2 + 0.0633515^2 \tag{6.50}$$
$$c_2 = 0.775311^2 + 0.156721^2 + 0.440504^2. \tag{6.51}$$

This is one way to get the projection.

6.4.2 Defining the projection through the environment part of the 1RDM

The projection on the impurity is, as stated before, just the unit matrix. We additionally showed in Eq. (6.27) that the environment part of the 1RDM gives the same set as

$$\hat{b}^\dagger_{\mathfrak{a}} = \sum_{i=1}^{5} \Xi_{\mathfrak{a}i} \hat{c}^\dagger_i. \tag{6.52}$$

The 1RDM defined on the environment is

$$\gamma_{N_{\text{env}}} = \begin{pmatrix} 0.666667 & 0.288675 & -0.166667 \\ 0.288675 & 0.5 & -0.105662 \\ -0.166667 & -0.105662 & 0.666667 \end{pmatrix}. \tag{6.53}$$

Diagonalizing yields the eigenvalues $\{0.0136200671, 0.8197132662, 1.\}$ and the eigenvectors

$$ev = \begin{pmatrix} -0.451557 & 0.856338 & 0.250563 \\ 0.708115 & 0.173099 & 0.684550 \\ -0.542834 & -0.486541 & 0.684550 \end{pmatrix} \tag{6.54}$$

The eigenvector belonging to the eigenvalue one is the orbital that does not have any overlap with the impurity. It can be neglected for the description of the impurity. Taking the eigenvectors belonging to the lowest eigenvalues, we can now define the projection as:

$$\hat{p}^\dagger = \begin{pmatrix} 1 & 0 & 0 & 0 \\ 0 & 1 & 0 & 0 \\ 0 & 0 & -0.451557 & 0.856338 \\ 0 & 0 & 0.708115 & 0.173099 \\ 0 & 0 & -0.542834 & -0.486541 \end{pmatrix} \tag{6.55}$$

which is the same as the projection defined from the wave function directly.

6.4.3 The 1RDM of the embedded system

We apply the projection $\hat{p}$ to the hopping Hamiltonian $\hat{t}$ to get the embedding Hamiltonian $\hat{t}_{\text{emb}}$

$\hat{p}^\dagger \hat{t} \hat{p} =$

$$= \begin{pmatrix} 1 & 0 & 0 & 0 & 0 \\ 0 & 1 & 0 & 0 & 0 \\ 0 & 0 & -0.4516 & 0.7081 & -0.5428 \\ 0 & 0 & 0.8563 & 0.1731 & -0.4865 \end{pmatrix} \begin{pmatrix} 0 & -1 & 0 & 0 & 0 \\ -1 & 0 & -1 & 0 & 0 \\ 0 & -1 & 0 & -1 & 0 \\ 0 & 0 & -1 & 0 & -1 \\ 0 & 0 & 0 & -1 & 0 \end{pmatrix} \begin{pmatrix} 1 & 0 & 0 & 0 \\ 0 & 1 & 0 & 0 \\ 0 & 0 & -0.4516 & 0.8563 \\ 0 & 0 & 0.7081 & 0.1731 \\ 0 & 0 & -0.5428 & -0.4865 \end{pmatrix}$$
$$= \begin{pmatrix} 0. & -1. & 0. & 0. \\ -1. & 0. & 0.4516 & -0.8563 \\ 0. & 0.4516 & 1.4083 & -0.0897 \\ 0. & -0.8563 & -0.0897 & -0.1280 \end{pmatrix} \equiv \hat{t}_{\text{emb}} \tag{6.56}$$

Diagonalizing the new hopping Hamiltonian yields the eigenvectors

$$\begin{pmatrix} -0.513869 & 0.634511 & -0.5 & -0.288675 \\ -0.705318 & 0.050269 & 0.5 & 0.5 \\ 0.099101 & -0.061637 & -0.625475 & 0.771467 \\ -0.478167 & -0.768810 & -0.329820 & -0.267405 \end{pmatrix} \tag{6.57}$$

with corresponding eigenvalues

$$\{-1.372562, -0.079225, 1., 1.732050\} \tag{6.58}$$

Taking the eigenvectors belonging to the lowest two eigenvalues and build the 1RDM from them yields

$$\gamma_{\text{emb}} = \begin{pmatrix} 0.666667 & 0.394338 & -0.090034 & -0.242103 \\ 0.394338 & 0.5 & -0.072996 & 0.298613 \\ -0.090034 & -0.072996 & 0.013620 & 0 \\ -0.242103 & 0.298613 & 0 & 0.819713 \end{pmatrix} \tag{6.59}$$

As can be seen by comparison, on the impurity (that is, in this case, for the first two sites) the 1RDMs of the full problem and of the embedding problem are the same.

6.5 Summary

In this chapter, with the help of the example of three spinless particles on five lattice sites, we have explicitly shown every step in the DMET algorithm in terms of the treated wave functions and in terms of the treated 1RDMs. We have shown that, both treatments lead to the same result.

Chapter 7

Practical implementation

Although very detailed, the above section might not be very helpful to understand the actual DMET algorithm, as it is implemented in the code[†]. Also, there are a few technicalities and difficulties that will be discussed in the following chapter.

The goal of this chapter is to give a practical guide for the implementation of the DMET code in the flavour which is used in this thesis. In the first section, for the example of the Hubbard model, we will guide the reader through the DMET steps which have to be implemented in the code. In the second section, we will discuss in detail a few of the subtleties and problems we have come across in the course of this thesis. We will reveal tricks that are used in the actual calculations and highlight some of the drawbacks of the DMET algorithm. While some of the drawbacks can be circumvented, as we will also show, other problems have to be considered in more detail.

7.1 Actual DMET steps

In this section, we will show each single step of the DMET code for the Hubbard Hamiltonian. The goal of this section is to show the reader how to practically implement her own DMET code.

$$\hat{H} = t \sum_{\langle i,j\rangle,\sigma} \hat{c}^{\dagger}_{i\sigma}\hat{c}_{j\sigma} + U \sum_{i} \hat{n}_{i\uparrow}\hat{n}_{i\downarrow}, \tag{7.1}$$

$$\hat{H}|\Psi\rangle = E|\Psi\rangle, \tag{7.2}$$

which we also show graphically in figure 7.1.

1. Setting up the Hamiltonians as tensors
As a first step, we define the full interacting Hamiltonian. The one-body (hopping term) $\hat{T}$ is then defined as a matrix with elements only on the first off-diagonal. The two-body (electron-electron interaction term) $\hat{U}$ is defined as a tensor of fourth order. In the Hubbard model, it only has diagonal terms $U(i,i,i,i)$.

2. Computing the mean field 1RDM
The next step is to compute the 1RDM of the mean field Hamiltonian $\hat{T}$. In the non-interacting case, the eigenfunctions of the 1RDM and of the Hamiltonian are the same. Thus, we diagonalize the mean field Hamiltonian (in the first iteration, this is simply the hopping Hamiltonian, after that, there will be an additional non-local potential added to it). The eigenvectors of this matrix are then the eigenstates of the 1RDM. The 1RDM consists only of the occupied orbitals, so we take the lowest $\frac{M}{2}$ eigenstates (each orbital can be occupied twice due to spin). We build the 1RDM in the lattice-site basis by computing each element as

$$\gamma_{ij} = \sum_{\mu=1}^{M/2} \varphi_i^{\mu}\varphi_j^{\mu}. \tag{7.3}$$

[†] The code implemented within the scope of this thesis is available upon request.

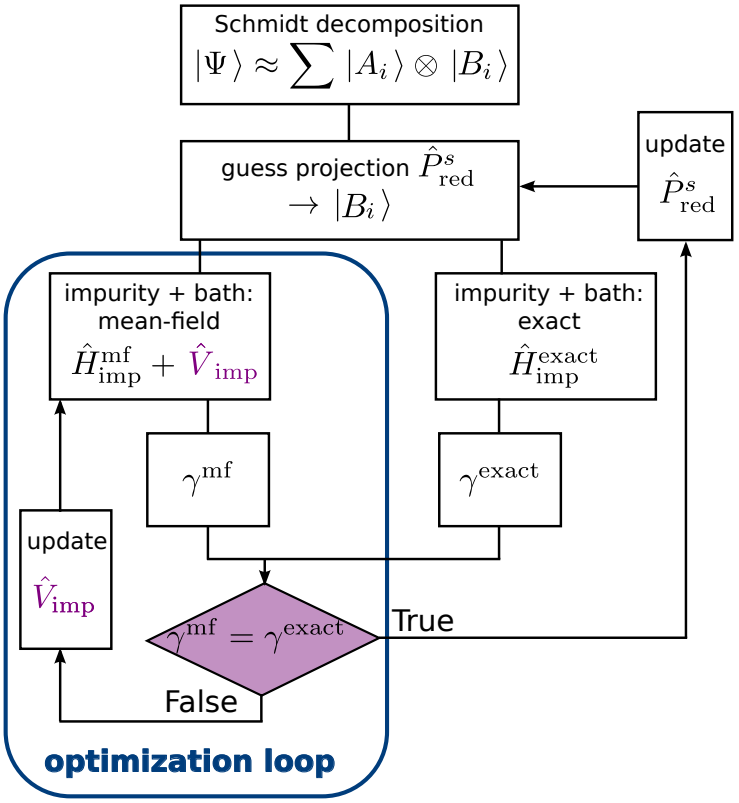

Figure 7.1: Schematic presentation of all DMET steps listed above.

3. Obtaining the projection from the mean field 1RDM
The projection should leave the impurity region of the Hamiltonian unchanged and just project the rest of the system onto a new basis set. Thus, the impurity part of the projection is simply a unitary matrix. To find the optimal orbitals which build up the incomplete basis set, we cut out only the part of the 1RDM that is not on the impurity and diagonalize it. We then get three different groups of eigenvalues

- Eigenvalues that are 0, belonging to the unoccupied orbitals of the 1RDM
- Eigenvalues that are 2, meaning that the full norm is in the environment. This also means that the eigenvectors belonging to the eigenvalue does not have an overlap with the impurity lattice sites
- Eigenvectors that are between 0 and 2. This means that the belonging eigenvectors do not have its full norm on the environment, thus having an overlap with the impurity. The eigenvectors belonging to these eigenvalues are the ones we choose to define the projection

The full projection has two parts: on the impurity, it is a unity matrix while the environment part consists of the eigenvectors belonging to the eigenvalues between zero and 2:

$$\hat{p} = \begin{pmatrix} \mathbb{1}_{N_{imp}} & 0 \\ 0 & \tilde{\xi}_{\text{env},1} \cdots \tilde{\xi}_{\text{env},2\text{N}_{\text{imp}}} \end{pmatrix} \tag{7.4}$$

Note that each of the eigenvectors ξ_α is of length N, so that the total projection matrix will be of the dimension $N \times 2N_{N_{\text{imp}}}$.

4. Obtaining the embedding Hamiltonian and calculating observables We use the projection to build the embedding Hamiltonian:

$$\hat{H}_{\text{emb}} = \hat{P}^{s\dagger}_{\text{red}} \hat{T} \hat{P}^s_{\text{red}} + \hat{P}^{s\dagger}_{\text{red}} \hat{P}^{s\dagger}_{\text{red}} \hat{U} \hat{P}^s_{\text{red}} \hat{P}^s_{\text{red}} \tag{7.5}$$

Note that here, $\hat{T}$ will always remain to be the simple hopping Hamiltonian, without additional nonlocal potential. The embedding Hamiltonian is now small enough to be solved accurately

with the method of choice (in this work, either by exact diagonalization or with DMRG). With the wave function on the embedded system $|\Psi_{\text{emb}}\rangle$, we compute the 1RDM

$$\gamma_{ij} = \langle \Psi_{\text{emb}} | \hat{c}_i^\dagger \hat{c}_i | \Psi_{\text{emb}} \rangle. \tag{7.6}$$

5. Computing the 1RDM of the non-interacting embedded system
We want to compare the 1RDM of the interacting system with the 1RDM of the non-interacting system. As the 1RDM of the interacting system is obtained with the embedding Hamiltonian, we also compute the 1RDM of the non-interacting system with the embedded hopping Hamiltonian.

6. Obtaining the non-local potential
We minimize the difference between the two 1RDMs by adding a non-local potential to the embedded hopping Hamiltonian used to calculate the non-interacting 1RDM. This is done until convergence.

7. Self-consistency
From the step before, we obtain a new mean field Hamiltonian $\hat{T}' = \hat{T} + \hat{V}$, where $\hat{V}$ is the non-local potential. Now instead of using the simple hopping Hamiltonian to define the projection, we use this new Hamiltonian. This will yield a different embedding Hamiltonian and different 1RDMs. We repeat the above steps until the non-local potential does not change anymore and $\hat{T}'_{\text{itr=L}} = \hat{T}'_{\text{itr=L+1}}$.

7.2 Problems and subtleties of DMET

In the last chapters, for the sake of clarity, we considered the straightforward and easiest possible way to derive and implement the DMET algorithm. There are however some subtleties and problems in DMET that we have come across and that are worth mentioning. In this section, we will mention all subtleties and problems known to the authors and offer solutions or bypasses if possible. Some of the subtleties with deeper meaning and and some problems will be explained and discussed in more detail in the last chapter 11.

7.2.1 Interacting and non-interacting bath picture

In the above derivation, we showed DMET in the so-called "interacting bath picture" [70, section 3.1/3.2], that is, we set up the original Hamiltonian to have interactions on all lattice sites. Differently stated, in the first step, we generate the full Hamiltonian $\hat{H} = \hat{T} + \hat{U}$, where the first part $\hat{T}$ is generated as an $N \times N$ matrix and the second part $\hat{U}$ is generated as a tensor of fourth order, $N \times N \times N \times N$. Although working well in theory, this method has the downside that we have to store the U-tensor, an object growing $\propto N^4$ with system size N which can get expensive with respect to the memory costs already for medium-sized lattices.

As the full system $\hat{H}$ is never actually calculated anyways and all the interactions between the impurity and the rest of the system are mimicked through the optimized one-body orbitals that are given by the projection $\hat{p}$, the storage of the full interacting problem is not necessary. Instead, the so called "non-interacting bath picture" can be implemented. Here, only the interactions within the impurity are taken into account, in other words, only the interaction tensor $U_{N_{\text{imp}}}$ of dimension $N_{N_{\text{imp}}} \times N_{N_{\text{imp}}} \times N_{N_{\text{imp}}} \times N_{N_{\text{imp}}}$ is built. Thus, the interactions within the embedded system and the interactions between impurity and embedded system are not taken into account when building the first projection $\hat{p}$ and are only later approximately included in the self-consistency loop.

7.2.2 Optimizing the full (embedded) 1RDM or only the 1RDM on the impurity

In order to find the non-local potential $\hat{W}$ that optimizes the projection $\hat{p}$, we minimize the difference between the 1RDM of the interacting system with the 1RDM of the non-interacting system. There are two possibilities how to do that in practice:

1. Compare the 1RDMs on the impurity
From the DMET calculation, we obtain the wave function of the embedded system $|\Psi_{\text{emb}}\rangle$. This wave function is in the original lattice-site basis on the impurity. Thus we can calculate the 1RDM on the impurity of the system

$$\gamma_{ij} = \langle\Psi_{\text{emb}}|\hat{c}_i^\dagger \hat{c}_j|\Psi_{\text{emb}}\rangle, \;\; i,j : 1..N_{\text{imp}} \tag{7.7}$$

and compare it with the 1RDM of the non-interacting system on the impurity

$$\gamma_{ij}^s = \langle\Phi|\hat{c}_i^\dagger \hat{c}_j|\Phi\rangle, \;\; i,j : 1..N_{\text{imp}}. \tag{7.8}$$

We see numerically that we can indeed find a non-local potential that leads to the same 1RDMs $\gamma_{ij}|_{N_{\text{imp}}} = \gamma_{ij}^s|_{N_{\text{imp}}}$. Unfortunately though, when comparing the 1RDMs restricted to the impurity, we encounter convergence issues for large interaction strength.

2. Compare the 1RDMs on the embedded system
Alternatively to solution 1, we can also compare the 1RDMs for the whole embedded system. In order to so, we also have to project the mean field Hamiltonian to the embedding basis

$$\hat{P}_{\text{red}}^{s\dagger} \hat{T} \hat{P}_{\text{red}}^s = \hat{T}_{\text{emb}}, \tag{7.9}$$

$$\hat{T}_{\text{emb}}|\Phi_{\text{emb}}\rangle = \tilde{E}|\Phi_{\text{emb}}\rangle \tag{7.10}$$

and then minimize

$$\min\left(\langle\Psi_{\text{emb}}|\hat{\text{c}}_\text{i}^\dagger \hat{\text{c}}_\text{j}|\Psi_{\text{emb}}\rangle - \langle\Phi_{\text{emb}}|\hat{\text{c}}_\text{i}^\dagger \hat{\text{c}}_\text{j}|\Phi_{\text{emb}}\rangle\right), \; \text{i,j} : 1...2\text{N}_{\text{imp}}. \tag{7.11}$$

In this approach, we see numerically that the two 1RDMs are never exactly the same which can lead to ambiguities in the non-local potential. It is far more stable for large interaction strength though, so in the following, this approach will be used.

The reason for the occuring instabilities and ambiguities will be analysed more in detail in chapter 11 of this thesis.

7.2.3 Symmetry breaking in DMET

In the DMET algorithm, we want to mimic the many body ground state wave function by a single Slater determinant which is the ground state wave function of an approximate mean field system. In other words: we want to describe a state that can only be determined exactly by a sum of Slater determinants by just one single Slater determinant.

In order to describe many body features in this way, we need to allow more degrees of freedom than usually existent in the mean-field description of the considered system. One way to expand the degrees of freedom of the Slater determinant is to explicitly break its symmetry at the cost of violating the conservation laws of the mean field description. In the DMET algorithm, this symmetry breaking is done with the non-local potential $\hat{W}_{N_{\text{imp}}}$.

In the self-consistency loop of the DMET algorithm, the non-local potential $\hat{W}_{N_{\text{imp}}}$, defined solely on the impurity is found which, added to the mean field embedding Hamiltonian $\hat{T}_{\text{emb}}$, yields the same 1RDM as the interacting embedding Hamiltonian $\hat{H}_{\text{emb}}$. Then, in order to improve the projection $\hat{P}_{\text{red}}^s$ we continue the $W_{N_{\text{imp}}}$ on full mean field Hamiltonian:

$$\hat{T}' = \hat{T} + \hat{V}. \tag{7.12}$$

The nonlocal potential $\hat{V}$ defined on the whole lattice is then

$$\hat{V} = \begin{pmatrix} \hat{V}_{N_{\text{imp}}} & 0 & 0 & 0 \\ 0 & \hat{V}_{N_{\text{imp}}} & 0 & 0 \\ 0 & 0 & \hat{V}_{N_{\text{imp}}} & 0 \\ 0 & 0 & 0 & \hat{V}_{N_{\text{imp}}} \end{pmatrix}. \tag{7.13}$$

Where we used the translational symmetry of the full system for the continuation of $\hat{V}_{N_{\text{imp}}}$ throughout the full system.

One condition the Hamiltonian $\hat{T}'$ has to fulfill (and that might not be seen immediately) is that it needs to break the translational symmetry that the system described by the exact Hamiltonian $\hat{H}$ has. If the translational symmetry of $\hat{T}'$ is not broken, the DMET procedure will immediately converge trivially and the gained observables from this DMET run will not approximate the interacting system in a good way. We explain this in more detail for the easy example of only 2 impurity lattice sites.

Example: Two impurity sites When taking into account only two impurity lattice sites, the $W_{N_{\text{imp}}}$ matrix only has two independent degrees of freedom: the densities n_1 and n_2 on the two sites are the same as both couple to each other and also to the embedding system equally, so translational invariance is preserved. The first off-diagonal elements, $\gamma_{12} = \gamma_{21}^*$ are each others complex conjugates. As we are only treating real numbers, $\gamma_{12} = \gamma_{21}$. So, after the first self-consistency loop, we get the correction matrix:

$$V_{N_{\text{imp}}} = \begin{pmatrix} v_1 & v_2 \\ v_2 & v_1 \end{pmatrix}. \tag{7.14}$$

Continuing as before through the whole lattice, we get

$$V = \begin{pmatrix} v_1 & v_2 & 0 & 0 & ... & v_2 \\ v_2 & v_1 & v_2 & 0 & ... & 0 \\ 0 & v_2 & v_1 & v_2 & ... & 0 \\ ... & ... & v_2 & v_1 & v_2 & ... \\ ... & ... & ... & ... & ... & \\ v_2 & 0 & 0 & ... & v_2 & v_1 \end{pmatrix}. \tag{7.15}$$

The V matrix, defined like this though does not change the projection at all: while the diagonal elements v_1 just add a phase to the Hamiltonian $\hat{T}'$, the off-diagonal elements v_2 trivially change the energy spectrum, but both elements do change the eigenfunctions of the Hamiltonian. This means that the DMET loop will stop after the first iteration and the projection will not be improved from the initial guess. So, we remain with the projection gained from the pure hopping Hamiltonian.

In order to fix this, instead of continuing $V_{N_{\text{imp}}}$ trivially, we break the translational symmetry by continuing like this:

$$V = \begin{pmatrix} v_1 & v_2 & 0 & 0 & ... & 0 \\ v_2 & v_1 & 0 & 0 & ... & 0 \\ 0 & 0 & v_1 & v_2 & ... & 0 \\ ... & 0 & v_2 & v_1 & 0 & .. \\ ... & ... & ... & ... & v_1 & v_2 \\ 0 & 0 & 0 & ... & v_2 & v_1 \end{pmatrix}. \tag{7.16}$$

This yields a new mean field Hamiltonian $\hat{T}'$ of the form:

$$\hat{T}' = \hat{T} + V = \begin{pmatrix} v_1 & v_2 & 0 & 0 & ... & -t \\ v_2 & v_1 & -t & 0 & ... & 0 \\ 0 & -t & v_1 & v_2 & ... & 0 \\ ... & 0 & v_2 & v_1 & -t & .. \\ ... & ... & ... & -t & v_1 & v_2 \\ -t & 0 & 0 & ... & v_2 & v_1 \end{pmatrix}. \tag{7.17}$$

When breaking the translational symmetry in this way, we get a non-trivial new projection which brings the 1RDMs of the interacting and the non-interacting embedding Hamiltonians closer and closer together and improves the results on the expense of violating a fundamental symmetry.

Generalizing the symmetry breaking While for the case of two impurity lattice sites, we have to introduce a symmetry breaking explicitly, this is not necessary if we consider more impurity lattice sites. The reason for this is that the symmetry in these cases will be automatically broken due to the projection of the exact Hamiltonian. Before the projection, we consider an on-site Hubbard

interaction that is only local on each site and a nearest neighbour hopping. While this remains exactly the same after the projection on the impurity, the interactions and correlations in the bath part of the Hamiltonian are changed dramatically by the projection: After rotating the Hamiltonian, each lattice site in the bath part of the embedding Hamiltonian is interacting with each other and also, the hopping term t' between any two lattice sites is non-zero. This leads to a different treatment of those impurity sites directly neighbouring the bath part of the Hamiltonian and those in the middle of the impurity: the lattice sites neighbouring the bath are now coupled to all bath lattice sites, while the lattice sites in the middle of the impurity remain only coupled to nearest neighbours by hopping and do not directly interact with each other.

This alone leads to a symmetry breaking in the matrix $V_{N_{\text{imp}}}$.

7.2.4 Degeneracy at the Fermi level

In step 2 of the practical implementation documented in section 7, it is stated that we build the 1RDM of the full system by filling up the natural orbitals with the lowest eigenenergies with two electrons per orbital. This is a problem though, if the eigenenergies of the one-particle spectrum are degenerate at the Fermi level because this means that there are two different orbitals with the same energy that need to be taken into account. For the one-dimensional Hubbard model, this problem occurs when the total particle number is divisible by four.

Solution 1
If we run into this problem, we can simply take into account all eigenvectors belonging to the same eigenenergy and occupy them with two, divided by the number of degenerate eigenvectors, $\frac{2}{\#\text{deg}}$.
In the one dimensional Hubbard model for example, we encounter a twofold degeneracy. We build the 1RDM taking the eigenvectors belonging to lowest $M/2-1$ eigenvalues. Then, we take the eigenvectors belonging to the eigenvalue of $M/2$ and $M/2+$, which has the same value and occupy each degenerate orbital once. This yields the correct 1RDM for the whole system.

When diagonalizing the environment 1RDM though, we see that not only N_{imp} of the eigenvalues are between zero and two but imp. We only choose the eigenvectors belonging to the inner $\#Imp$ to build the bath orbitals. As the correlated system has a gap, this problem only occurs in the first iteration and therefore does not yield a big error.

Solution 2
An (easier) way to circumvent this problem instead of solving it, is to choose the system properties so that no degeneracy occurs at the Fermi level: This can be done by choosing anti-periodic boundary conditions for the one-dimensional Hubbard model. As in this work, we mostly consider very big systems, and the behaviour of the system is not changed dramatically by anti-periodic instead of periodic boundary conditions, this is the solution we choose for the calculations depicted in part IV of this thesis.

Solution 3
Instead of changing the boundary conditions such that the degeneracy of the mean field system is broken, it is also possible to include a fictitious temperature in the mean field system. Analogue to implementing anti-periodic boundary conditions, this would also lead to a mean field system without degeneracy at the Fermi level.

7.3 Summary

In this chapter, we have given a recipe for the implementation of the DMET algorithm. Further, we have illustrated subtleties and tricks that can be found in the practical DMET implementation and indicated a few problems of this method.

Part III

Quantum phase transitions in the Hubbard-Holstein model

Chapter 8

The Hubbard Holstein model

Changing the phase of a material means changing its properties in a fundamental way, such as melting or freezing. While normal transitions in classical systems are usually driven by the competition between inner energy and entropy, in a quantum system even at temperature zero, phase transitions can be observed. Quantum phase transitions [62] do not occur, like classical phase transitions, due to thermal fluctuations, but due to the interplay of competing interactions in the Hamiltonian describing the system.

In quantum materials, the electron-electron and the electron-phonon interactions naturally compete against each other. This is most easily understood by noting that the Coulomb interaction between two electrons is generically repulsive, whereas electron phonon interactions can lead to effectively attractive electron-electron interactions. A good example for this is the Cooper pairing mechanism in conventional superconductors [2]. In strongly correlated low-dimensional materials, the competition between electron-electron and electron-phonon interactions has lead to longstanding debates for instance about the origin of high-temperature superconductivity and the anomalous normal states observed in entire classes of materials [57, 38]. At the same time, competing interactions lead to competing ground states and phase transitions that pose a major roadblock on the way towards reliable numerical solutions for the quantum many-body electron-phonon problem. In many-body quantum physics, interactions in the system are described by a Hamiltonian and phase transitions are driven by the competition of different terms in the Hamiltonian.

The goal of this part of the thesis is to characterize and understand quantum phase transitions in one dimensional systems and how this problem can be treated with the DMET method presented before. In orde to do that, we will first discuss the considered model and describe the analytically known limiting cases. After that, we will discuss the methods used to treat the full model. The first method is a generalization of the DMET method presented in the chapter before to electron-phonon systems. We also briefly present the generalization of the DMRG method to electron-phonon methods. Both generalizations have been derived by the author of this thesis in the scope of this thesis. Finally, the results obtained from the DMET method will be presented and compared to the results obtained by DMRG calculations and by a purely electronic DMET, where the lattice vibrations are taken into account for with the Born Oppenheimer approximation.

The work presented in this part of this thesis has been summarized in [53]

8.1 Hamiltonian

We choose the simplest possible model that can still describe electron-electron as well as electron-phonon interactions which is the one-dimensional Hubbard-Holstein Hamiltonian [14, 63]

$$\hat{H}_{\mathrm{el-phon}} = \underbrace{t \sum_{\langle i,j\rangle,\sigma} \hat{c}^\dagger_{i\sigma}\hat{c}_{j\sigma}}_{A} + \underbrace{U \sum_i \hat{n}_{i\uparrow}\hat{n}_{i\downarrow}}_{B} + \underbrace{\omega_0 \sum_i \hat{a}^\dagger_i \hat{a}_i}_{C} + \underbrace{\sum_{i,\sigma} \alpha_i (\hat{n}_{i\sigma})(\hat{a}^\dagger_i + a_i)}_{D} \tag{8.1}$$

Here, the first two terms describe the electronic part of the system:

A is a simplified description of the kinetic energy of the electrons where $\hat{c}_{j\sigma}$ is the particle annihilation and $\hat{c}^{\dagger}_{i\sigma}$ the particle creation operator of particles with spin $\sigma = \{\uparrow, \downarrow\}$: we assume that the itinerancy of the electrons decays exponentially with the distance, which is why we only consider next-neighbours hopping. Electrons can hop from one site to the adjacent site.

B is a simplified description of the Coulomb interaction between the electrons, where $\hat{n}_{i\uparrow} = \hat{c}^{\dagger}_{i\uparrow}\hat{c}_{i\uparrow}$ and $\hat{n}_{i\downarrow} = \hat{c}^{\dagger}_{i\downarrow}\hat{c}_{i\downarrow}$ are the density operators of spin up and down: We neglect long-range interactions of the electrons and only consider an on-site repulsion.

The third and fourth terms in the Hamiltonian describe the interactions of the electrons with the phonons. Phonons are quasi particles that we use to describe the lattice vibrations of solids. In the one dimensional Hubbard-Holstein Hamiltonian, they are approximately described by a harmonic linear chain. This is why we describe the phonons by a distorted quantum harmonic oscillators:

C describes the quantum harmonic oscillators in second quantization, where $\hat{a}_i$ is the phononic particle annihilation and $\hat{a}^{\dagger}_i$ the phononic particle creation operator.

D describes the coupling of the electrons to the phonons: electrons and phonons are coupled through the electronic density which distorts the phononic oscillator from its origin. $\left(\hat{a}^{\dagger}_i + a_i\right)$ corresponds to the displacement operator of the phonons on lattice site i.

In the Hubbard Holstein model, three competing forces that drive the system to different quantum phases can be detected: first, the electron hopping strength t, that leads to mobilization of the electrons and will put the system in a metallic phase. Second, the electron-electron interaction U that, if dominant, leads to an immobilized spin wave for the electronic degrees of freedom, that is, a Mott phase, which is insulating. Third, the electron-phonon coupling g, that, if dominant, leads to a Peierls phase, that is the position of the electrons on the lattice is distorted from their initial position, forming a charge density wave. Also the Peierls phase is insulating.

For the two limiting cases of no electron-phonon interaction and no electron-electron interaction, the Hamiltonian in Eq. (8.1) can be solved exactly and we know which phase to expect: In the case of no electron-phonon interaction, the interplay between the kinetic and the repulsion term of the electronic Hamiltonian plays a major role, which will result in a Mott phase. When neglecting electron-electron interactions, we expect to see a Peierls phase.

In between the two insulating phases (the Mott phase for strong electron-electron interactions and weak electron-phonon interactions and the Peierls phase for the opposite scenario), a metallic phase can be found. This phase occurs due to strong quantum fluctuations of the phonons, that can destroy the Peierls phase if the electron-electron interactions are not too strong to prevent this. This is why, we expect a metallic phase, when the two couplings, i.e. the electron-electron and the electron-phonon coupling compensate each other. We expect the metallic phase to be distinct when considering high phonon frequencies ω_0 in comparison to the itineracy of the electrons t. In contrast, if the phonon frequency is small compared to the electronic hopping, the metallic phase should, if existent, be smaller than for the opposed case.

Before discussing the full Hubbard Holstein model, we will first present known, exact results for the limiting cases and sketch their derivations.

8.2 Mott phase

The gapped phase of a Mott insulator, as opposed to conventional band insulators, occurs purely due to electron-electron interactions and is thus a true correlation effect. This is why, in order to predict the insulating Mott phase, conventional band theory, in which the interactions of the electrons are not considered, is not enough. In the Mott picture, whether a material is a metal or an insulator depends on the ratio between the interaction strengths of the electrons and the kinetic hopping term $\frac{U}{t}$. The material is in the metallic phase if the hopping term dominates over the electron electron repulsion $t \gg U$. On the other hand, the material is insulating for $t \ll U$. In the one dimensional case and for the purely electronic case at half filling it has been shown that the gap is always bigger than zero if $U > 0$ [41]. In order to gain a better understanding of where the Mott gap originates from, we

will briefly present the idea of the proof here. Considering the Hubbard model with N_α sites and N electrons on it:

$$\hat{H}_{\text{el}} = t \sum_{\langle i,j\rangle,\sigma} \hat{c}^\dagger_{i\sigma}\hat{c}_{j\sigma} + U \sum_i \hat{n}_{i\uparrow}\hat{n}_{i\downarrow} \tag{8.2}$$

As we do not include spin-flip terms in this Hamiltonian, the number of electrons with up- spin M and down-spin M' are conserved ($M + M' = N$). Assuming that $E(M, M'; U)$ is the ground state energy of the above Hamiltonian for a fixed number of particles and using particle-hole symmetry, one can show:

$$E(M, M'; U) = -(N_\alpha - M - M')\,U + E(N_\alpha - M, N_\alpha - M'; U)\,. \tag{8.3}$$

We define the gap $\Delta\mu = \mu_+ - \mu_-$ as the difference between the chemical potentials:

$$\mu_+ \equiv E(M+1, M; U) - E(M, M; U) \tag{8.4}$$
$$\mu_- \equiv E(M, M; U) - E(M-1, M; U) \tag{8.5}$$

inserting equation 8.3 into equation 8.4 yields:

$$\mu_+ = U - \mu_- \tag{8.6}$$

The proof of Lieb and Wu shows that, for temperature zero, in one dimension and for a half-filled system, the Hubbard Hamiltonian will always be in a gapped state, irrespective of the strength of the electron-electron interaction (excluding $U = 0$).

When including electron-phonon interactions though, even in one dimension a richer phase diagram, including a metallic phase and a Peierls phase can be found. On the other hand, this problem is not addressable analytically anymore.

8.3 Peierls phase

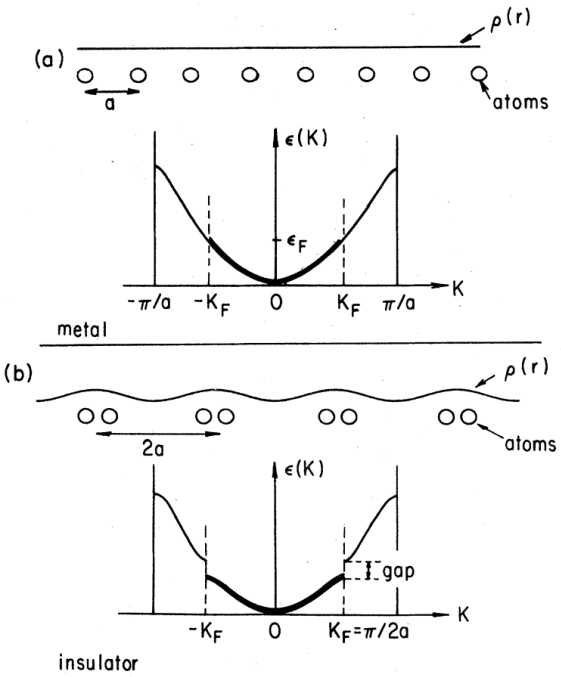

Figure 8.1: Without electron-electron interaction and for a half filled Holstein system at temperature 0, the ions in the lattice always lead to a dimerization of the electronic chain. This situation is energetically more favorable because, due to the doubling of the period, more bands appear, leading to a gap opening at the Fermi level. This graph is from the book "Density waves in solids" by George Grüner [18].

The Peierls instability or dimerization occurs when the electron-phonon interaction dominates the electron-electron interaction. For a half filled system without electron-electron interaction and at

temperature zero, a dimerization of the lattice always occurs, that is, this lattice will always be in the Peierls phase. This can be proven exactly [31], but also intuitively understood as is explained in the book by Peierls himself [50]. Consider a 1D electron chain with a constant distance between the electrons of a.

The Bloch band of this setup will then look like figure 8.1: For a half filled system, the electrons will fill up the band until the Fermi energy ϵ_F which corresponds to a position in k-space of K_F. If the distance between nuclei is not uniform, but instead they are dimerized in pairs of two due to the electron-phonon interaction (which in the Holstein model is an interaction of the electron density with the phononic distortion from the zero position), this corresponds to the doubling of the unit cell to 2a. It leads to a loss in energy between the electrons that are now closer together, but a gain in energy between the electrons that are further apart. For the half filled system at temperature zero, the energy gain due to gap opening is always bigger than the loss of elastic energy of the electrons.

8.4 Summary

In this chapter, we discussed the term quantum phase transitions in connection with the Hubbard Holstein model, which is a minimal model for the quantum mechanical description of coupled electron-phonon systems. We then investigated the phase diagram of the Hubbard Holstein model by discussing the analytically known limiting case of the Mott and the Peierls phase and showing what is expected for the full model.

Chapter 9

Methods

The one dimensional Hubbard Holstein model, although it is the easiest model that considers both electron-electron as well as electron-phonon interactions, cannot be solved analytically. However, it has been studied with a lot different numerical methods, such as the Density Matrix Renormalization group (DMRG) [13], Quantum Monte-Carlo (QMC) [8, 19, 22, 66, 48, 28] and dynamical mean field theory (DMFT) [68, 45, 3]. In this thesis, we analyze the quantum phase transitions discussed in chapter 8 with the Density Matrix Embedding Theory introduced in part II and compare to results obtained with a DMRG solver.Also, in the DMET method, we use a DMRG solver to diagonalize the small embedding. In the following, we will very briefly discuss the expansion of the DMRG solver implemented by Claudius Hubig to treat electron phonon systems. Then, we will discuss more in detail the expansion of the DMET algorithm to coupled electron-phonon systems.

9.1 DMRG for coupled electron-phonon systems

Throughout this thesis, we use the Density Matrix Renormalizatiom Group, specifically, the syten library [24, 25], as a solver for our DMET systems. In order to use DMRG for the coupled electron-phonon system at hand, we expanded the syten library to be able to treat electron-boson systems.

As explained in section 2.2, DMRG is an efficient wave function method. In this method, the wave function is decomposed as a Matrix Product State (MPS) and the Hamiltonian as a Matrix Product Operator (MPO). Using the gauge freedom of this description (as explained in detail in section 2.2.3) makes it possible to apply the Hamiltonian (MPO) locally to each lattice site (MPS) and then updating the whole system.

In the syten library, instead of defining one MPS consisting of N tensors, where N is the number of lattice sites in the system, an MPS consisting of $2N$ lattice sites is defined. All even lattice sites are then phononic and all odd lattice sites are electronic. The electronic sites are treated with the fermionic commutation relations while the phononic sites are treated with the bosonic commutation relations, making it possible to have a big number of basis functions per site.

Additionally, local MPOs, that is, the local particle creation and annihilation operators $\hat{c}_i^\dagger, \hat{c}_i$ for the fermionic particles and $\hat{a}_i^\dagger, \hat{a}_i$ for the bosonic particles are defined such that the bosonic MPOs only interact with the bosonic MPS lattice sites and the fermionic MPOs only interact with the fermionic MPS lattice sites.

The gloabl Hamiltonian $\hat{H}_{\mathrm{el-phon}}$ is then build up from these local operators where the transition elements $t_{ij}, U_{ijkl}, \omega_{ij}, g_{ijk}$ of the individual parts of the Hamiltonian are handed over to the syten code explicitly when starting the calculation.

Then, the interactions between two bosonic, between two fermionic and between a bosonic and a fermionic site are defined differently. With this setup of a new lattice with $2 \cdot N$ lattice sites, the ususal DMRG algorithm can be used.

Scaling of DMRG

The purely fermionic syten-DMRG code scales with $\propto m^3 \cdot d \cdot w$, where m is the bond dimension (as explained in section 2.2), d is the physical dimension of the local MPS (that is, 4 for fermions and N_{phon} for bosons) and w is the bond dimension of the MPO.

This means that, due to the phonons, the DMRG code will be linearly slowed down due to the doubling of the total lattice sites (N fermionic and N bosonic sites) and due to the higher amount of basis functions per lattice site d.

9.2 DMET for coupled electron-phonon systems

In order to generalize DMET to coupled electron-phonon systems, we need to find a projection P that projects the whole, coupled electron-phonon Hamiltonian

$$\hat{H}_{\text{el-ph}} = \hat{T}_{\text{el}} + \hat{U}_{\text{el}} + \hat{T}_{\text{ph}} + \hat{U}_{\text{el-ph}} \tag{9.1}$$

into a new embedding basis:

$$\hat{H}^{\text{emb}}_{\text{el-ph}} = \hat{P}^\dagger \hat{H}_{\text{el-ph}} P. \tag{9.2}$$

Similar to the purely electronic case, we find this projection by assuming a non-interacting system, which then allows us to make a product ansatz between the electronic and phononic degrees of freedom as is visualized in figure 9.1. Instead of finding one projection for the coupled electron-phonon system, we thus have to find two projections, one for the electrons and one for the phonons. The electronic projection is then, as in the original scheme, approximated by the ground state of $\hat{H}^{\text{proj}}_{\text{el}}$ (section 5.2.6)

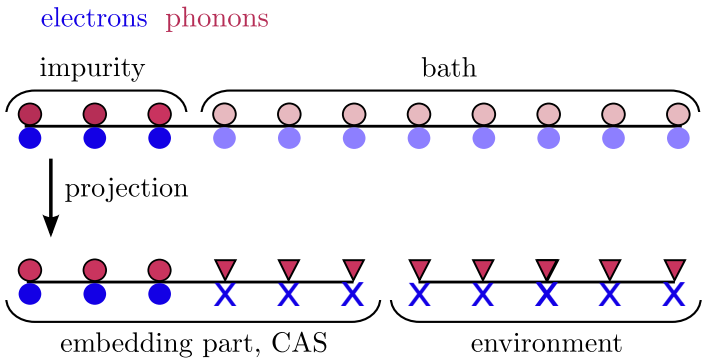

Figure 9.1: Visualization of the decomposition of the electron-phonon model system via the projection P: Starting with a 1D lattice in real space that on each site has both electronic (blue) as well as phononic (red) degrees of freedom, we choose one part of the system that is from then on called impurity, whereas the rest is the bath. The projection leaves the basis on the impurity the same (a real space lattice), whereas it projects the bath degrees of freedom into a new basis set whose physical meaning is abstract. Within this new basis set, the environmental degrees of freedom can be divided into those having an overlap with the impurity lattice sites and those that do not have an overlap with the impurity lattice site, called environment. The physics on the impurity is determined by the impurity and the embedding part of the system only. Sketch from [53].

9.2.1 Generalized coherent states

In order to find the projection for the phononic degrees of freedom we choose a set of shifted harmonic oscillators, which is a Hamiltonian of the same form as the electron-phonon Hamiltonian Eq. (8.1):

$$\hat{H}_{\text{ph}} = \sum_i \omega_0 \hat{a}_i^\dagger \hat{a}_i + \sum_{i,\sigma} g_i (\hat{a}_i^\dagger + \hat{a}_i) = \hat{T}_{\text{ph}} + \hat{C}_{\text{ph}}. \tag{9.3}$$

The first part of this Hamiltonian is set of simple quantum harmonic oscillators (one harmonic oscillator for each lattice site i), while the second part describes a distortion $z_i = \left\langle \hat{a}_i^\dagger + \hat{a}_i \right\rangle$ from the resting position on lattice site i. In order to describe the state of the system on lattice site i with Fock

number states (that is, the eigenstates of the quantum harmonic oscillator that are usually used), an infinite number of these Fock number states is needed and the particle number for each lattice site is not fixed:

$$|\xi_i\rangle = \sum_{\alpha}^{\infty} \xi_i^{\alpha} \hat{a}_{\alpha}^{\dagger} |0\rangle \tag{9.4}$$

As this is not an optimal description of the problem, we redefine the eigenstates of the harmonic oscillator allowing us to effectively describe the shifted harmonic oscillator [6, pp.18]. The ground state wave function of the shifted harmonic Oscillator is the product state of coherent states on each lattice site k:

$$|Z\rangle = \bigotimes_k \alpha_k |z_k\rangle \tag{9.5}$$

$$|z_k\rangle = e^{a_k^{\dagger} z_k}|0\rangle = e^{-|z_k|^2/2} \sum_{j=0}^{\infty} \frac{(z_k)^j}{\sqrt{j!}} |j\rangle. \tag{9.6}$$

A coherent state $|z_k\rangle$ is a quantum harmonic oscillator that is shifted with respect to its initial position, where $z_k = \left\langle \hat{a}_k^{\dagger} + \hat{a_k} \right\rangle$ is the shift of the phonon mode from the initial position on the lattice site k. In order to describe the non-interacting Hamiltonian defined in 9.3, only one state $|z_k\rangle$ per site is needed. For the interacting problem though, the simple shifted harmonic oscillator is not the exact eigenstate, as here, electron-phonon interactions need to be included. Thus, in order to describe the full Hamiltonian, we choose a linear combination of coherent states to describe the interacting problem.

Similar to the electronic case Eq. (5.60), we determine the phononic projection by splitting the phononic wave function up into three parts:

$$|Z\rangle = \sum_{\alpha,\beta}^{N_{\mathrm{ph}}^{N_{\mathrm{imp}}}} |A_{\alpha}^{\mathrm{ph}}\rangle |B_{\beta}^{\mathrm{ph}}\rangle \otimes \sum_{j}^{N_{\mathrm{ph}}^{N-N_{\mathrm{imp}}}} |\tilde{B}_j^{\mathrm{ph}}\rangle. \tag{9.7}$$

Here, the $|A_{\alpha}^{\mathrm{ph}}\rangle$ are again just defined on the impurity region of the lattice, $|B_{\beta}^{\mathrm{ph}}\rangle$ is composited by those coherent states that have an overlap over the impurity region and $|\tilde{B}_j^{\mathrm{ph}}\rangle$ is composited by the coherent states that do not have an overlap over the impurity region. Neglecting again the part of the wave function that does not have an influence on the impurity, we define the phononic projection as:

$$P'_{\mathrm{ph}} = \sum_{\alpha,\beta}^{N_{\mathrm{ph}}^{N_{\mathrm{imp}}}} |A_{\alpha}^{\mathrm{ph}}\rangle |B_{\beta}^{\mathrm{ph}}\rangle \langle B_{\beta}^{\mathrm{ph}}| \langle A_{\alpha}^{\mathrm{ph}}| = \sum_{\alpha,\beta}^{N_{\mathrm{ph}}^{N_{\mathrm{imp}}}} |A_{\alpha}^{\mathrm{ph}} C_{\beta}^{\mathrm{ph}}\rangle \langle A_{\alpha}^{\mathrm{ph}} C_{\beta}^{\mathrm{ph}}|. \tag{9.8}$$

Then, analogous to the electronic procedure, we again define

$$|A_{\alpha}^{\mathrm{ph}} B_{\beta}^{\mathrm{ph}}\rangle = |\tilde{C}_{\alpha}^{\mathrm{ph}}\rangle + |\tilde{C}_{\alpha}^{*\mathrm{ph}}\rangle \tag{9.9}$$

such that

$$|\tilde{C}_{\alpha}^{\mathrm{ph}}\rangle = |A_{\alpha}\rangle, \qquad \text{for } \alpha : 1, ...\mathrm{N}_{\mathrm{ph}}^{\mathrm{N_{imp}}}, \tag{9.10}$$

$$|\tilde{C}_{\alpha}^{\mathrm{ph}}\rangle = 0, \qquad \text{otherwise}, \tag{9.11}$$

$$|\tilde{C}_{\alpha}^{*\mathrm{ph}}\rangle = 0, \qquad \text{for } \alpha : 1, ...\mathrm{N}_{\mathrm{ph}}^{\mathrm{N_{imp}}}, \tag{9.12}$$

$$|\tilde{C}_{\alpha}^{*\mathrm{ph}}\rangle = |B_{\alpha}\rangle, \qquad \text{otherwise}, \tag{9.13}$$

which yields the projection

$$\begin{aligned} \hat{P}'_{\mathrm{ph}} &= \sum_{\gamma=1}^{4^{N_{\mathrm{imp}}}} \left(|\tilde{C}_{\alpha}^{\mathrm{ph}}\rangle \langle \tilde{C}_{\alpha}^{\mathrm{ph}}| \; + \; |\tilde{C}_{\alpha}^{*\mathrm{ph}}\rangle \langle \tilde{C}_{\alpha}^{*\mathrm{ph}}| \right), \\ &= \sum_{\gamma=1}^{2\cdot 4^{N_{\mathrm{imp}}}} |\tilde{C}_{\gamma}^{\mathrm{ph}}\rangle \langle \tilde{C}_{\gamma}^{\mathrm{ph}}| \qquad \tilde{C}_{\alpha}^{\mathrm{ph}} = \tilde{C}_{\gamma} \;\text{ for }\; \alpha = 1, ..., \mathrm{N_{imp}}, \gamma = 1, ...\mathrm{N_{imp}}, \\ &\qquad\qquad\qquad\qquad \tilde{C}_{\alpha}^{*\mathrm{ph}} = \tilde{C}_{\gamma}^{\mathrm{ph}} \;\text{ for }\; \alpha = \mathrm{N_{imp}} + 1, ..., 2\mathrm{N_{imp}}, \gamma = 1, ...\mathrm{N_{imp}}. \end{aligned} \tag{9.14}$$

The $\tilde{C}_\gamma^{\mathrm{ph}}$ are not normalized yet:

$$\hat{P}'_{\mathrm{ph}} = \sum_{\gamma=1}^{2\cdot 4^{N_{\mathrm{imp}}}} \|\tilde{C}_\gamma^{\mathrm{ph}}\| |C_\gamma^{\mathrm{ph}}\rangle\langle C_\gamma^{\mathrm{ph}}|. \tag{9.15}$$

We thus define the projection used in the phononic DMET algorithm as

$$\hat{P}_{\mathrm{ph}} = \sum_{\gamma=1}^{2\cdot 4^{N_{\mathrm{imp}}}} |C_\gamma^{\mathrm{ph}}\rangle\langle C_\gamma^{\mathrm{ph}}|. \tag{9.16}$$

Due to the bosonic nature of the phonons, the number of basis functions per site, N_{ph} will go to infinity for an accurate calculation. As the coherent state basis is very close to the optimal basis for the description of the Hubbard Holstein Hamiltonian though, taking 8 basis states per phononic sites is enough to converge the results within our error estimate.

9.2.2 Projection of the full Hamiltonian

Knowing the two projections, we are now able to find the embedding Hamiltonian of the coupled system

$$\hat{H}^{\mathrm{emb}}_{\mathrm{el-ph}} = \hat{P}^\dagger_{\mathrm{ph}}\hat{P}^\dagger_{\mathrm{el}}\hat{H}_{\mathrm{el-ph}}\hat{P}_{\mathrm{el}}\hat{P}_{\mathrm{ph}}. \tag{9.17}$$

The purely electronic part of the Hamiltonian is treated as before with the electronic projection $\hat{P}_{\mathrm{el}}$ (this has been explained in detail in section 5.3):

$$\hat{H} = \hat{T}_{\mathrm{el}} + \hat{U}_{\mathrm{el}} + \hat{T}_{\mathrm{ph}} + \hat{U}_{\mathrm{el-ph}} \tag{9.18}$$

$$\hat{T}^{\mathrm{emb}}_{\mathrm{el}} = \hat{P}^\dagger_{\mathrm{el}}\hat{T}_{\mathrm{el}}\hat{P}_{\mathrm{el}} \tag{9.19}$$

$$\hat{U}^{\mathrm{emb}}_{\mathrm{el}} = \hat{P}^\dagger_{\mathrm{el}}\hat{P}^\dagger_{\mathrm{el}}\hat{U}_{\mathrm{el}}\hat{P}_{\mathrm{el}}\hat{P}_{\mathrm{el}}. \tag{9.20}$$

The purely phononic part of the Hamiltonian, $\hat{T}_{\mathrm{ph}}$, is treated analogously to the electronic hopping part of the Hamiltonian Eq. (5.114), but with the phononic part of the Projection $\hat{P}_{\mathrm{ph}}$:

$$\hat{T}^{\mathrm{emb}}_{\mathrm{ph,ab}} = \sum_i \sum_{a,b} \hat{P}^{\dagger,ai}_{\mathrm{ph}}\hat{T}_{\mathrm{ph,ii}}\hat{P}^{ib}_{\mathrm{ph}} \tag{9.21}$$

$$= \sum_i \sum_{a,b} \omega_0 \hat{P}^{\dagger,ai}_{\mathrm{ph}}\hat{a}^\dagger_i\hat{a}_i\hat{P}^{ib}_{\mathrm{ph}} \tag{9.22}$$

$$= \sum_{a,b} \omega_0 \hat{a}'^\dagger_a\hat{a}'_b. \tag{9.23}$$

The interaction part of the Hamiltonian, contains electronic as well as phononic degrees of freedom:

$$\hat{U}_{\mathrm{el-ph}} = \sum_{i,\sigma} \alpha(\hat{c}^\dagger_{i\sigma}\hat{c}_{i\sigma})(\hat{a}^\dagger_i + \hat{a}_i) \tag{9.24}$$

$$= \sum_{i,\sigma} \alpha(\hat{c}^\dagger_{i\sigma}\hat{c}_{i\sigma})\hat{a}^\dagger_i + \sum_{i,\sigma} \alpha(\hat{c}^\dagger_{i\sigma}\hat{c}_{i\sigma})\hat{a}_i \tag{9.25}$$

Specifically, we have two electronic degrees of freedom and one phononic degree of freedom that need to be rotated. Similar to Eq. (5.115), we define the projection of the phononic creation and annihilation operators as:

$$\sum_i P^\dagger_{\mathrm{ph},\alpha i}\hat{a}^\dagger_i = \hat{a}^\dagger_{\alpha,\mathrm{emb}} \tag{9.26}$$

$$\sum_i \hat{a}_{i\sigma}P_{\mathrm{ph,i}\alpha} = \hat{a}_{\alpha\sigma,\mathrm{emb}}. \tag{9.27}$$

From this definition, we find the projected electron-phonon interaction term as:

$$\hat{U}^{\text{emb}}_{\text{el-ph}} = \sum_{a,b,c}\sum_{i,\sigma} \alpha(\hat{P}^{\dagger,ai}_{\text{el}}\hat{c}^{\dagger}_{i\sigma}\hat{c}_{i\sigma}\hat{P}^{ib}_{\text{el}})\hat{P}^{\dagger,ci}_{\text{ph}}\hat{a}^{\dagger}_{i} + \sum_{a,b,c}\sum_{i,\sigma} \alpha(\hat{P}^{\dagger,ai}_{\text{el}}\hat{c}^{\dagger}_{i\sigma}\hat{c}_{i\sigma}\hat{P}^{ib}_{\text{el}})\hat{a}_{i}\hat{P}^{ic}_{\text{ph}} \tag{9.28}$$

$$= \sum_{a,b,c,\sigma} \alpha(\hat{c}^{'\dagger}_{a\sigma}\hat{c}'_{b\sigma})\hat{a}^{'\dagger}_{c} + \sum_{a,b,c,\sigma} \alpha(\hat{c}^{'\dagger}_{a\sigma}\hat{c}'_{b\sigma})\hat{a}'_{c} \tag{9.29}$$

$$= \sum_{a,b,c,\sigma} \alpha(\hat{c}^{'\dagger}_{a\sigma}\hat{c}'_{b\sigma})(\hat{a}^{'\dagger}_{c} + \hat{a}'_{c}). \tag{9.30}$$

Note that, although the Hamiltonian before the rotation had a diagonal form (that is, the sum was only over one index, i), it is not diagonal anymore after the transformation. In fact, the new embedding Hamiltonian $\hat{H}_{\text{emb}}$ does not have any structured form any more after transformation. Also, as there are long-range interactions in this new Hamiltonian, the DMRG calculation gets more costly as larger bond dimensions have to be considered.

9.2.3 Improving the projection

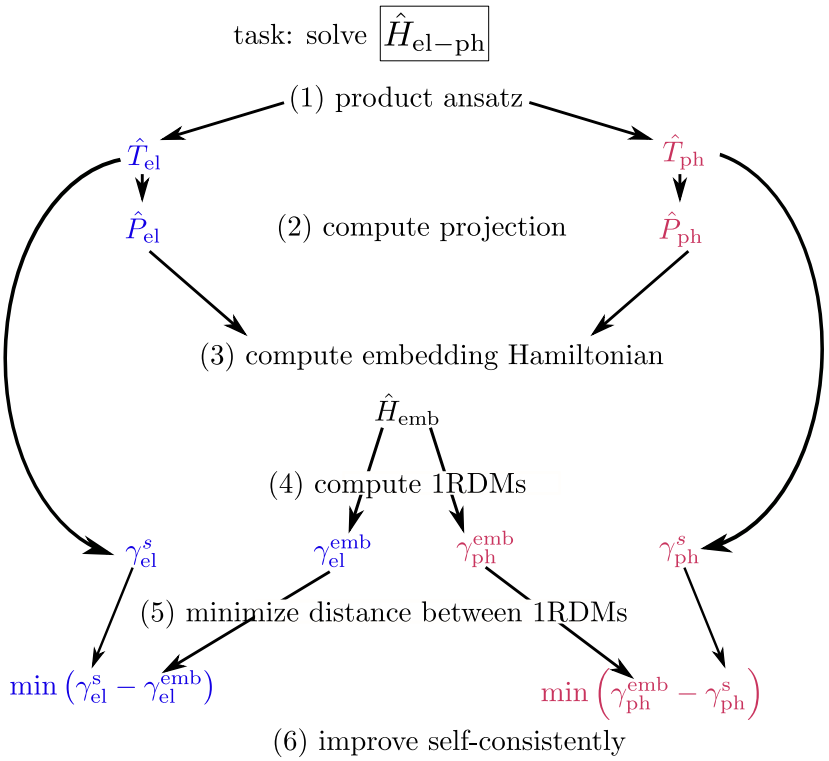

Figure 9.2: Visualization of the DMET procedure: from the purely electronic and the purely fermionic projection Hamiltonians $\hat{H}^{\text{proj}}_{\text{el}}$ and $\hat{H}^{\text{proj}}_{\text{ph}}$, we get the projections $\hat{P}_{\text{el}}$ and $\hat{P}_{\text{ph}}$. Applied to the full Hubbard-Holstein Hamiltonian $\hat{H}_{\text{el-ph}}$ these yield the embedding Hamiltonian $\hat{H}^{\text{emb}}_{\text{el-ph}}$ that, due to its small size, can be calculated accurately. In order to improve the projections $\hat{P}_{\text{el}}$ and $\hat{P}_{\text{ph}}$, we aim at making the (electronic and phononic) 1RDM properties of the interacting ($\gamma^{\text{emb}}_{\text{ph}}$ and $\gamma^{\text{emb}}_{\text{ph}}$) and the non interacting systems (γ^{s}_{ph} and γ^{s}_{ph}) as similar as possible. This is done by adding non-local potentials to the projecting Hamiltonians that minimize the difference between the one-body observables of the interacting system and the non-interacting systems. When the new potentials are found, new projections can be calculated which yield a new embedding Hamiltonian. This procedure is repeated until self-consistency.

Again the initial guess for the projection is not necessarily very good as additionally to assuming a non-interacting active space for both the electrons as well as the phonons, it also assumes a product state between electronic and phononic degrees of freedom. We self-consistently optimize the electronic and the phononic projection, where for the electronic case we proceed similar as for the purely electronic problem as explained in section 5.4.

For the phonons, we have to compare two properties as the initial Hamiltonian also has two terms:

$$\hat{H}^{\text{proj}}_{\text{ph}} = \hat{T}_{\text{ph}} + \hat{V}_{\text{ph}} + \hat{C}_{\text{ph}} + \hat{W}_{\text{ph}}. \tag{9.31}$$

While $\hat{V}_{\text{ph}}$ is dependent on the phononic reduced one-particle density matrix $\langle \hat{a}_i^\dagger \hat{a}_j \rangle$, $\hat{W}_{\text{ph}}$ depends on the shift of the phonons from zero $\langle \hat{a}_i^\dagger + \hat{a}_i \rangle$. The potentials are again found by minimizing the difference between the properties of the interacting and the mean field system:

$$\begin{aligned} \min \Bigg| & \sum_{i,j \in \text{imp}} \left\langle \Psi_{\text{emb}} | a_i^\dagger a_j | \Psi_{\text{emb}} \right\rangle - \left\langle Z | a_i^\dagger a_j | Z \right\rangle \\ & + \sum_{i \in \text{imp}} \left\langle \Psi_{\text{emb}} | \hat{a}_i^\dagger + \hat{a}_i | \Psi_{\text{emb}} \right\rangle - \left\langle Z | \hat{a}_i^\dagger + \hat{a}_i | Z \right\rangle \Bigg|, \end{aligned} \tag{9.32}$$

where $|Z\rangle$ is the ground-state wave function of the Hamiltonian defined in Eq. (9.31) and $|\Psi\rangle$ is the ground state wave function of the full Hubbard Holstein Hamiltonian defined in Eq. (9.1). The whole DMET procedure is visualized in figure 9.2.

The small embedding problem is then solved using the DMRG code generalized to phonon-electron problems, explained in section 9.1.

9.3 Born Oppenheimer approximation

The question arises whether the extensive treatment of the fully quantized electron-phonon Hamiltonian is necessary in order to capture the full phase diagram of the Hubbard Holstein model. In order to clarify this question, we compare our results with the Born Oppenheimer (BO) Hamiltonian in the one dimensional Hubbard Holstein mode, where the quantum nature of the electrons is fully conserved but the phonons are treated as classical nuclei.

In order to do so we derive the Born Oppenheimer Hamiltonian. The full Hubbard Holstein Hamiltonian, as already written in section 8 reads:

$$\hat{H}_{\text{el-phon}} = t \sum_{\langle i,j \rangle, \sigma} \hat{c}_{i\sigma}^\dagger \hat{c}_{j\sigma} + U \sum_i \hat{n}_{i\uparrow} \hat{n}_{i\downarrow} + \omega_0 \sum_i \hat{a}_i^\dagger \hat{a}_i + \sum_{i,\sigma} \alpha_i (\hat{n}_{i\sigma})(\hat{a}_i^\dagger + a_i) \tag{9.33}$$

The particle creation and annihilation operators are defined as

$$\hat{a}_i = \sqrt{\frac{\omega_0}{2}} \left(\hat{x}_i + \frac{i}{\omega_0} \hat{p}_i \right) \tag{9.34}$$

$$\hat{a}_i^\dagger = \sqrt{\frac{\omega_0}{2}} \left(\hat{x}_i - \frac{i}{\omega_0} \hat{p}_i \right) \tag{9.35}$$

from which follows

$$\hat{a}_i^\dagger \cdot \hat{a}_i = \frac{\omega_0}{2} \hat{x}_i^2 + \frac{1}{2\omega_0} \hat{p}_i^2 \tag{9.36}$$

$$\hat{a}_i^\dagger + \hat{a}_i = \sqrt{2\omega_0} \hat{x}_i \tag{9.37}$$

rewriting the Hamiltonian to:

$$\hat{H}_{\text{el-phon}} = t \sum_{\langle i,j \rangle, \sigma} \hat{c}_{i\sigma}^\dagger \hat{c}_{j\sigma} + U \sum_i \hat{n}_{i\uparrow} \hat{n}_{i\downarrow} + \omega_0 \sum_i \left(\frac{\omega_0}{2} \hat{x}_i^2 + \frac{1}{2\omega_0} \hat{p}_i^2 \right) + g n_i \sqrt{2\omega_0} \hat{x}_i. \tag{9.38}$$

In the Born-Oppenheimer approximation, we assume the nuclei on the one hand side to be classical particles and on the other hand to be much slower than the electrons; thus we can neglect their kinetic energy, which yields:

$$\hat{H}_{\text{el-phon}} = t \sum_{\langle i,j \rangle, \sigma} \hat{c}_{i\sigma}^\dagger \hat{c}_{j\sigma} + U \sum_i \hat{n}_{i\uparrow} \hat{n}_{i\downarrow} + \sum_i \frac{\omega_0^2}{2} x_i^2 + \cancel{\sum_i \frac{1}{2} p_i^2} + \sum_i g n_i \sqrt{2\omega_0} x_i. \tag{9.39}$$

We can now treat this Hamiltonian with purely electronic DMET, where the ionic term is simply a constant in the energy contribution In the DMET calculation, we optimize the distortion of the nuclei $\hat{x}_i$ to minimize the total energy, yielding the electronic potential energy surfaces.

Chapter 10

Results for the computation of the Hubbard Holstein model

10.1 Defining observables and parameters

10.1.1 Observables

In order to describe the phase transition of the one dimensional Hubbard Holstein model, we need to define observables that unambiguously show which phase the system is in. One observable that unambiguously shows whether we are in an insulating or a metallic phase is the energy gap, defined as

$$\Delta c_{\mathrm{SP}} = 2 \cdot E_0^{\mathrm{N}/2} - E_0^{\mathrm{N}/2-1} - E_0^{\mathrm{N}/2+1}, \tag{10.1}$$

where $E_0^{N/2}$ is the ground state energy of the Hamiltonian for half filling, $E_0^{N/2-1}$ is the ground state energy of the system for half filling minus one and $E_0^{N/2+1}$ is the energy of the system for half filling plus one.

While it is in general possible (but cumbersome) to treat open shell systems in the DMET method, we did not include this feature in our implementation. Thus, we cannot measure the energy gap defined in Eq. (10.1) directly. We thus choose a relatively simple approximation: Instead of doing three calculations with different particle numbers, we consider our *sophisticated mean field* Hamiltonian

$$\hat{H}_{\mathrm{el-ph}}^{\mathrm{proj}} = \hat{T}_{\mathrm{el}} + \hat{V}_{\mathrm{el}} + \hat{T}_{\mathrm{ph}} + \hat{V}_{\mathrm{ph}} + \hat{C}_{\mathrm{ph}} + \hat{W}_{\mathrm{ph}} \tag{10.2}$$

which is optimized to have similar one-body properties as the interacting Hamiltonian. We calculate the spectrum $\{\epsilon_i\}$ of this non-interacting Hamiltonian by diagonalizing it and then approximate the gap by defining

$$\begin{aligned} \Delta c &= 2 \cdot E_0^{\mathrm{N}/2} - E_0^{\mathrm{N}/2-1} - E_0^{\mathrm{N}/2+1} \\ &= 2 \cdot \sum_{i=1}^{N/2} \epsilon_i - \sum_{i=1}^{N/2-1} \epsilon_i - \sum_{i=1}^{N/2+1} \epsilon_i, \end{aligned} \tag{10.3}$$

In order to further monitor the phase transitions of the Hubbard Holstein model and to distinguish between the Mott and the Peierls phase (which are both gapped phases), we additionally show two more observables, namely the the double occupancy $\langle n_{i\uparrow} n_{i\downarrow} \rangle$ and the electronic density difference between neighbouring sites $\langle n_i \rangle - \langle n_{i+1} \rangle$ which are both local properties and can simply be calculated on one arbitrary (impurity) site.

The double occupancy measures the probability of finding two electrons (one electron with spin up and one electron with spin down) on one lattice site. For half filling and in the limiting case of the system being deeply in the Peierls phase (that is, very small electron-electron interaction and high electron-phonon interaction) or far in the regime of a Mott phase (that is, very strong electron-electron interaction and weak electron-phonon interaction), one can intuitively understand what to

expect: If we have a strong Peierls phase, the electron density will not be homogeneous anymore. The maximum density deviation between adjacent electronic sites possible is to have two electrons on one site and zero electrons on the adjacent site. This situation will lead to a double occupancy of $\langle n_{i\uparrow} n_{i\downarrow} \rangle = \left\langle \frac{n_{i\uparrow} n_{i\downarrow} + n_{i+1\uparrow} n_{i+1\downarrow}}{2} \right\rangle = \frac{1+0}{2} = 0.5$ for the whole system. In the case of an extreme Mott phase, we expect the opposite: the electron-electron repulsion is strong in comparison to the hopping, leading to electrons that are localized on the lattice site; per lattice site, only one electron can be found, leading to a double occupancy of zero. In the metallic phase and for a half filled system, the electrons are not bound to the lattice sites; on average, we find every possible distribution to equally probable. This leads to a double occupancy of $\langle n_{i\uparrow} n_{i\downarrow} \rangle = \langle 0.5 \cdot 0.5 \rangle = 0.25$.

The electronic density difference between neighbouring sites only indicates the transition to the Peierls phase: While in the Mott phase, the electronic density distribution stays homogeneous, in the Peierls phase we observe an electronic density oscillation, that is, the electronic density on site i will be much higher/lower than on site $i+1$.

10.1.2 Parameters

The phase transition depends on the itineracy of the electrons ($\propto t$), the electron-electron repulsion ($\propto U$), the electron-phonon interaction ($\propto g$) and the phonon frequency with respect to the electrons. This is why, we introduce the adiabaticity ratio

$$\alpha = \frac{\omega_0}{t} \tag{10.4}$$

accounting for the relation between the kinetic hopping energy of the electrons t and the frequency of the phonons ω_0 and we also decide to discuss our results in terms of dimensionless coupling constants:

$$u = \frac{U}{4t}, \quad \lambda = \frac{g^2}{2t\omega_0} \tag{10.5}$$

Computational scaling

One of the biggest selling points of DMET is low computational costs in comparison to methods such as DMRG or the different flavours of DMFT. In DMET, we calculate the big system with a low accuracy method, whose computational costs scales quadratic with total lattice size. Additionally, we diagonalize the interacting Hamiltonian of the small embedding system; this calculation scales like the chosen solver (in our case, DMRG) for the impurity size. As we improve the estimate of the projection, the whole calcuation has to be performed various times until self-consistency.

As already mentioned, in this work we use a DMRG solver that scales approximately with $\left(N_{\text{imp}}^{\text{el}}\right)^3 \cdot \left(N_{\text{imp}}^{\text{ph}}\right)^3$, leading to a total scaling of $\eta \left[\left(N_{\text{imp}}^{\text{el}}\right)^3 \cdot \left(N_{\text{imp}}^{\text{ph}}\right)^3 \cdot \left(N^{\text{el}}\right)^2 \cdot \left(N^{\text{ph}}\right)^2\right]$, where η is the amount of iterations needed until convergence.

10.2 Extrapolation and convergence

While the Hubbard-Holstein model describes a translational invariant, infinite solid, in our simulations, we can only consider finite systems. This discrepancy can lead to errors in our calculation which in the following, we try to annihilate or, if not possible, discuss in detail.

In this thesis, we are discussing two different methods, DMRG and DMET and compare them; for both methods, we need to perform extrapolations and consider convergences with system size. In order to not make the discussion in this thesis too lengthy though, we will only perform the extrapolations and convergence discussion of the DMET method for selected observables here, as this method is also the core of this thesis. The interested reader can find the remaining discussion of the rest for the DMRG method and the remaining DMET observables in the appendix in chapter 15.

10.2.1 Phonon basis functions per site

As explained in section 9.2.1, we use a generalized coherent state basis in order to describe the phononic part of the wave function which is an optimized basis set for our problem. Still, as phonons obey the bosonic commutation relation, we need in principle infinitely many of those basis functions per lattice site to describe the phononic degrees of freedom. As this is not possible numerically, we make sure that the number of phononic basis functions leads to qualitatively converged results for the chosen observables.

We will show the convergence with phononic basis functions for the DMET and the DMRG calculation both in the adiabatic as well as in the anti-adiabatic limit for the energy gap $\Delta c/t$ here. The interested reader can find the discussion about other observables (the total energy and the double occupancy) in the appendix.

In figure 10.1, we show the convergence of the energy gap in the anti-adiabatic ($\alpha = 5.0$) as well as for the adiabatic limit ($\alpha = 0.5$) for the DMET calculation.

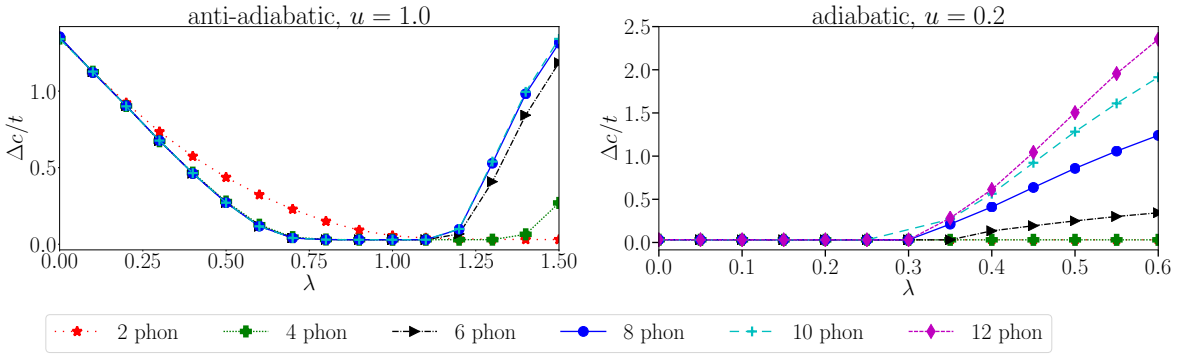

Figure 10.1: Convergence of the energy gap with the number phononic basis functions per site for a total system size of $N = 408$. While for the anti-adiabatic case, the results are converged for a considered number of basis function of phon = 8, in the adiabatic limit, even for 12 phonon basis functions per site we see no convergence in the Peierls phase. The position of the quantum phase transitions is predicted quantitatively for both cases and a number of basis functions per site of 8. Graph from [53].

While the results are quantitatively converged for a number of phonon basis functions of 8 in the anti-adiabatic limit and in the Mott regime of the adiabatic limit the gap in the Peierls phase is not converged even for 12 basis functions per site. As we are only interested in the position of the gap (which is always quantitatively predicted for 8 basis functions per site) and to not drive the computational costs any higher, we still consider 8 basis functions in the following.

10.2.2 Finite size scaling

The Hubbard-Holstein model is defined in infinite space and is therefore translational invariant. Numerically though, we are only able to consider finite systems and therefore have to consider finite size effects and the influence of the boundaries on the observables. This is why we do a finite size scaling. In the DMET method, there are two scales to be considered: the size of the whole considered system as well as the impurity size.

Finite size scaling of the whole system

As the computational costs with respect to the whole system size only grows quadratic, we can regard very big systems and therefore perform the finite size scaling with system sizes of $N = 408$, $N = 816$ and $N = 1632$ sites, as shown in figure 10.2. While for the energy gap, the finite size scaling is necessary, for the local observables, namely the density difference of the electrons between neighbouring sites $\langle n_i \rangle - \langle n_{i+1} \rangle$ and the double occupancy $\langle n_{i\uparrow} n_{i\downarrow} \rangle$, we observe that the finite size effects and the influence of the boundaries for a system size of $N = 408$ are already negligible (as can be observed in figure 10.2).

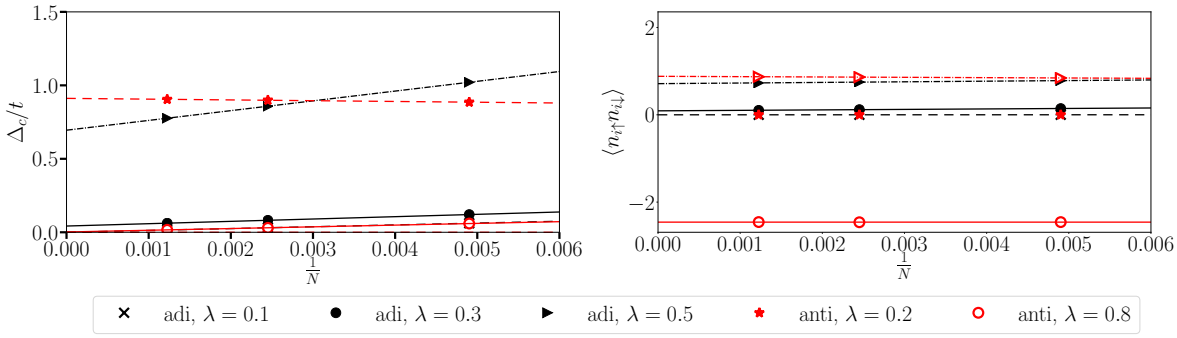

Figure 10.2: Finite size scaling for the energy gap $\Delta c/t$ (left hand side) and double occupancy $\langle n_{i\uparrow}n_{i\downarrow}\rangle$ (right hand side) in the DMET calculation. We show some examples, both for the adiabatic limit ($\lambda = 0.15; 0.35; 0.55$ and $u = 0.2$) as well as for the anti-adiabatic limit ($\lambda = 0.25; 0.85; 1.45$ and $u = 1.0$). The extrapolation is done with system sizes of $N = 408; 816; 1632$. The scaling is linear, making it possible to remove finite size effects. We also observe that for the double occupancy, the values do not differ for the different system sizes, which leads us to the conclusion that for this observable, the finite size effects are already negligible for system sizes ≥ 408. Left graph from [53]

Finite size scaling of the impurity

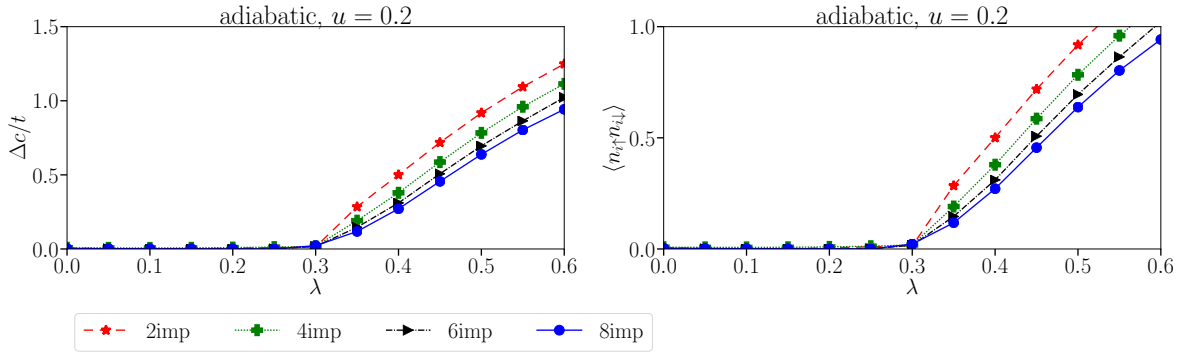

Figure 10.3: Finite size scaling of the impurity for the energy gap $\Delta c/t$ (left hand side) and the double occupancy $\langle n_{i\uparrow}n_{i\downarrow}\rangle$ (right hand side) in the DMET calculation: we plot the dependence of energy gap $\frac{\Delta c}{t}$ on the electron-phonon coupling strength λ for different impurity sizes, going from $N_{\text{imp}} = 2$ to $N_{\text{imp}} = 8$ in steps of 2. While both observables seem to decrease with increasing impurity size, the scaling seems to converge for the double occupancy while that is not the case for the energy gap.

In DMET, while the impurity part of the system is considered as accurately as possible, the rest of the system is only taken into account on a mean field level. This is why, with increasing impurity size, long range correlations are captured more accurately. Unfortunately though, this leads to a nonlinear scaling of the observables with respect to the impurity size.
In the following, we will discuss the scaling of our non-local observable $\Delta c/t$ as well as the scaling of the (locally defined) double occupancy $\langle n_{i\uparrow}n_{i\downarrow}\rangle$ with increasing impurity sizes. We start the discussion for the adiabatic limit ($\alpha = 0.5, u = 0.2$) and refer the interested reader to the appendix for further data for different parameter sets.
In figure 10.3, we plot the energy gap $\frac{\Delta c}{t}$, as defined in section 10.1.1 for different electron-phonon coupling strengths λ in the adiabatic limit ($\alpha = 0.5$, $u = 0.2$). We observe an apparently non-linear decrease of the estimation of the energy gap for increasing impurity sizes.

In order to quantify the finite size scaling more in detail, we choose different data sets of λ for the four impurity sizes. In figure 10.4, we see the development of $\frac{\Delta c}{t}$ for increasing impurity sizes. The convergence for all values of λ with increasing impurity size is nonlinear, making its quantification nontrivial. While the scaling for small values of $\lambda \leq 0.3$ cannot even be described qualitatively as the values go up and down with no visible rules, the values of the gap for large values of $\lambda \geq 0.3$ is going monotonously down with increasing impurity sizes.

From the discussion in sections 8.2 and 8.3 we expect a Mott phase for small values of λ and a Peierls phase for high values of λ. The Mott phase occurs due to electron-electron correlation and does not exhibit long range order which explains that with increasing impurity sizes, the result is not monotonously converging. The Peierls phase on the other hand breaks translational invariance (and thus a symmetry); it exhibits long range order and thus is improved upon considering larger regions

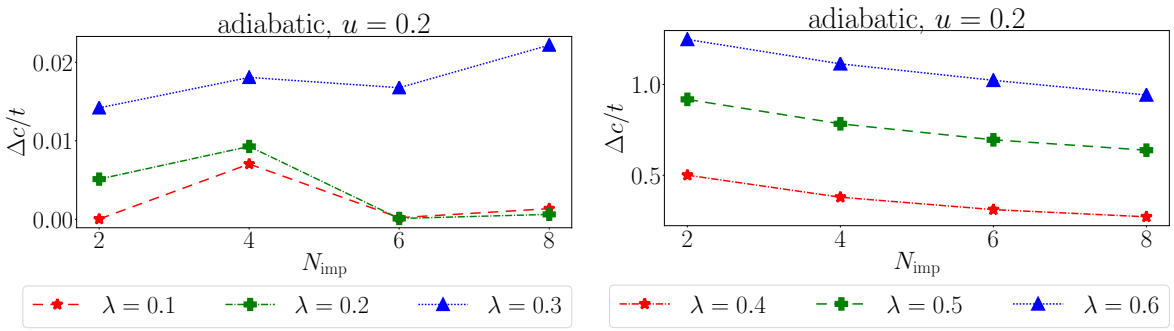

Figure 10.4: Finite size scaling for the energy gap with increasing impurity sizes in the DMET calculation. We show different values of the electron-phonon coupling strengths λ with increasing impurity sizes. On the left hand side, we show coupling strengths $\lambda \leq 0.3$ belonging to the Mott phase, on the right hand side, we show coupling strengths $\lambda \geq 0.3$ belonging to the Peierls phase.

of the system more accurately. Additionally, the decrease in the energy gap with increasing impurity size seems reasonable as with growing impurity size, we include more electron-electron correlation, which work against the Peierls phase.

Similar to the non-local energy gap, we also plot the double occupancy $\langle n_{i\uparrow} n_{i\downarrow} \rangle$ for different impurity sizes and values of electron-phonon coupling strengths λ (Fig. 10.4). While also the values for this observable seem to decrease with increasing impurity size, the scaling seems to converge, which could not be observed for the energy gap. Again considering the results more in detail by plotting single

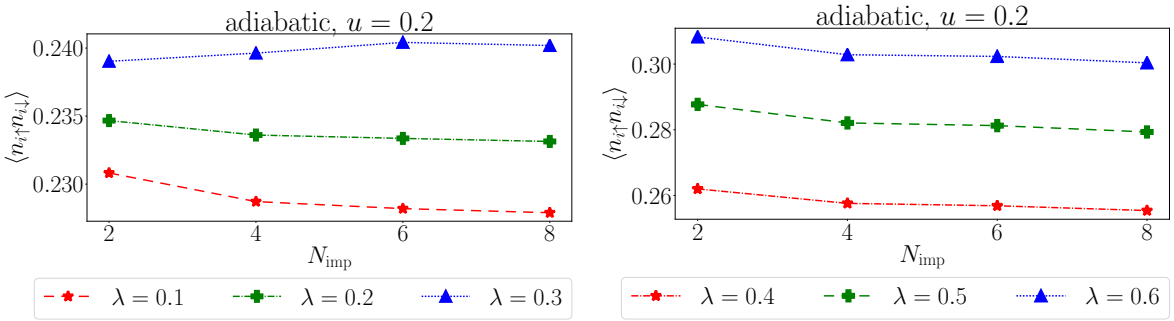

Figure 10.5: Finite size scaling for the double occupancy $\langle n_{i\uparrow} n_{i\downarrow} \rangle$ with increasing impurity sizes in the DMET calculation. We show the energy gap $\Delta c/t$ as a function of different values of the electron-phonon coupling strengths λ with increasing impurity sizes. On the left hand side, we show coupling strengths $\lambda \leq 0.3$ belonging to the Mott phase, on the right hand side, we show coupling strengths $\lambda \geq 0.3$ belonging to the Peierls phase. The double occupancy, being a local observable, converges much faster with increasing impurity size.

electron-phonon coupling strengths, we observe that, while the decrease is only strictly monotonic for values $\geq \lambda = 0.3$, the results seem to be almost converged for an impurity size of 8. We explain this with the locality of this observable, which is influenced less by long-range correlations than the energy gap.

As already mentioned, DMET's success origins partly in its computational cheapness, making it possible to relatively easy consider large coupled electron-phonon systems. To keep the computational costs low and because we do not observe any qualitative changes in the behaviour of the observables, in the following, we will choose an impurity size of 6. For 6 impurity sites, the computational cost per calculation is approximately 3 hours (in comparison, calculations for 8 impurity sites are already taking around 12 hours on average), making it much cheaper than the DMRG calculations used to compare to this study which on average took 72 hours per calculation.

10.3 Energy per site

Although not being an observable of physical interest, the energy per site is an important property to show how well two methods agree with each other.

10.3.1 DMET vs. DMRG

In order to benchmark the results of the DMET calculation, we therefore compare the results for the calculated energy per site E_{site} with those from the DMRG calculation. In figure 10.6, we show the energy per site for the anti-adiabatic ($\alpha = 5.0,\ u = 1.0$) as well as for the adiabatic limit ($\alpha = 0.5,\ u = 0.2$) for DMRG and DMET. Of course also for the DMRG calculation, a finite size scaling with respect to the total system size has been made. This discussion as well as the finite size scaling of the energy in the DMET calculation can be found in sections 15.2 and 15.1 in the appendix. For both cases, the results agree on a quantitative level.

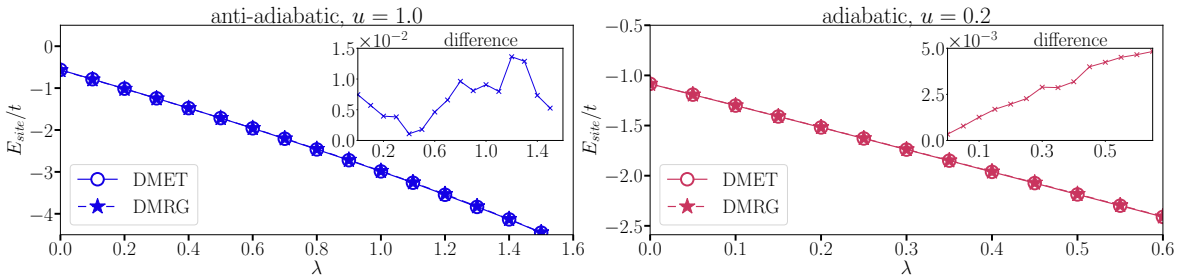

Figure 10.6: Comparison of the energy per site E_{site}, calculated with the DMRG and with the DMET method. In the upper graph, we show the anti-adiabatic limit ($\alpha = 5.0,\ u = 1.0$), in the lower graph, the adiabatic limit ($\alpha = 0.5,\ u = 0.2$). For both limits, the results agree quantitatively. Graph from [53]

10.3.2 DMET vs. DMET with BO approximation

Additionally, we also compare the energies per site between the full Hubbard-Holstein model and the Hubbard-Holstein model in BO approximation in figure 10.7. For the anti-adiabatic limit, the energy per site shows approximately the same behavior while not agreeing quantitatively. In the adiabatic limit, a qualitative agreement can be observed. In this section, we show a comparison of the energy per

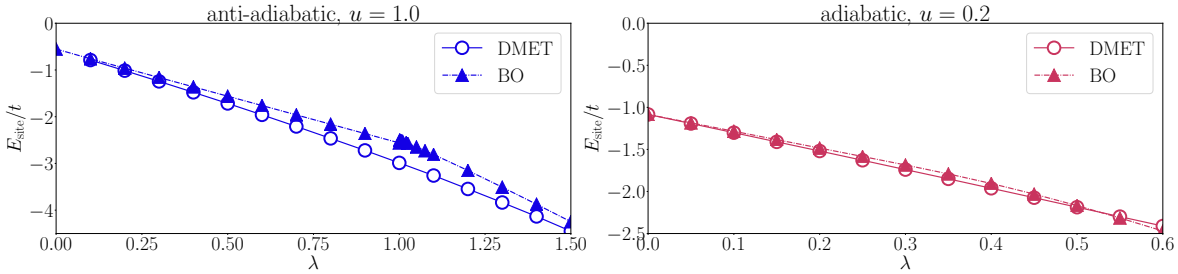

Figure 10.7: Comparison of the energy per site E_{site} for the full electron-phonon system (DMET calculation), with the energy per site from the same system under the BO approximation. On the right hand side, we show the anti-adiabatic ($\alpha = 5.0,\ u = 1.0$), on the left hand side the adiabatic limit ($\alpha = 0.5,\ u = 0.2$). While the behaviour only approximately coincides for the anti-adiabatic case, a qualitative agreement between the two methods for the adiabatic limit can be observed. Graph from [53]

site for the three considered methods: DMET for coupled electron-phonon systems, DMRG for coupled electron-phonon systems and DMET for purely electronic systems in the BO approximation. For the first two methods, we get a quantitative agreement between the energy per site, while, when comparing the two different DMET approaches, we only observe a qualitative agreement. We therefore hope to get good agreement in the quantities of physical interest between the DMET and DMRG methods for coupled electron-phonon systems but are already warned that the BO approximation might not fully be able to reproduce the full physics of the Hubbard Holstein model.

10.4 Phase diagram of the Hubbard Holstein model

10.4.1 Anti-adiabatic limit

In figure 10.8, we plot the energy gap $\Delta c/t$, the electronic density difference between neighbouring sites $\langle n_i \rangle - \langle n_{i+1} \rangle$, and the double occupancy $\langle n_{i\uparrow} n_{i\downarrow} \rangle$ (as defined in section 10.1.1) in the anti-adiabatic limit ($\alpha = 5.0$) for an electron-electron repulsion of $u = 1.0$ and for different electron-phonon coupling strengths λ.
For all three observables, we observe a Mott phase for $0 \leq \lambda \leq 0.7$. With growing λ, we indeed observe a distinct metallic phase ($0.7 \leq \lambda \leq 1.1$) which is followed by a Peierls phase for $1.1 \leq \lambda$.

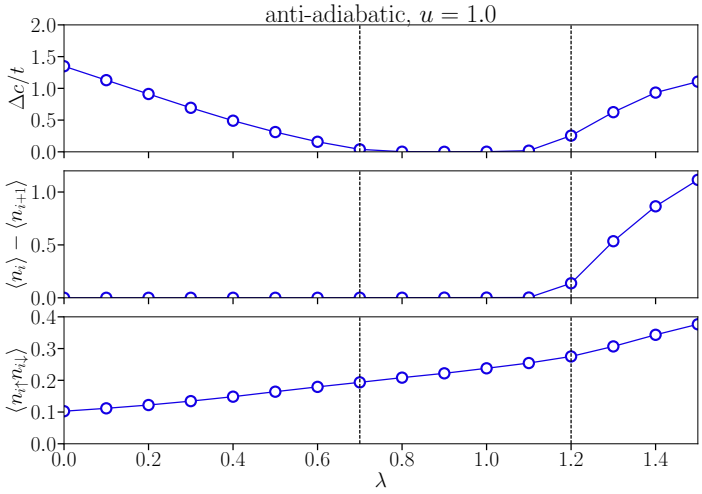

Figure 10.8: Energy gap $\Delta c/t$, density difference of the electrons between neighbouring sites $\langle n_i \rangle - \langle n_{i+1} \rangle$ and double occupancy $\langle n_{i\uparrow} n_{i\downarrow} \rangle$ for the anti-adiabatic limit $\alpha = 5.0$ and an electron-electron coupling of $u = 1.0$ for different electron-phonon couplings λ. For $0 \leq \lambda \leq 0.7$, a Mott phase is observed, which changes into a metallic phase for $0.7 \leq \lambda \leq 1.1$. Above coupling values of $1.1 \leq \lambda$, we observe a Peierls phase. Graph from [53]

10.4.2 Adiabatic limit

As explained in section 8.1, the occurrence of a pronounced metallic phase in the anti-adiabatic limit was to be expected; it is however not clear whether this phase also occurs for all electron-electron interaction strengths u in the adiabatic limit, where the phonon frequency is small in comparison to the electronic hopping and thus, the quantum fluctuations of the phonons are suspected to be smaller.
In figure 10.9, we again show the energy gap $\Delta c/t$, the electronic density difference between neighbouring sites $\langle n_i \rangle - \langle n_{i+1} \rangle$ and the double occupancy $\langle n_{i\uparrow} n_{i\downarrow} \rangle$ (as defined in section 10.1.1) in the adiabatic limit ($\alpha = 0.5$) for different electron-electron repulsions, ($u = 0.0; 0.2; 0.4$) and different electron-phonon coupling strengths λ. When the electron-electron interaction is absent, we do not observe a Mott phase, but a direct transition from the metallic to the Peierls phase at $\lambda = 0.2$. This result is as expected as the Mott phase is driven by the electron-electron interaction and therefore cannot occur in this limit.
For a small electron-electron interaction, $u = 0.2$, the Mott phase exists for very small electron-phonon interactions $0 \leq \lambda \leq 0.1$. The gap indicating the Mott phase though is very small in comparison to the gap that indicates the pronounced Peierls phase for $0.3 \leq \lambda$. Between Mott and the Peierls, we observe a small metallic phase for electron phonon coupling values of $0.1 \leq \lambda \leq 0.3$.
When considering stronger electron-electron interactions $u = 0.4$, the size of the gap indicating the Mott gap grows considerably, as does the range of the Mott phase: for $0 \leq \lambda \leq 0.25$, we observe a Mott phase, followed again by a narrow metallic phase for $0.25 \leq \lambda \leq 0.45$. Afterwards, we observe a Peierls phase, whose gap is less pronounced than for lower u, but still clearly visible.
Our results for the adiabatic limit of the Hubbard Holstein model are summarized in the phase diagram shown in figure 10.10. We observe that the Mott phase, while not existent at all for $u = 0.0$, grows more and more pronounced for growing electron-electron coupling values u. The range of the metallic phase stays approximately constant for different u-values, but shifts from small values for

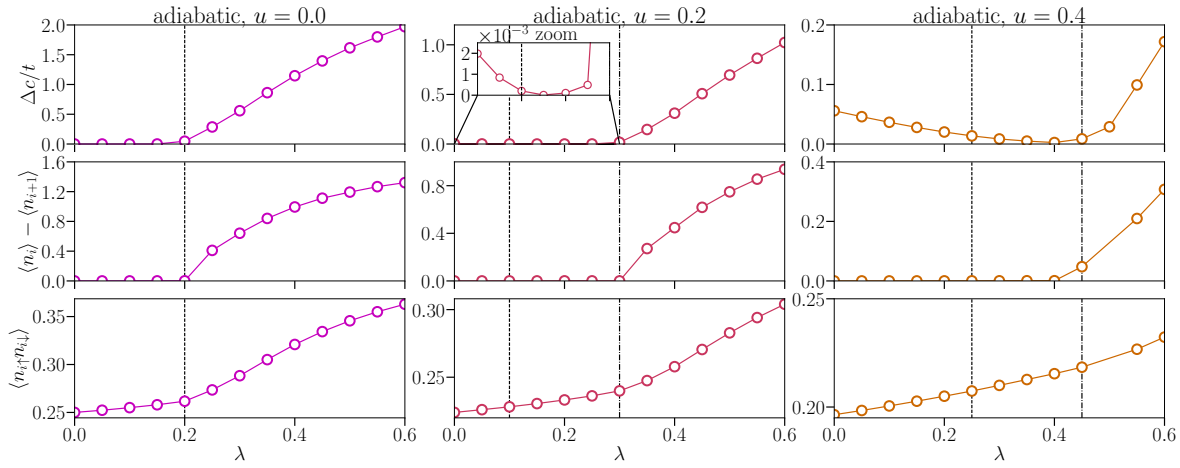

Figure 10.9: Energy gap $\Delta c/t$, density difference of the electrons between neighbouring sites $\langle n_i \rangle - \langle n_{i+1} \rangle$ and double occupancy $\langle n_{i\uparrow} n_{i\downarrow} \rangle$ for the adiabatic limit $\alpha = 0.5$ and three different electron-electron couplings, $u = 0.0$, $u = 0.2$ and $u = 0.4$ for different electron-phonon couplings λ. For $u = 0.0$ (absent electron-electron coupling), we do not observe any Mott phase but a direct transition from the metallic to the Peierls phase at $\lambda = 0.2$. For a value of $u = 0.2$, the Mott phase exists for values of $0 \leq \lambda \leq 0.1$ but the gap is very small. For values $0.1 \leq \lambda \leq 0.3$, a metallic phase can be observed, followed by a Peierls phase for $\lambda \geq 0.3$. For bigger electron-electron couplings ($u = 0.4$) the energy gap indicating the Mott phase (from $0 \leq \lambda \leq 0.25$) gets more pronounced. The range of the metallic phase ($0.25 \leq \lambda \leq 0.45$) stays the same for this u-value while the gap due to the Peierls phase for $0.45 \leq \lambda$ becomes less pronounced (but still visible). Graph from [53]

electron-phonon interaction λ to intermediate values. The Peierls phase is getting less pronounced for growing u.

10.4.3 Comparison with DMRG calculation

In order to benchmark our results, we compare with the DMRG method. As explained in section 9.1, for this purpose we expanded the syten library to be able to treat coupled fermion-boson systems.

In figure 10.11, we compare the DMRG and the DMET results for both the anti-adiabatic limit ($\alpha = 5.0, u = 1.0$) and the adiabatic ($\alpha = 0.5, u = 0.2$) limit. Up to an electron-phonon coupling value of $\lambda = 1.2$, we observe a quantitative agreement of the energy gap, although different approximations where made to calculate this property (while in the DMET calculation, we only take the HOMO-LUMO gap of the mean field system, in the DMRG calculation we calculate the energy gap for systems with half, half plus one and half minus one filling, as explained in section 10.1.1). While for higher values of λ, the actual value of the gap differs, the point of the quantum phase transition is predicted equivalently with both the DMRG and the DMET calculation. For a value of $\lambda = 1.3$, the gap measured by the DMET calculation abruptly increases, while it only increases slightly in the DMRG calculation. Reasons for this discrepancy could be either the mean field nature of the calculation of the gap in the DMET treatment, which overestimates the Peierls phase, or the too early cutting of the Fock space (with a maximum amount of 8 phononic basis function per site, see the discussion in section 10.2.1) which could lead to an under-estimation of the Peierls phase in the DMRG calculation.

In figure 10.11, we compare the DMRG and the DMET results for the adiabatic limit ($\alpha = 0.5$) and an electron-electron repulsion of $u = 0.2$. While the position of the phase transitions both between the Mott and the metallic phase as well as between the metallic and the Peierls phase agree quantitatively, the actual sizes of the gaps only agree qualitatively: In the Mott and metallic phase, the gap measured by the DMRG calculation is bigger than the gap measured in the DMET calculation. While in the metallic phase, the DMET gap closes up to a value of 10^{-4}, the value stays at a value of $5 \cdot 10^{-3}$ in the DMRG calculation. These deviations are within the error limit of the finite size convergence presented in section 10.2.2.

In the Peierls phase, as also observed in the anti-adiabatic limit, the size of the gap in the DMET calculation is bigger as in the DMRG calculation. As already discussed before, this can have its origin either in the mean field nature of the calculation of the DMET gap or in the cutting of the Fock space in the DMRG calculation.

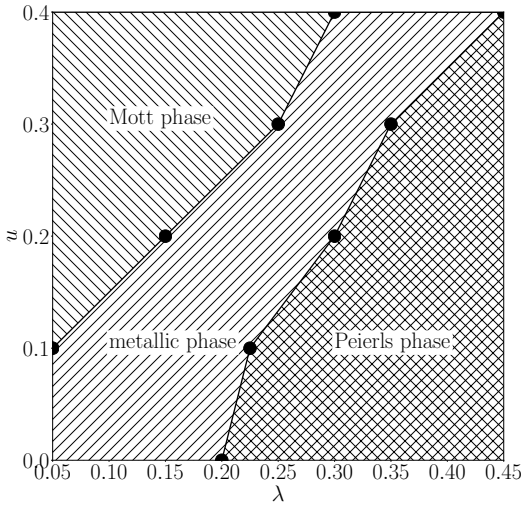

Figure 10.10: Phase diagram for the adiabatic limit ($\alpha = 0.5$) of the Hubbard Holstein model. For different electron-electron coupling values u and different electron-phonon coupling values λ, the phase of the model at these parameters is indicated. While not existent at all for $u = 0$, the Mott phase gets more and more pronounced with growing u and small λ values. The Peierls phase, while always existing in this range, needs higher electron-phonon coupling strengths to occur when the electron-electron interactions are also growing bigger. Graph from [53]

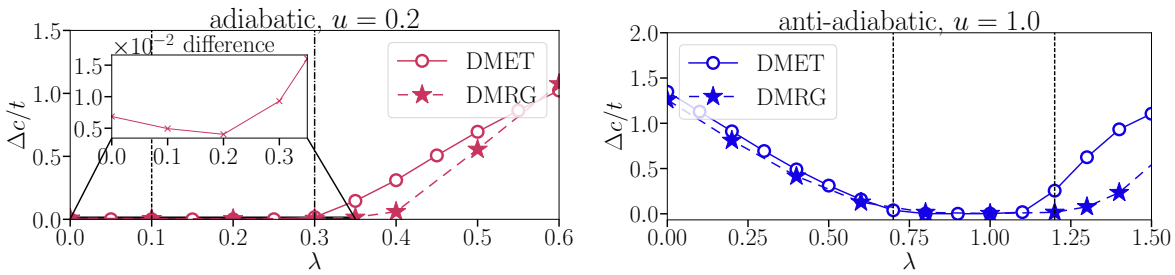

Figure 10.11: Comparison of the energy gap $\Delta c/t$ for the DMRG and the DMET calculation in the adiabatic limit $\alpha = 0.5$ (left side) and the anti-adiabatic limit (right side). Plotted are different electron-phonon coupling values λ for a constant electron-electron coupling of $u = 0.2$. We observe a quantitative agreement in the position of the phase transitions between Mott and metallic phase at $\lambda = 0.1$ and between metallic and Peierls phase at $\lambda = 0.3$. For the Mott phase and the Peierls phase both, the size of the gap is only in qualitative agreement. Graph from [53]

10.4.4 Comparison with results from the Born Oppenheimer approximation

As discussed in section 9.3, we can also make the Born Oppenheimer approximation, which means treating the phononic degrees of freedom classically ions which are distorted from the resting position, where this distortion of the ions $\hat{x}_i$ is optimized to minimize the total energy. In figure 10.12, we compare the double occupancy $\langle n_{i\uparrow} n_{i\downarrow} \rangle$ and the distortion of the electronic density $\langle n_i \rangle - \langle n_{i+1} \rangle$ for the BO system and the fully quantum mechanical system in the anti-adiabatic ($\alpha = 5.0, u = 1.0$) and the adiabatic limit ($\alpha = 0.5, u = 0.2$). In the anti-adiabatic limit, we observe that for both observables, the Born-Oppenheimer description of the phase transition is not accurate. While in the full quantum mechanical model, the transition between metallic and Mott phase occurs for a value of $\lambda = 1.1$, in the Born-Oppenheimer model, this transition already occurs for $\lambda = 1.0$. Also, more importantly, the actual phase transition is of second order, while the Born-Oppenheimer treatment predicts a phase transition of first order.

In the adiabatic limit, while still not accurate (the phase transition is predicted too early, at $\lambda = 0.25$ (BO) instead of $\lambda = 0.3$ (full)), at least the qualitative nature of the phase transition as being of second order is captured.

This result confirms our expectation that in order to treat the quantum phase transitions of the Hubbard Holstein model, both the quantum mechanical nature of the electrons as well as of the phonons needs to be taken into account. Especially when considering the phononic frequency to be high in comparison to the electronic kinetic hopping, the BO approximation, which assumes the phonons to be moving much slower than the electrons, fails.

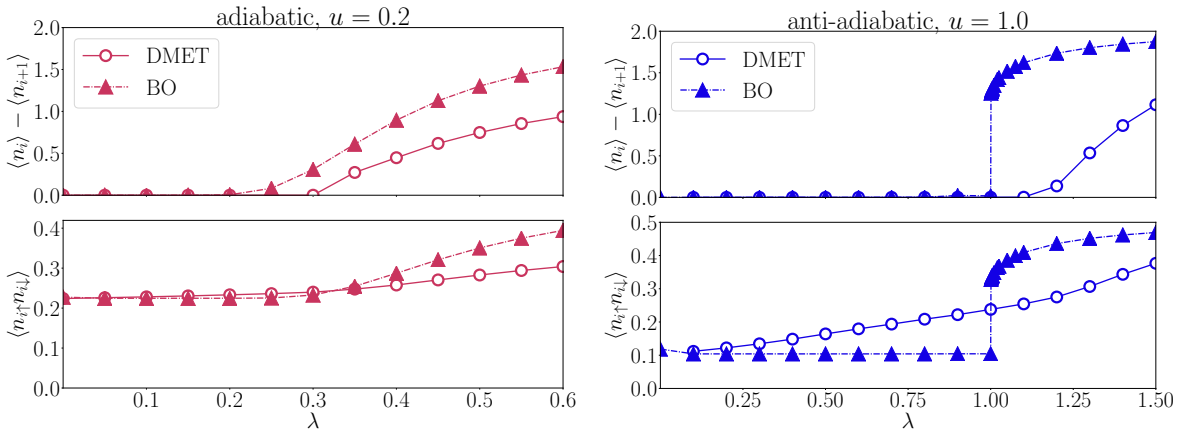

Figure 10.12: Comparison of the density difference of the electrons between neighbouring sites $\langle n_i \rangle - \langle n_{i+1} \rangle$ and the double occupancy $\langle n_{i\uparrow} n_{i\downarrow} \rangle$ in the adiabatic (left side) and the anti-adiabatic (right side) limit for the fully quantum mechanical treatment and the Born Oppenheimer approximation of the Hubbard Holstein model. Both calculations are performed with DMET. For both the adiabatic and the anti-adiabatic case, the position of the gap is not predicted accurately with the BO approximation, in the anti-adiabatic limit, also the nature of the phase transition is predicted wrong (first order instead of second order phase transition). Parameters are $\alpha = 0.5$, $u = 0.2$, $t_{\text{elec}} = t_{\text{phon}} = 1$, $N_{\text{imp}} = 6$, $N_{\text{phon}} = 8$ (adiabatic) and $\alpha = 5.0$, $u = 1.0$, $t_{\text{elec}} = t_{\text{phon}} = 1$, $N_{\text{imp}} = 6$, $N_{\text{phon}} = 8$ (anti-adiabatic). Graph from [53]

10.5 Summary

In this chapter, we showed results for all three methods that we introduced before. First, a finite size extrapolation is performed. Then, four properties of the system, that is, the energy per site, the energy gap, the double occupancy and the density difference of the electrons between neighbouring sites were considered and discussed. While we showed good agreement between the electron-phonon DMRG method and the electron-phonon DMET methods for all properties, in the BO approximation, only the energy per site can be reproduced qualitatively and the rest of the description of the Hubbard Holstein model is not accurate.

We have expanded the DMET method towards the calculation of electron-boson systems and benchmarked this expansion with the Hubbard-Holstein model, which describes coupled electron-phonon problems. With this new method, we expect to be able to also treat electron-photon systems. In this field, there have been recent, very exciting developments in experimental physics, specifically in cavity quantum-electrodynamical engineering of materials properties [39, 9, 56, 54, 43, 10, 32, 1]. We hope that our DMET method could be further expanded to theoretically model some of those experiments as DMET is able to deal with correlated electron-boson lattice systems from weak to strong coupling.

Part IV

Functionalizing Density Matrix Embedding Theory

Chapter 11

Goals and pitfalls of DMET

In part II of this thesis, we derived and explained the DMET method in great detail. In DMET, the system of interest is split into two parts, an impurity and the rest of the system called environment. While for the environment certain approximations are made, the impurity is treated as accurately as possible.

But which properties on the impurity are supposed to be reproduced? Or, in other words, what are the goals of DMET? In this chapter, we will analyse the goals of DMET for the specific case of the Hubbard model, described by the Hamiltonian

$$\hat{H} = t \sum_{\langle i,j\rangle,\sigma} \hat{c}^\dagger_{i\sigma}\hat{c}_{j\sigma} + U \sum_i \hat{n}_{i\uparrow}\hat{n}_{i\downarrow}, \tag{11.1}$$

$$\hat{H}|\Psi\rangle = E|\Psi\rangle. \tag{11.2}$$

The Hubbard system is translationally invariant and particle and spin conserving. By restricting ourselves to a homogeneous system, we find the simplest possible case in which we can investigate in great detail what can be achieved in DMET. Additionally, we do not consider any of the tricks that are possible in DMET and that were discussed in section 7.2 in order to investigate the limitations of this method in a clear-cut setting.

11.1 Wave function

The property that describes the full physics and from which all observables can be calculated is the wave function on the impurity.

We start with the wave function of the original system $|\Psi\rangle$ restricted to the impurity as has been defined in Eq. (5.13). This is the property of the full system we can maximally hope to describe accurately.

In the DMET method, we find a projection $\hat{P}^s_{\text{red}}$ from the mean field system

$$\hat{T} = t \sum_{\langle i,j\rangle,\sigma} \hat{c}^\dagger_{i\sigma}\hat{c}_{j\sigma} \tag{11.3}$$

$$\hat{T}|\Phi'\rangle = \tilde{E}|\Phi'\rangle \tag{11.4}$$

$$|\Phi'\rangle = \sum_{\alpha=1}^{2\cdot 4^{\text{imp}}} \lambda_\alpha |C_\alpha\rangle, \tag{11.5}$$

$$\rightarrow \hat{P}^s_{\text{red}} = \sum_{\alpha=1}^{2\cdot 4^{\text{imp}}} |C_\alpha\rangle\langle C_\alpha|. \tag{11.6}$$

As discussed before, with $\hat{P}^s_{\text{red}}$, the interacting Hamiltonian $\hat{H}$ is projected into an embedding basis $\hat{H}_{\text{emb}}$ that leaves the Hamiltonian on a small part of the system, called impurity, the same while it

changes the Hamiltonian on the rest of the system.

$$\hat{H}_{\text{emb}}|\Psi_{\text{emb}}\rangle = E'|\Psi_{\text{emb}}\rangle, \tag{11.7}$$

$$\hat{H}_{\text{emb}}|_{\text{imp}} = \hat{H}|_{\text{imp}}. \tag{11.8}$$

The projection is improved self-consistently by adding a non-local potential to the mean field system

$$\hat{T}' = t \sum_{\langle i,j\rangle,\sigma} \hat{c}^\dagger_{i\sigma}\hat{c}_{j\sigma} + \sum_{i,j,\sigma} v_{ij}\hat{c}^\dagger_{i\sigma}\hat{c}_{j\sigma} = \hat{T} + \hat{V}. \tag{11.9}$$

The non-local potential $\hat{V}$ is chosen such that the 1RDMs of the interacting embedded system and the non-interacting mean field system are the same. The new Hamiltonian $\hat{T}'$ yields a new projection, which leads to a self-consistency cycle that converges once the 1RDMs of both systems are the same.

The developers of DMET claim [70, 34, 35], that after the above procedure is converged, the wave function of the interacting embedded system, restricted to the impurity lattice sites, $|\Psi_{\text{emb}}\rangle|_{\text{imp}}$ is the same as the wave function of the non-interacting mean field system that is used to generate the projection, $|\Phi\rangle|_{\text{imp}}$

$$|\Psi_{\text{emb}}\rangle|_{\text{imp}} \overset{!}{=} |\Phi\rangle|_{\text{imp}}. \tag{11.10}$$

Additionally, if the method is to yield useful results, also the wave function of the embedded system, restricted to the impurity should be the same (or similar) to the wave function of the original system on the impurity

$$(|\Psi_{\text{emb}}\rangle|_{\text{imp}} - |\Psi\rangle|_{\text{imp}}) = \delta, \tag{11.11}$$

where δ is small. Note: what we mean by small here and how we intend to compare the wave functions will be explained in more detail later in this work.

We will now first derive whether it is possible to meet the first demand (Eq. 11.10) and then numerically check if the second demand (Eq. 11.11) is met. Then, we can conclude if the wave function on the impurity is a sensible target property.

11.1.1 First demand

Dimensions

As a first step, we consider the dimensions of the Hilbert spaces the different wave functions are defined in. If the dimension of the Hilbert space of the embedded wave function on the impurity and the Hilbert space of the mean field system, restricted to the impurity are the same, it is in principle possible that also the wave functions are the same.

Dimensions in the interacting system

The ground state wave function of the original Hamiltonian $\hat{H}$ is in general defined in the full Fock space of a N lattice site system $\mathcal{F}$. For the Hubbard Hamiltonian that is particle number conserving though, we can restrict the Fock space to the part of M particles:

$$|\Psi\rangle \in \mathcal{F}_N|_M. \tag{11.12}$$

After the projection, we only consider $2\cdot\text{imp}$ "sites" (they are actual sites on the impurity region and different basis functions on the rest of the system). Also, we only consider the maximal number of particles that can possibly be on the impurity region, which are $2\cdot\text{imp}$ particles

$$|\Psi_{\text{emb}}\rangle \in \mathcal{F}_{2\text{imp}}|_{2\text{imp}}. \tag{11.13}$$

The amount of basis functions needed to set up the Fock space is the binomial coefficient

$$\dim\left(\mathcal{F}_{2\text{imp}}|_{2\text{imp}}\right) = \frac{2\text{imp}!}{\frac{2\text{imp}-\text{imp}}{2}!\frac{2\text{imp}+\text{imp}}{2}!} = \frac{2\text{imp}!}{\frac{\text{imp}}{2}!\frac{3\text{imp}}{2}!}. \tag{11.14}$$

For the homogeneous Hubbard system we can additionally use that the particle number per site is constant,

$$p = \frac{M}{N}, \tag{11.15}$$

where p is the number of particles on each site. Thus, in the homogeneous case we can also restrict the Fock space on the impurity to

$$|\Psi_{\text{emb}}\rangle|_{\text{imp}} \in \mathcal{F}_{\text{imp}}|_{p\cdot\text{imp}}. \tag{11.16}$$

This yields a total amount of basis functions needed to set up this Fock space of

$$\dim\left(\mathcal{F}_{\text{imp}}|_{\text{p}\cdot\text{imp}}\right) = \frac{\text{imp!}}{\frac{\text{imp}-\text{p}\cdot\text{imp}}{2}!\frac{\text{imp}+\text{p}\cdot\text{imp}}{2}!} \equiv \aleph, \tag{11.17}$$

which is much smaller than the number of basis functions needed to set up the other Fock spaces.

Like all wave functions, we can write the wave function restricted to the impurity in its Slater determinant basis set, where only Slater determinants with $p \cdot \text{imp}$ particles on it are allowed.

$$|\Psi_{\text{emb}}\rangle|_{\text{imp}} = \sum_{i=1}^{\aleph} c^i |\Phi^i_{\text{imp}}\rangle. \tag{11.18}$$

Dimensions in the non-interacting system

The non-interacting system is described by the Hamiltonian $\hat{T}$, its ground state wave function is a Slater determinant with a fixed particle number of M. This means that the Fock space describing this problem, similar to the interacting case, is

$$|\Psi\rangle \in \mathcal{F}_N|_M. \tag{11.19}$$

After the projection, the Slater determinant describing the mean field embedding Hamiltonian $\hat{T}_{\text{emb}}$ is restricted to the Fock space

$$\mathcal{F}_{\text{2imp}}|_{\text{2imp}} \tag{11.20}$$

as we consider a system with 2imp particles in it.

Considering the wave function projected on the impurity lattice sites $|\Phi\rangle|_{\text{imp}}$, we know that there is (possible) particle transfer between the impurity and the embedding part of the system. For the converged DMET calculation though, the particle number on the impurity needs to be the same as in the interacting case which means that there have to be $p\cdot$imp particles on the impurity. We know that the wave function describing the embedded system is a Slater determinant. This does not imply that the wave function describing the impurity is a Slater determinant. Like the interacting wave function on the impurity, we can also write the non-interacting wave function on the impurity as

$$|\Phi_{\text{emb}}\rangle|_{\text{imp}} = \sum_{i=1}^{\aleph} c^i |\Phi^i_{\text{imp}}\rangle. \tag{11.21}$$

Considering the dimensions of the Fock spaces the wave functions are defined on, it is possible that the demand in Eq. (11.10),

$$|\Psi_{\text{emb}}\rangle|_{\text{imp}} \overset{!}{=} |\Phi\rangle|_{\text{imp}}, \tag{11.22}$$

can be fulfilled.

Reasoning that the wave functions can not be the same

Consider without loss of generality two systems (one with, the other without interaction), with respectively two particles:

$$\hat{H} = \hat{t}_1 + \hat{t}_2 + \hat{u}(1,2), \tag{11.23}$$
$$\hat{H}|\Psi\rangle = E_0|\Psi\rangle, \tag{11.24}$$
$$\hat{T} = \hat{t}_1 + \hat{t}_2 + \hat{v}_1 + \hat{v}_2, \tag{11.25}$$
$$\hat{T}|\Phi\rangle = \tilde{E}_0|\Phi\rangle, \tag{11.26}$$
$$\tag{11.27}$$

We can choose a gauge such that $E_0 = \tilde{E}_0 = 0$ which yields

$$\hat{t}_1 + \hat{t}_2 + \hat{u}(1,2)|\Psi\rangle = 0 \tag{11.28}$$
$$\hat{t}_1 + \hat{t}_2 + \hat{v}_1 + \hat{v}_2|\Phi\rangle = 0 \tag{11.29}$$

Assume that the wave functions $|\Psi\rangle$ and $|\Phi\rangle$

$$|\Psi\rangle|_{\text{imp}} \overset{!}{=} |\Phi\rangle|_{\text{imp}}. \tag{11.30}$$

Eqns. (11.28) and (11.29) imply that

$$\left(\hat{t}_1 + \hat{t}_2\right)|\Psi\rangle = -\hat{u}(1,2)|\Psi\rangle, \tag{11.31}$$
$$\left(\hat{t}_1 + \hat{t}_2\right)|\Phi\rangle = \left(-\hat{v}(1) - \hat{v}2\right)|\Psi\rangle. \tag{11.32}$$

subtracting Eq. (11.32) from Eq. (11.31) yields:

$$0 = \left(-\hat{u}(1,2) + \hat{v}(1) + \hat{v}2\right)|\Phi\rangle|_{\text{imp}}. \tag{11.33}$$

As the term $-\hat{u}(1,2) + \hat{v}(1) + \hat{v}2$ can never be zero, the wave functions $|\Psi\rangle|_{\text{imp}}$ and $|\Phi\rangle|_{\text{imp}}$ can only be the same if they are zero:

$$|\Psi\rangle|_{\text{imp}} = |\Phi\rangle|_{\text{imp}} \iff |\Psi\rangle|_{\text{imp}} = |\Phi\rangle|_{\text{imp}} = 0. \tag{11.34}$$

From this reasoning it seems highly unlikely that the interacting and the non-interacting wave functions are locally the same in general. Further, due to the dimensionality of the wave function and the potential, it is only possible to control a wave function with a potential that is of the same dimension. As the wave function is gained from a system which includes two-particle terms $\hat{v}'(1,2)$, in order to control this wave function, we would also need a controlling potential depending on two particles, which would be an interacting wave function.

11.1.2 Second demand

Although we have derived that the non-interacting and the interacting wave functions of the embedded system on the impurity will usually not be the same, it still might be that the interacting wave function of the embedded system becomes very similar to the wave function of the original system on the impurity,

$$(|\Psi_{\text{emb}}\rangle|_{\text{imp}} - |\Psi\rangle|_{\text{imp}}) = \delta_\Psi. \tag{11.35}$$

In order to test this assumption, we first have to clarify how we intend to compare the wave functions on the impurities. Further, we have to define what we mean by "δ_Ψ being small" .

1. How to compare the wave functions?
All information of the wave function is also contained in the density matrix

$$\rho = \Psi^* \Psi, \tag{11.36}$$

also called M-RDM Γ^N, where M is the number of particles in the system. Thus, for a system with only one particle, the 1RDM describes the whole system, for a system with 2 particles, the 2RDM describes the whole system and so on.

In order to see if the projection is improving with increase of the impurity region, we compare the imp-RDMs of the embedded system with the imp-RDMs of the whole system, which for this purpose we solved with our DMRG solver

2. What does δ is small mean?
It is hard to quantify what "similar" in terms of wave functions or N-RDMs means. This is why, we the difference between the NRDMs of the original and of the DMET system with the difference between the original system and a system, which we project trivially so that it is cut after 2imp lattice sites. We call the trivial projection $\hat{P}^{DMRG}$. The costs of calculating this system is the same as one DMET self-consistency loop as the system size considered here is the same as the size of the embedded system in DMET. The N-RDMs being "close" thus in our setting means that δ_{DMRG}, the difference of the wave functions obtained by the two DMRG calculations is significantly bigger than δ_{DMET}, the difference of the full DMRG wave function and the DMET wave function.

For this calculation, we considered a full system of 24 lattice sites and impurity sizes of 1, 2, 3 and 4 sites at half filling so that number of particles = number of impurity lattice sites. In figure 11.1,

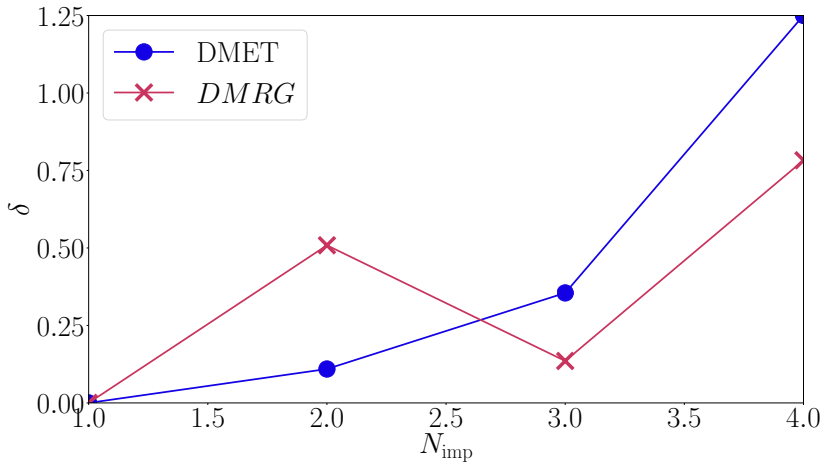

Figure 11.1: Difference between the N-RDM of the full system and the system cut after $2N_{\text{imp}}$ lattice sites (red line, crosses) and the difference between the N-RDM of the full system and the DMET system (blue line, dots)

we plot the difference between the N-RDMs of the embedded systems, once gained with the trivial projection $\hat{P}^{DMRG}$ and once gained with the DMET projection $\hat{P}^s_{\text{red}}$,

$$\left(\Gamma^{N_{\text{imp}}}|_{\text{imp}} - \Gamma^{N_{\text{imp}}}_{\text{emb}}|_{\text{imp}}\right)^2 = \delta \tag{11.37}$$

We observe that the distance between the original system and the embedded system, obtained by the trivial projection $\hat{P}^{DMRG}$, (in blue labelled with "DMRG" in the graph), is of the same order of magnitude as the distance between the original system and the embedded system, obtained by the DMET projection $\hat{P}^s_{\text{red}}$ (in red and labelled with "DMRG" in the graph). Additionally, we know by construction that the DMRG projection will converge to the exact solution if the embedded system is of the same size as the original system, which is not obvious for the DMET projection. Also, the DMET calculus is more expensive as, instead of performing the computation of the embedded system once, it has to be repeated until convergence of the projection.

In this chapter, we have shown that the wave function on the impurity of the embedded interacting and non-interacting systems in DMET are usually not the same. Moreover, the DMET algorithm does not provide a wave function on the impurity that is closer to the wave function on the impurity of the original system than a simple cutting of the full space would yield.

We deduce from these insights that the wave function on the impurity is not a sensible target property in the DMET algorithm.

11.2 1RDMs

If the wave function on the impurity is not a sensible target, a next good candidate would be the 1RDM. In this section, we will investigate

1. If it is possible to make the 1RDMs of the embedded mean field and the embedded interacting system the same

$$\gamma_{\text{emb}}|_{\text{imp}} \stackrel{?}{=} \gamma^s_{\text{emb}}|_{\text{imp}}, \tag{11.38}$$

where γ_{emb} is the 1RDM of the interacting and γ^s_{emb} is the 1RDM of the mean-field system.

2. If the embedding 1RDM γ_{emb} on the impurity is close to the 1RDM from the original system γ on the impurity

$$(\gamma_{\text{emb}}|_{\text{imp}} - \gamma|_{\text{imp}}) = \delta \tag{11.39}$$

11.2.1 Comparison of the 1RDM of the embedded mean field and the embedded interacting system

1RDMs on the embedded system

Considering the 1RDMs of the embedded systems, γ^s_{emb} and γ_{emb}, we see immediately that they can never be the same,

$$\gamma^s_{\text{emb}} \neq \gamma_{\text{emb}}, \tag{11.40}$$

by looking more closely to the definitions of the two 1RDMs:

The 1RDM of the mean field system is defined as

$$\gamma^s_{\text{emb,ij}} = 2 \cdot \sum_{k=1}^{P/2} \tilde{\varphi}^k_i \tilde{\varphi}^k_j \tag{11.41}$$

where P is the total particle number in the embedded system and the $\tilde{\varphi}^\mu$ are the eigenvectors of single-particle Hamiltonian belonging to the lowest $P/2$ eigenvalues.

$$\hat{t}_{\text{emb}}|\tilde{\varphi}^k\rangle = \epsilon^k|\tilde{\varphi}^k\rangle. \tag{11.42}$$

The determinant of these eigenvectors builds the many body ground state wave function of the mean field Hamiltonian in Fock space:

$$\hat{T}_{\text{emb}}|\Phi_{\text{emb}}\rangle = E|\Phi_{\text{emb}}\rangle, \tag{11.43}$$

$$|\Phi_{\text{emb}}\rangle = \det\{\tilde{\varphi}^\mu\}_{\mu:1\ldots P} \tag{11.44}$$

The ground state of the interacting system $|\Psi\rangle_{\text{emb}}$ can be written as a sum of Slater determinants

$$|\Psi\rangle_{\text{emb}} = \sum_{k=1}^{\alpha} c^k|\Phi^k_{\text{emb}}\rangle, \tag{11.45}$$

where $\alpha > 1$. This means that in order to determine $|\Psi\rangle_{\text{emb}}$, not only the lowest eigenvectors of the single-particle system are needed, but a linear combination of all Slater determinants in the span $\{\tilde{\chi}^{\text{k}}\}_{\text{k:1...P}}$. Therefore, the 1RDM of the interacting system can be written as

$$\gamma_{\text{emb,ij}} = \sum_{k=1}^{\eta} n_k \tilde{\chi}^k_i \tilde{\chi}^k_j, \tag{11.46}$$

where $\tilde{\chi}^k_i$ are the natural orbitals of the interacting 1RDM and $P > \eta > P/2$.

1RDMs on the impurity

The 1RDM of the mean field embedded system is defined by the $\{\tilde{\varphi}^\alpha\}_{\text{imp}}$ which are the eigenfunctions of the single-particle Hamiltonian $\hat{t}$:

$$\sum_j \hat{t}_{ij}\tilde{\varphi}_j^\alpha = \epsilon^\alpha \tilde{\varphi}_i^\alpha \Longleftrightarrow \gamma_{ij}^s = \sum_{i=1}^{N_{\text{imp}}} \tilde{\varphi}_i^\alpha \tilde{\varphi}_j^\alpha \tag{11.47}$$

We can split each orbital into one part that is only defined on the impurity and one part that is only defined on the bath:

$$\tilde{\varphi}^\alpha = \tilde{\varphi}_{\text{imp}}^\alpha + \tilde{\varphi}_{\text{env}}^\alpha \tag{11.48}$$

Then, the 1RDM of the embedded system can be written as

$$\gamma_{\text{emb,ij}}^s = \sum_{\alpha=1}^{N_{\text{imp}}} \tilde{\varphi}_{\text{imp,i}}^\alpha \tilde{\varphi}_{\text{imp,j}}^\alpha + \sum_{\alpha=1}^{N_{\text{imp}}} \tilde{\varphi}_{\text{env,i}}^\alpha \tilde{\varphi}_{\text{env,j}}^\alpha, \tag{11.49}$$

Considering now only the 1RDM on the impurity,

$$\gamma_{\text{emb,ij}}^s|_{\text{imp}} = \gamma_{\text{imp,ij}}^s = \sum_{\alpha=1}^{N_{\text{imp}}} \tilde{\varphi}_{\text{imp,i}}^\alpha \tilde{\varphi}_{\text{imp,j}}^\alpha, \tag{11.50}$$

we observe that the single-particle wave functions on the impurity $\tilde{\varphi}_{\text{imp}}^\alpha$ are no longe normalized. Renormalizing them yields

$$\gamma_{\text{imp,ij}}^s = \sum_{\alpha=1}^{N_{\text{imp}}} \|\tilde{\varphi}\|_{\text{imp}}^2 \varphi_{\text{imp,i}}^\alpha \varphi_{\text{imp,j}}^\alpha. \tag{11.51}$$

We see that $\gamma_{\text{imp,ij}}^s$ has the same form as the 1RDM of the interacting system by considering the 1RDM of the interacting system

$$\gamma_{\text{emb,ij}} = \sum_{k=1}^{2N_{\text{imp}}} n_k \tilde{\chi}_i^k \tilde{\chi}_j^k. \tag{11.52}$$

Note that the sum here goes over all possible one-particle orbitals. Splitting the $\tilde{\chi}^k$ into impurity and bath

$$\tilde{\chi}^k = \tilde{\chi}_{\text{imp}}^k + \tilde{\chi}_{\text{env}}^k \tag{11.53}$$

yields the 1RDM

$$\gamma_{\text{emb,ij}} = \sum_{\alpha=1}^{2N_{\text{imp}}} \tilde{\chi}_{\text{imp,i}}^\alpha \tilde{\chi}_{\text{imp,j}}^\alpha + \sum_{\alpha=1}^{2N_{\text{imp}}} \tilde{\chi}_{\text{env,i}}^\alpha \tilde{\chi}_{\text{env,j}}^\alpha. \tag{11.54}$$

Considering the 1RDM on the impurity and renormalizing yields

$$\gamma_{\text{imp,ij}} = \sum_{\alpha=1}^{N_{\text{imp}}} n_k \cdot \|\tilde{\chi}\|_{\text{imp}}^2 \chi_{\text{imp,i}}^\alpha \chi_{\text{imp,j}}^\alpha. \tag{11.55}$$

Note that, due to the renormalization, the sum now only goes until N_{imp} as the full sub-space of the 1RDM on the impurity is set up by N_{imp} orbitals.

We see that Eq. (11.51) and Eq. (11.55) have the same form. So, it is possible to make the 1RDMs of the embedded interacting and the embedded mean field system, restricted to the impurity exactly the same. In order to do that, we need to choose the natural orbitals of the mean field 1RDM such that they are the same on the impurity

$$\varphi_{\text{imp},\alpha:1..\text{imp}}^\alpha = \chi_{\text{imp,k:1...imp}}^k. \tag{11.56}$$

Additionally, we have to make the norms the same:

$$n_k \cdot \|\tilde{\chi}\|^2_{\text{imp}} = \|\tilde{\varphi}\|^2_{\text{imp}} \tag{11.57}$$

In fact, there is not only one possible choice for the set of eigenfunctions of the mean field Hamiltonian $\hat{t}'$, but infinitely many. The Hamiltonian

$$\hat{t}_{ij} = \sum_{\alpha=1}^{N_{\text{imp}}} \epsilon^\alpha \|\tilde{\varphi}\|^2_{\text{imp}} \varphi^\alpha_{\text{imp,i}} \varphi^\alpha_{\text{imp,j}} + \sum_{\alpha=1}^{N_{\text{imp}}} \epsilon^\alpha \left(1 - \|\tilde{\varphi}\|_{\text{imp}}\right)^2 \varphi^\alpha_{\text{env,i}} \varphi^\alpha_{\text{env,j}} \tag{11.58}$$

yields the exact same 1RDM on the impurity as the Hamiltonian

$$\hat{t}'_{ij} = \sum_{\alpha=1}^{N_{\text{imp}}} \epsilon'^\alpha \|\tilde{\varphi}\|^2_{\text{imp}} \varphi^\alpha_{\text{imp,i}} \varphi^\alpha_{\text{imp,j}} + \sum_{\alpha=1}^{N_{\text{imp}}} \epsilon'^\alpha \left(1 - \|\tilde{\varphi}\|_{\text{imp}}\right)^2 \varphi'^\alpha_{\text{env,i}} \varphi'^\alpha_{\text{env,j}}, \tag{11.59}$$

where the environment orbitals $\varphi'^\alpha_{\text{env}}$ can be chosen arbitrarily.

A consequence of this arbitrariness is that we can find a non-interacting Hamiltonian $\hat{t}'$ that yields the same 1RDM as the interacting Hamiltonian much simpler than through the minimization of the standard DMET procedure:

The interacting 1RDM of the embedded system, γ_{ij}, yields $2N_{\text{imp}}$ natural orbitals $\tilde{\chi^k}$, Eq. (11.52). As in a non-interacting system, the natural orbitals are equal to the eigenfunctions of the single particle hopping Hamiltonian

$$\hat{t}'_{ij} = \sum_{k=1}^{2N_{\text{imp}}} \epsilon_k \tilde{\chi}^k_i \tilde{\chi}^k_j \tag{11.60}$$

we can directly find the Hamiltonian $\hat{t}'_{ij}$ from the natural orbitals, where we choose the ϵ_k arbitrarily. The condition this Hamiltonian needs to fulfill is that it yields a 1RDM which is on the impurity exactly the same as the 1RDM of the interacting system on the impurity:

$$\gamma^s_{\text{imp,ij}} = \gamma_{\text{imp,ij}}. \tag{11.61}$$

This condition is trivially fulfilled when just taking the natural orbitals $\tilde{\chi}^k$ obtained from the diagonalization of the interacting 1RDM. But it is also fulfilled for any single particle orbitals $\eta^k = \eta^k_{\text{imp}} + \eta^k_{\text{env}}$, where the orbitals on the impurity are the same as before,

$$\eta^k_{\text{imp}} = \tilde{\varphi}^k_{\text{imp}}. \tag{11.62}$$

The eigenfunctions on the environment, $\tilde{\varphi}^k_{\text{env}}$ are completely arbitrary as they do not influence the 1RDM on the impurity at all. This can be seen intuitively by considering a simple explicit example.

This arbitrariness in the eigenfunctions on the environment leads to severe convergence issues in the DMET algorithm.

11.2.2 Comparison of the 1RDM of the embedded interacting with the original interacting system

We have shown that it is possible to make the 1RDMs of the mean field and the interacting system on the impurity the same and which consequences this has. This equivalence does not state anything about the similarity of the interacting 1RDM of the embedded system and the original 1RDM though.

Equally to our study for the wave functions, we also examine the difference between the original 1RDM restricted to the impurity $\gamma|_{\text{imp}}$ and the 1RDM obtained from the embedded system $\gamma_{\text{emb}}|_{\text{imp}}$. We again compare to the 1RDM obtained from a system that is simply cut after 2imp lattice sites. This is equivalent to comparing the efficiency of the projection obtained from the DMET self-consistency loop $\hat{P}^s_{\text{red}}$ and the trivial projection that is unity on the first 2imp lattice sites and zero otherwise. In figure 11.2, we show the result of this comparison: while the difference between the 1RDMs for the DMRG calculation and the cut DMRG system is high for small impurity sizes, it decreases drastically with increasing impurity sizes. For this approach, we now see that both solution will coincide for equal system sizes. Comparing the 1RDM of the full system with the DMET system, we observe that they are already relatively similar for small impurity sizes, but the difference in the 1RDMs increases with growing impurity size.

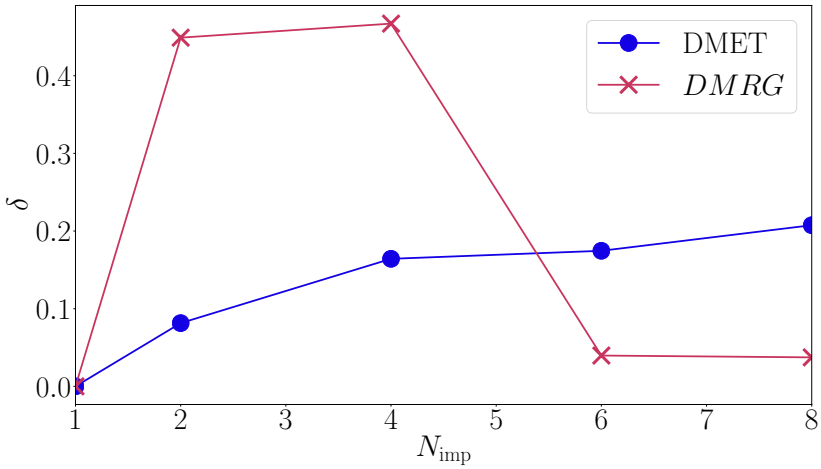

Figure 11.2: Difference between the 1RDM of the full system and the system cut after $2N_{\text{imp}}$ lattice sites (red line, crosses) and the difference between the 1RDM of the full system and the DMET system (blue line, dots)

11.3 Summary

In this chapter, we have examined the claims found in literature about the targets of the DMET algorithm.

We conclude that the wave function on the impurity is not a good target for two reasons. On the one hand, we usually cannot even locally make the wave function of an interacting and a non-interacting system the same. On the other hand, the wave function of the embedded system on the impurity does not become similar to the wave function of the original system on the impurity.

The 1RDM restricted to the impurity is a better property as it is possible to make the 1RDMs of the interacting and the non-interacting systems the same. Also, for small impurity sizes, the difference between the 1RDM from the DMET calculation and the original system is relatively small, making it a good target for DMET. Unfortunately though, there is an ambiguity in the choice of the non-interacting 1RDM and thus, in the non-local potential of the mean field system, leading to convergence issues in the numerical code.

11.3.1 Solutions: How to make the projection well-defined

There are three possible solutions, that we can think of, to fix the ambiguity issue discussed in the section before:

1. Minimizing the 1RDMs on the full system
Instead of making the 1RDMs on the impurity the same

$$\gamma^s_{\text{emb}}|_{\text{imp}} = \gamma_{\text{emb}}|_{\text{imp}}, \tag{11.63}$$

we can try to minimize the distance between the full 1RDMs on the embedded system:

$$\min\left(\gamma^s_{\text{emb}} - \gamma_{\text{emb}}\right). \tag{11.64}$$

This is what is often done in practice and also most of the results obtained in this work were performed by minimizing the full 1RDMs on the embedded system. Still, as the 1RDMs on the full system can never be exactly the same, the mean field 1RDM (and with that the full mean field system), are neither unique nor well defined when taking this path. In practice, we observe that convergence issues can be minimized in this way.

1. Including temperature
It can be shown [15] that in the grand canonical ensemble, that is, including temperature in the system, it is possible to make the 1RDM of a non-interacting system the same as the 1RDM of an interacting system

$$\gamma^{gk,s}_{\text{emb}} = \gamma^{gk}_{\text{emb}}. \tag{11.65}$$

Including temperature in the system is therefore one possible way to solve the ambiguity problem, we will not treat this topic in this thesis though.

2. Using insights from functional theory
In functional theories discussed in section 3.1 of this thesis, there has been done a lot of research on the topic of uniquely mapping properties of non-interacting systems to interacting systems.

We can use these insights by, instead of choosing the 1RDMs as target of the DMET algorithm, choosing a different property such that a unique convergence is achievable.

In the next chapter, we will explore two possible properties that meet this demand.

Chapter 12

Using insights from Functional Theory for DMET

12.1 Density functional theory

As discussed in section 3.1 of this thesis, the foundation of Density Functional Theory is that there is a one-to-one correspondence between the density and the wave function of a chosen system. In other words, the density fully determines the full system, there cannot be two different densities yielding the same ground-state wave function.

For our DMET approach this means that, instead of making the 1RDMs of the interacting and the non-interacting embedded systems the same, we choose to make the densities the same

$$n^s_{\text{emb}} = n_{\text{emb}}. \tag{12.1}$$

When changing the target of DMET in this way, it is on the one hand possible to find a non-interacting Hamiltonian $\hat{T}'$ that exactly meets this demand. On the other hand, we can also be sure that, once we have found it $\hat{T}'$, it is the only (non interacting) Hamiltonian yielding exactly this density. Thus, changing the target from the 1RDM to the density the code should converge more easily.

For our homogeneous Hubbard system, the density on the whole system is also homogeneous

$$n_{ii} = \frac{M}{N}. \tag{12.2}$$

From this property, it follows that also the non-local potential $\hat{V}$ we add to the mean field Hamiltonian

$$\begin{aligned} \hat{T}' &= \hat{T} + \hat{V} \\ &= t \sum_{\langle i,j\rangle,\sigma} \hat{c}^\dagger_{i\sigma}\hat{c}_{j\sigma} + \sum_{i,\sigma} v_{ii}\hat{c}^\dagger_{i\sigma}\hat{c}_{i\sigma} \end{aligned} \tag{12.3}$$

is homogeneous on the impurity. As we continue the non-local potential on the impurity throughout the full system, this means that the mean field Hamiltonian is also homogeneous on the whole system.

Unfortunately, this new Hamiltonian $\hat{T}'$ just changes the phase of the system and does not change the initial guess of the projection $\hat{P}^s_{\text{red}}$, as explained in section 7.2.3. The DMET self-consistency cycle thus converges trivially after one iteration.

So, for homogeneous systems, the density is not enough as a target property.

12.2 Kinetic energy Kohn Sham

As the density is not enough to determine a reduced projection $\hat{P}^s_{\text{red}}$ which can be improved in the self-consistency loop in the homogeneous case, we have to find a property that can yield a projection that can be improved. Preferably, this property should also be uniquely defined though, that is, for a

given non-interacting system, there should only be one external potential yielding a certain value of this property.

One observable fulfilling the above demand is the kinetic energy density K_i that is defined as

$$K_i = 2t_i \cdot \gamma_{i,i+1}, \tag{12.4}$$

where $\gamma_{i,i+1}$ is the first off-diagonal element of the 1RDM and t_i is the prefactor of the next-neighbour hopping term.

For the Hubbard model defined in Eq. (11.1), the non-interacting Hamiltonian which yields the same density n_i and kinetic energy density K_i has the form:

$$\hat{T} = \sum_{\langle i,j\rangle,\sigma} t_i^s \hat{c}_{i\sigma}^\dagger \hat{c}_{j\sigma} + \sum_{i\sigma} v_i^s \hat{c}_{i\sigma}^\dagger \hat{c}_{i\sigma} \tag{12.5}$$

$$\hat{T}|\Phi\rangle = \tilde{E}|\Phi\rangle. \tag{12.6}$$

It can be shown [60] that for a homogeneous system, there is one and only one external potential which yields the same kinetic energy density than the kinetic energy density of the interacting system:

In the interacting system, the hopping element $t_i = t$ is constant. The kinetic energy density K_i thus only depends on the first off-diagonal term of the 1RDM $\gamma_{i,i+1}$ which is the same for all lattice sites i in the homogeneous system. The 1RDM, and with that, the kinetic energy density, thus only depends on the interaction strength in units of the hopping U/t and the relative filling per site $\frac{M}{N}$.

As the 1RDM does not depend on any shifts or phases of the Hamiltonian, as we have discussed in section 7.2.3, the 1RDM of the non-interacting system only depends on the relative filling per site $\frac{M}{N}$.

Thus, we can find a relative hopping of the non-interacting system:

$$t_i^s = \frac{t \cdot \gamma_{i,i+1}}{\gamma_{i,i+1}^s} \tag{12.7}$$

We can adapt our DMET algorithm to not target the 1RDM, but the density n_i and the kinetic energy density K_i in the self-consistency cycle

$$\min\left(\gamma_{\text{emb}} - \gamma_{\text{emb}}^s\right) \to \min\left[\left(n_{\text{emb}} - n_{\text{emb}}^s\right) + \left(K_{\text{emb}} - K_{\text{emb}}^s\right)\right], \tag{12.8}$$

yielding an effective local potential v_i and an effective hopping parameter t_i on the impurity. Note that in order to create a non-trivial self-consistency cycle as a first step the two parameters have to be found on the impurity. Then, in a second step they have to be continued throughout the system by breaking the translational symmetry, as explained in detail in section 7.2.3.

12.2.1 Comparing the kinetic energy density of the original system with the embedded system

In Kinetic Energy Kohn Sham theory, is is always possible to make the kinetic energy density of a mean field and an interacting system the same. Equivalent to the above cases of the wave function and the 1RDM, this does not state anything about the similarity of the kinetic energy density of the embedded system and the original kinetic energy density of the original system though.

In this chapter, like for the wave function and the 1RDM, we examine the difference between the original kinetic energy density, restricted to the impurity $K_i|_{\text{imp}}$ and the kinetic energy density obtained from the embedded system $K_{i\text{emb}}|_{\text{imp}}$, which we will denote by *KEKS 2* here. We again compare to the kinetic energy density obtained from a system that is simply cut after 2imp lattice sites. Additionally, we also compare to the kinetic energy density obtained from the original DMET calculation and from a DMET calculation, where, instead of minimizing the full 1RDM in the self-consistency loop, we just minimize the diagonal and first-off diagonal elements of the 1RDM (which is a property proportional to the kinetic energy density, we will call this method *KEKS 1* here).

In figure 12.1, we see the result of this comparison. The performance of the DMRG calculation as well as the performance of the DMET calculation is very similar to the comparison of the full 1RDMs: The DMRG calculation yields a big difference between the K_i for small impurity sizes and the decreases

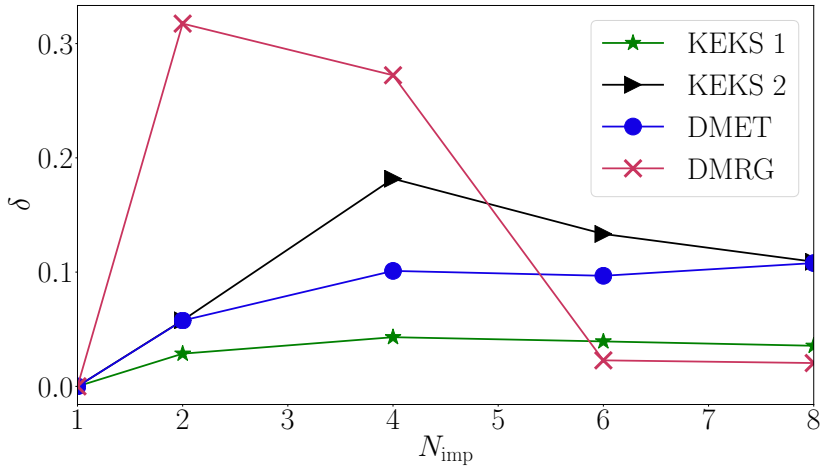

Figure 12.1: Difference between the kinetic energy density K_i of the full system and the system cut after $2N_{\text{imp}}$ lattice sites (red line, crosses), the difference between K_i of the full system and the DMET system (blue line, dots), the difference between K_i for the full system and the Kinetic-Energy-DMET calculation (green, stars) and the difference between K_i for a minimization of the diagonal and first off-diagonal element in the DMET calculation.

with increasing impurity size. In the DMET calculation, the difference between the K_i is already small for small impurity sizes, but increases for growing impurity sizes.

The *KEKS 1* method yields lower values in the of the K_i difference to the full system, which is not surprising as it is optimized to that property. Interestingly though, the difference does not increase with increasing impurity sizes but instead decreases starting from an impurity size of 4. This effect can be seen more drastically when considering the *KEKS 2* method: here, although the difference of the K_i to the full system is bigger than for all other methods (except DMRG), the difference decreases with increasing impurity size.

12.3 Summary

In this chapter, we combined Density Matrix Embedding Theory with insights from functional theory. By changing the target in DMET from making the 1RDMs of the embedded interacting and the mean field systems the same to making the density and the kinetic energy density the same, we improve the method in two ways:

1. Arbitrariness of the projection
In standard DMET, the projection into the embedded system is not unique, leading to convergence issues. Due to the one-to-one correspondence between the kinetic energy and the external potential of our considered homogeneous system, in our method, this arbitrariness is avoided.

2. Agreement of target of the original and the embedded system
We compare the kinetic energy density on the impurity of the embedded system and the original system the same for standard DMET and with our adapted method. The results show that the difference between K_i increases with increasing impurity sizes for standard DMET, but decreases for our method. This shows that agreement between this target for the original system and the embedded system is possible.

The insights presented in this chapter will be published in [59] soon. The expansion of DMET towards functional theories results naturally from an explicit derivation of DMET and the examination of the goals of DMET as we have shown in 11.2.1. This is why we believe that combining DMET with functional theories, which can be either seen as solving numerical and mathematical issues in the DMET code or as finding a new group of functionals in functional theory is a promising pathway towards the description of more realistic, strongly correlated systems. In the future, we aim at testing our new methods for observables beyond the density and the kinetic energy density.

Chapter 13

DMET calculation of the bond stretching in H_2

In section 12.1, we concluded that for a homogeneous system, the density is not a good target as in this case, it only adds a trivial phase to the mean field system. For non-homogeneous systems however, comparing the interacting with the non-interacting density leads to a non-homogeneous local potential in the mean field Hamiltonian.

In this chapter, we combine insights from DMET and DFT to a new method that we call Self-consistent density embedding (SDE). Doing this, we hope to address difficulties in both techniques: As discussed in section 11, in DMET, the mean field system from which the projection is found can never be exact. As a result, the embedded system which is used for the computation of all physical observables is also never exact (although it can be very similar to the original system) leading to numerical convergence issues. This can be improved by using insights from DFT: in Kohn-Sham DFT, as discussed in section 3.2, the mean field system (which is the Kohn-Sham system) is exact as it has the same density as the interacting system and all observables are functionals of the density. Using insights from DFT thus can help to improve the DMET algorithm.

From the DFT perspective, there are two challenges that still have to be faced: on the one hand side, DFT functionals often struggle to describe the physics of strongly correlated systems. Also, once a functional in DFT is found, it cannot be improved anymore. As DMET is designed to treat strongly correlated systems and can be improved systematically by increasing the size of the impurity, with the help of DMET we can also try to find new functionals in DFT.

We test and explain our SDE method which combines DFT and DMET for a simple example system that is not easy to describe with commonly used approximate DFT functionals: the two electrons bond stretching of a heteroatomic molecule in one dimension (see Fig.13.1). Part of the work presented here has been published in the paper [44].

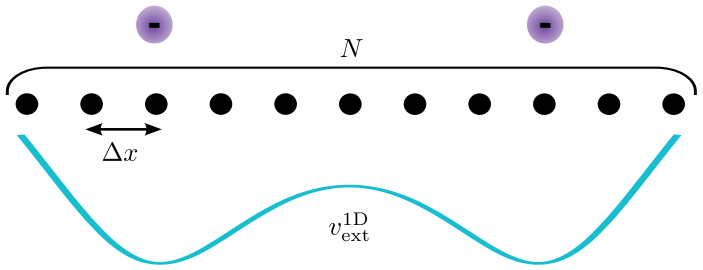

Figure 13.1: Visualization of the 1D H_2 molecule. The real space is discretized on a lattice. The two atoms are modelled through a symmetric double well potential. Sketch from [44]

13.1 Model Hamiltonian for heteroatomic bond stretching

We model the two electron bond stretching with the Hamiltonian[†] : [42]

$$\begin{aligned}\hat{H} = &-\frac{1}{2\,\Delta x^2}\sum_{i,\sigma}(\hat{c}^\dagger_{i+1,\sigma}\hat{c}_{i,\sigma} + \hat{c}^\dagger_{i,\sigma}\hat{c}_{i+1,\sigma} - 2\hat{n}_{i,\sigma}) \\ &+ \sum_{i,\sigma} v_{i,\text{ext}}\hat{n}_{i,\sigma} + \sum_{i,j,\sigma,\sigma'}\frac{\hat{n}_{i\sigma}\hat{n}_{j\sigma'}}{2\sqrt{\left(\Delta x(i-j)\right)^2 + \alpha}},\end{aligned} \tag{13.1}$$

Here, $\hat{c}^\dagger_{i,\sigma}$ and $\hat{c}_{i,\sigma}$ are the creation and annihilation operators of an electron with spin σ on lattice site i, as defined in section 2.1.3. We further define $\hat{n}_{i,\sigma} = \hat{c}^\dagger_{i,\sigma}\hat{c}_{i,\sigma}$, which is the density operator. We consider a one-dimensional box of size L with N lattice points which determines the lattice spacing Δx. Additionally, we employ an external potential v_{ext} which has the form of a double well.

The three terms of the Hamiltonian are describing the energy contribution in the system: The first term is, similar to the kinetic term in the Hubbard model, a next-neighbours hopping term. The second term mimics the ions of the molecule, as we do not explicitly consider these degrees of freedom here, it takes the form of an external potential. It depends on the considered dimension and has the form

$$v_{i,\text{ext}} = -\frac{z_1}{\sqrt{\left(x_i - \frac{d}{2}\right)^2 + \alpha}} - \frac{z_2}{\sqrt{\left(x_i - \frac{d}{2}\right)^2 + \alpha}} + \frac{z_1 z_2}{2\sqrt{(d^2 + \alpha)}} \tag{13.2}$$

while $x_i = \Delta x\left(i - \frac{N-1}{2}\right)$ is the distance between two grid points, the numbers z_1 and z_2 determine the depth of each well respectively. z_1 and z_2 take values between 0 and 2, we will characterize the potential by their difference $\Delta z = z_1 - z_2$.

The third term of the Hamiltonian is the interaction term between the electrons and has a different form than the on-site repulsion of the Hubbard model: We consider a more realistic kind of interaction by not only taking into account the interactions of two electrons on the same lattice site, but also more long-range interactions. This is done with the so-called soft-Coulomb interaction, which has the same form as the normal Coulomb interaction, but avoids the singularity at zero distance which occurs in the one-dimensional case by including a softening parameter $\alpha = 1$.

In a problem including only two electrons, instead of having to do a numerical inversion, we can analytically invert the density n of the problem to yield the Hartree-exchange-correlation potential v_{Hxc}. In our considered Hamiltonian, the ground state of the two-electron problem is always a singlet. This is why we can write the density as

$$n(\boldsymbol{r}) = 2\left|\varphi_0(\boldsymbol{r})\right|^2. \tag{13.3}$$

In section 3.1 of this thesis, we have established the Kohn Sham equations as

$$\left(-\frac{\nabla^2}{2} + v_{\text{S}}(r)\right)\varphi_j(r) = \varepsilon_j\varphi_j(r) \tag{13.4}$$

$$n(r) = \sum_j |\varphi_j(r)|^2. \tag{13.5}$$

We can then insert Eq. (13.3) into Eq. (13.4) yields [21], which yields us an explicit expression for the Hartree-exchange correlation potential in dependence of the density:

$$\hat{v}_{\text{Hxc}}(\boldsymbol{r}) = -\frac{\hat{h}(\boldsymbol{r})\sqrt{n(\boldsymbol{r})}}{\sqrt{n(\boldsymbol{r})}} + \epsilon_0, \tag{13.6}$$

where $\hat{h}(\boldsymbol{r})$ is the single-particle Hamiltonian of the system.

13.2 DMET for non-homogeneous systems

So far we only have treated homogeneous systems. As we treat a non-homogeneous system, the algorithm presented in chapter 7 needs to be adapted.

[†] Both authors contributed equally to this paper.

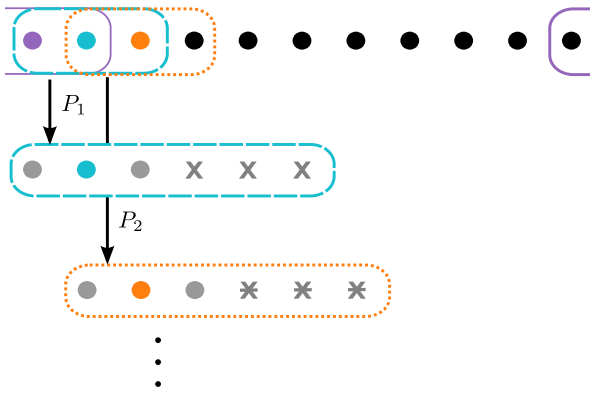

Figure 13.2: Visualization of the patching procedure: In order to obtain a continuous density, we sweep through the system by just going one site forward for each impurity calculation. Then, only the physical properties of the centering site are taken into account and patched together. Sketch from [44]

13.2.1 Patching together the single impurities

For homogeneous systems, the DMET algorithm is simpler insofar as that in order to compute properties of the full system, only one impurity plus embedded system needs to be calculated. As the system is locally the same everywhere, the properties on one impurity can simply be continued throughout the whole system. For non-homogeneous systems, this is not that simple. Different regions in the system can have different densities. In order to compute properties of the whole system we thus have to divide the full system into impurities and perform one DMET self-consistency cycle for each of them. Afterwards, the system is patched back together. Of course, the patching has to be such that the whole system is covered.

In DMET the system is divided into non-overlapping impurities causing artificial discontinuities in local observables [67].

In order to make sure that all impurities connect smoothly to one another, we introduce a continuous patching, where the system is covered by overlapping impurities. In practice, we sweep through the system by just going one site further for each impurity calculation (figure 13.2). When patching the system back together, we only take into account the site in the middle of each impurity. Real space lattices, for which we formulate the theory, have an intrinsic discontinuity (due to discretization of the real space) and our patching procedure is constructed such that the local observables remain as continuous as they can possibly be on a real space lattice.

Further, we have to make sure that when patching the system back together, we retain the correct particle number $\mathcal{N}$ in the full system

$$\langle \hat{\mathcal{N}} \rangle - \mathcal{N} \stackrel{!}{=} 0. \tag{13.7}$$

Following [70], we achieve this by adding and self-consistently optimizing a chemical potential μ to the embedding Hamiltonian of each impurity

$$\hat{H}_{\text{emb}} \to \hat{H}_{\text{emb}} + \mu \sum_{i \in N\text{imp}} \hat{n}_i, \tag{13.8}$$

where $\hat{n}_i$ denotes the density operator on site i. The constant μ in Eq. (13.8) is added only to the impurity part of each H_{emb} in order to achieve a correct particle number on both the impurity and the environment, respectively. In other words, the chemical potential is a Lagrange multiplier, which assures that the constrain in Eq. (13.7) is fulfilled.

13.2.2 Inversion instead of minimizing

For the specific example of targeting the density of the interacting and non-interacting mean field system to be the same on the impurity, instead of minimizing the difference between the two densities and finding a non-local potential yielding the new projection, we can use additional insights from DFT: As in the normal DMET calculation, starting with an initial guess, which is obtained from the one-body part of the Hamiltonian $\hat{h}$, we calculate the projected Hamiltonian $\hat{H}_{\text{emb}}$ and then diagonalize it to obtain the many body wave function $|\Psi_{\text{emb}}\rangle$ of the embedded system. From the wave function,

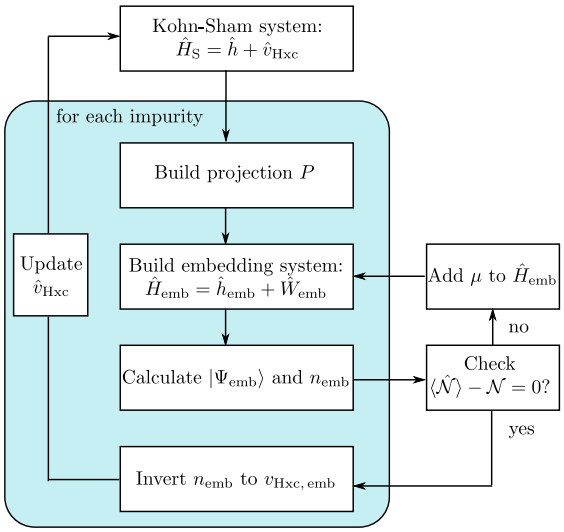

Figure 13.3: Visualization of the SDE algorithm: First, an initial guess for the Kohn-Sham system is made from which the projection is built. Then, the embedding Hamiltonian is calculated and the corresponding ground state wave function and density are computed. The density is then inverted and yields an updated v_{Hxc} which is then used to update the Kohn-Sham system. This is repeated until self-consistency. An additional self-consistency cycle is added in order to maintain the correct particle number. Sketch from [44]

we calculate the density n_{emb} on the impurity. But now, instead of minimizing the difference between the interacting and the non-interacting density with a Simplex algorithm as explained in section 5.4, we use the Hohenberg-Kohn theorem on the mean field system, which is equivalent to a Kohn-Sham system in DMET. From the Hohenberg-Kohn theorem it follows that in real space, every interacting density has a corresponding non-interacting wave function $|\Phi\rangle$ and local potential v_S.

Thus, having calculated the density exactly on the impurity, we can find the corresponding Kohn-Sham potential for this impurity by inversion [21, 29, 27, 47]. Inverting the density on every impurity yields the new Kohn-Sham Hamiltonian $\hat{h} + \hat{v}_{Hxc}$. Note that the inversion is performed independently for each impurity and the total Kohn-Sham potential is patched together as we describe in detail in section 13.2.1. We then use the new Kohn-Sham Hamiltonian to calculate a new projection $\hat{P}^s_{red}$. This is done, similar to the original DMET algorithm, until convergence (see Fig. 13.3).

13.3 Results

13.3.1 Dissociation of the H_2 molecule

As a first step, we consider Δz in above defined Hamiltonian, which means that the external double well potential has two wells of the same depth. With in total two particles in the system, this corresponds to the modelling of the H_2 model. We vary the bond length of the model, that is, the distance between the two wells of the external potential to show the behaviour of the bond stretching of the H_2 molecule. We expect the following behaviour: For a specific distance between the two cores, we compute a minimal energy E_0 which is the stable distance between the two cores. When changing the bondlengths either to smaller or to bigger values, the energy should always increase. In the case of smaller bond lengths, this is a drastic increase due to the repulsive core-core interaction. In the case of bigger distance, the bonding energy that makes it possible to form molecules is decreasing. For very large core distances $d \to \infty$, this contribution goes to zero as we now have two separate H atoms.

In Fig. 13.4, we show the ground state energy E_0 of the Hamiltonian described in 13.1. We observe that our SDE method describes exactly the behaviour we are expecting. Additionally, comparing to results from an exact diagonalization calculation, we see that our method quantitatively agrees with the exact solution. The advantage of our method is the much lower computational cost: While for the exact solution, the computational costs grow exponentially with the number of orbitals N (4^N), in the SDE method, only the costs of the impurity calculation is exponential. The underlying mean field calculation is growing quadratic with the amount of orbitals, multiplied by the number of

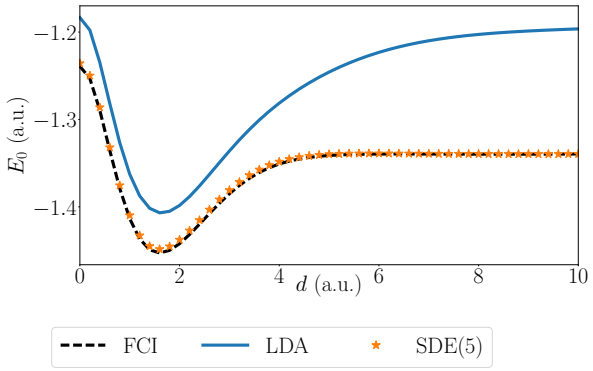

Figure 13.4: Ground state energy of the H_2 molecule, modeled in 1D calculated with SDE and $N_{\text{imp}} = 5$ (orange stars), Full-CI (black dashes line) and one dimensional LDA (solid blue line). When varying the distance of the two core potentials d, the energy curve has a minimum corresponding to a stable molecule. For smaller core distances, the energy grows due to the repulsion of the two cores. Increasing the distance $d \to \infty$ leads to the vanishing of the binding energy resulting in two separate atoms. Following set of parameters has been used (see section 13.1): number of real space lattice sites $N = 120$, box size $L = 20$, potential well difference $\Delta z = 0$, softening parameter $\alpha = 1$. Graph from [44]

impurities N, and the needed self-consistency iterations η ($4^{2 \cdot N_{\text{imp}}} \cdot N^3 \cdot \eta$). We additionally compare the results with those from a one dimensional LDA-DFT [20] calculation, whose computational costs are even lower. The costs for the LDA calculation grow quadratic with the number of lattice sites times the self-consistency iterations ($N^2 \cdot \eta$) but they also do not describe the behaviour of the H_2 bond stretching accurately. Specifically, the LDA calculation fails to describe the ground state energy of the system for large bond lengths.

13.3.2 Peaks and steps in the Kohn-Sham potential

In Kohn-Sham DFT, a non-interacting system is used to describe an interacting one. Here, the interaction consists of the repulsion of the two electrons in the H_2 model. As the Kohn Sham system does not include an actual interaction term, this repulsion needs to be mimicked by the (external) Kohn-Sham potential. In order to do so, we expect to see a peak that prevents the two electrons from being at the same atom, as has been investigated in previous work [61, 16, 21].

We consider the density and the Kohn-Sham potential from the SDE calculation in Fig. 13.5 to observe this peak. Specifically, we consider one computation with 5 impurity sizes (denoted as SDE(5) in the figure) and one computation with 9 impurity sizes (denoted as SDE(9) in the figure) and compare with the density and Kohn Sham potential obtained from the ED calculation.

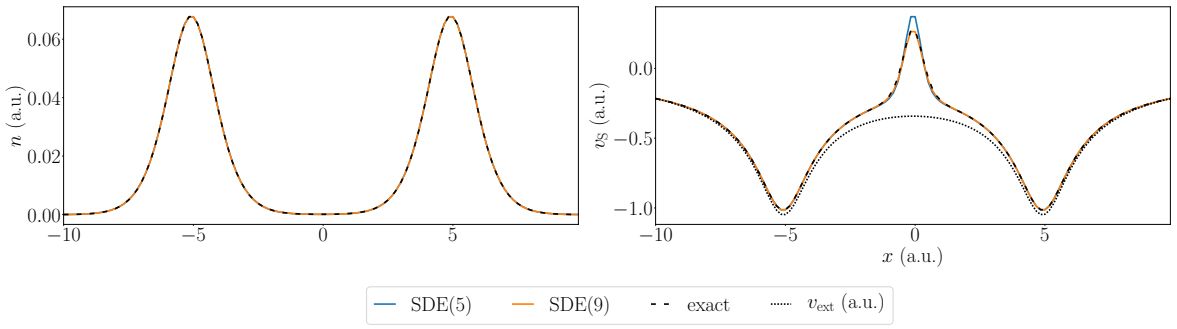

Figure 13.5: Density distribution $n(x)$ and Kohn-Sham potential $v_S(x)$ with SDE(5) (solid blue line), SDE(9) (solid orange line) and full CI (dashes black line). The exact and the SDE solution agree quantitatively. The SDE Kohn-Sham potential shows the expected peak in the center which mimics the electron-electron interaction. For small impurity sizes, this behaviour is overestimated, but converges quickly to a quantitatively exact result for bigger impurity sizes. The following set of parameters has been used: $N = 120$, $L = 20$, $d = 10$, $\Delta z = 0$. Graph from [44]

On the left hand side, we plot the density of the model and observe that both SDE calculations agree quantitatively with the exact calculation. Considering the right hand side, where we plotted the Kohn Sham potential, we observe a peak at position $x = 0$ in for both SDE calculations and the exact calculation. For an impurity size of 5, this peak is overestimated, for an impurity size of 9 it

agrees quantitatively with the exact solution. We can thus conclude that we can reproduce the exact Kohn-Sham potential for the one-dimensional H_2 model.

As a next step, we consider the external double well potential to be asymmetric, that is $\Delta z = 0.5$. This Hamiltonian can be used to mimic heteroatomic molecules and their behaviour under bond stretching.

Considering again the density and the Kohn Sham potential in figure 13.6, we first of all observe that the density of the molecule is not symmetric for an asymmetric external potential, which not only makes sense but also agrees quantitatively with the exact solution. On the right hand side of

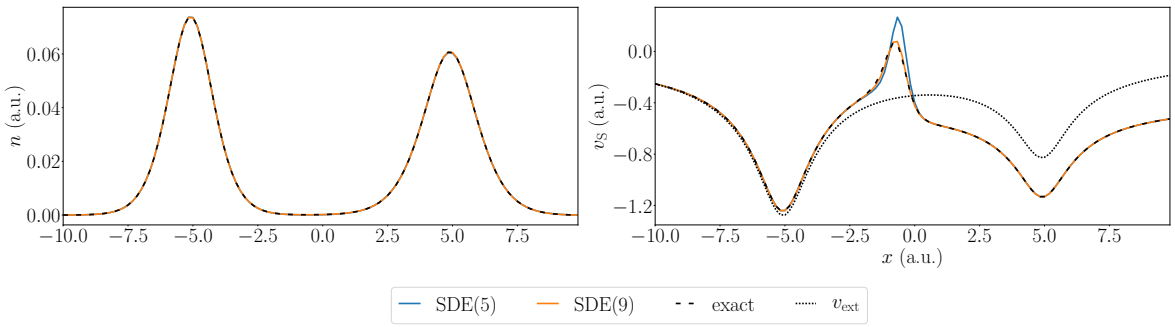

Figure 13.6: Density distribution $n(x)$ and Kohn-Sham potential $v_S(x)$ for an asymmetric external core potential with SDE(5) (solid blue line), SDE(9) (solid orange line) and full CI (dashes black line). To account for the asymmetry in the density distribution, in addition to the peak we observe a step going from the right side of the molecule to its left side. The following set of parameters has been used: $N = 120$, $L = 20$, $d = 10$, $\Delta z = 0.5$. Graph from [44]

the figure, we again consider the Kohn-Sham potential. As for the symmetric external potential, we observe a peak separating the two electrons from each other, which corresponds to the mimicking of the electron-electron repulsion in the interacting case. Additionally, we observe a step between the potential on the left and the right side. This step is necessary to obtain an asymmetric density.

13.4 Summary

In this chapter, we combined DMET with DFT to a new method which we call SED. We tested this method on the bond stretching of H_2 and find very good results.

Part V

Summary and Outlook

Chapter 14

Summary and Outlook

14.1 Summary

The first goal of this thesis was to understand some of those methods and their implications towards our understanding of nature. In the first part of this thesis, we decided on one specific setting, that is, non-relativistic many body quantum mechanics on a discretized real space lattice. We presented different techniques that are widely used for the numerical solution of model systems in this setting. Specifically, we presented two groups of approaches which are used to solve the models mentioned above, namely wave function methods and the functional methods. We highlighted advantages and problems of both groups of methods. In the second part of this thesis, we analyzed and presented in great detail a method that takes a third approach in between the two above mentioned groups. The method, called Density Matrix Embedding Theory, is an embedding technique, where one part of the system is treated with a wave function method and the connection towards the remaining system can be understood in terms of functional theory.

The second goal of this thesis was to expand DMET to be able to treat coupled electron-boson systems. We then tested DMET for coupled electron-phonon systems on the Hubbard-Holstein model, which describes the fundamental interactions between electrons and phonons. In order to be able to describe the physics of the Hubbard-Holstein model, we needed to decide which observables to consider. Here, we took great care of excluding or at least quantifying the limitations of the method, making sure that problems such as finite size effects are controlled. Comparing with the Tensor Network method, we found that our electron-phonon DMET is able to describe the quantum phase transitions of the Hubbard-Holstein model

The third goal of this thesis was to expand the DMET method to bridge functional methods and wave function methods thus forming a possible pathway towards being able to treat ab initio systems with strong correlations. Upon a profound analysis of the DMET method, we found the connection to functional methods already inside the method itself, which lead towards an improvement of the DMET method or, seen from the functional perspective, towards the possibilities of finding functionals in a different way. We showed that the expansion of DMET towards functional methods is in principle possible for two different settings: In the homogeneous case, we can include insights from Kinetic Energy Kohn Sham theory in the DMET technique and for inhomogeneous systems, we can use Density Functional Theory. The latter approach has been proven to be successful for the treatment of a model system of H_2.

14.2 Outlook

This thesis is, of course, just a small piece in a much bigger puzzle. Besides the fact that there are obviously a lot of other approaches towards a better understanding of nature, there are also a lot of pathways starting from this thesis. There are three ways in which the work presented in this thesis can be continued

14.2.1 DMET for electron-boson systems

We have considered the one-dimensional Hubbard-Holstein model which describes the coupling of electrons to phonon modes but the expansion of the DMET method is general and allows the treatment of any coupled electron-boson system. Thus, in a next step we can also describe electron-photon or even electron-phonon-photon coupling with DMET. Also an expansion towards two-dimensional systems, which for the purely electronic DMET has already been explored, is possible.

14.2.2 Improving DMET with further insights from functional theory

We have shown two possible ways DMET can be improved with Kinetic Energy Kohn Sham Theory or with Density Functional Theory, but so far we have only applied this new method to a H_2 toy model. In a next step, we can treat a more complicated system with our new method.

In the literature the presentation of DMET is convoluted and relatively implicit. In this thesis, we have taken the first steps toward a more mathematical formulation of this theory but we still have not fully analyzed the implications and relations of the projection in the DMET system. A more fundamental analysis could help to improve DMET even further.

14.2.3 Finding new functionals with DMET

As functional theory shows up naturally in the DMET methods, it makes sense to include DMET in embedding DFT methods.

The DMET-DFT approach allows to find a density-to-potential mapping in a completely new setting that does not follow the energy minimization which is usually done in DFT approaches. Additionally, this approach seems to work well especially for strongly correlated systems.

Of course it is also possible, on a larger scope, to combine all above mentioned proposals. Seeing DMET and DFT not as two separate but as one hybrid method would make it possible to find functionals for coupled electron-boson systems that are able to treat strongly correlated systems and that additionally can be improved systematically. Recent experiments on coupled electron-photon systems in a cavity set-up [39, 9, 54, 43, 10, 32, 1] show the need for the ab-initio treatment of coupled electron-photon systems.

Chapter 15

Appendix

15.1 Finite size extrapolation for the DMRG data

In the DMRG calculation, opposed to the DMET calculation, we only have two sources of possible errors due to finite size effects: the system size itself and the maximal number of considered basis functions in the phononic Fock space N_{phon}. We discuss both in this section.

15.1.1 Phonon basis functions per site

Similar to the convergence discussion for the DMET method, we show the convergence of the DMRG calculation with increasing number of phononic basis functions per site. We choose two observables: the energy gap in figure 15.1 and the convergence of the energy per site in 15.2 and show results both for the anti-adiabatic ($\alpha = 5.0$) as well as for the adiabatic limit ($\alpha = 0.5$).

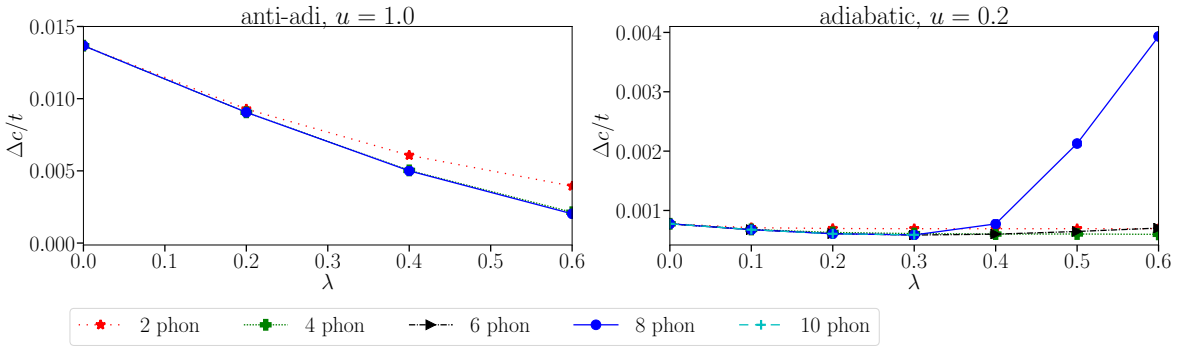

Figure 15.1: Scaling with the number of phononic basis functions per lattice site of the energy gap $\Delta c/t$. For the anti-adiabatic limit, the results are converged for a number of basis functions of 8 while in the adiabatic-limit in the Peierls phase, no convergence is reached even for a number of basis functions of 10. The position of the gap is predicted correctly for a number of basis functions of 8.

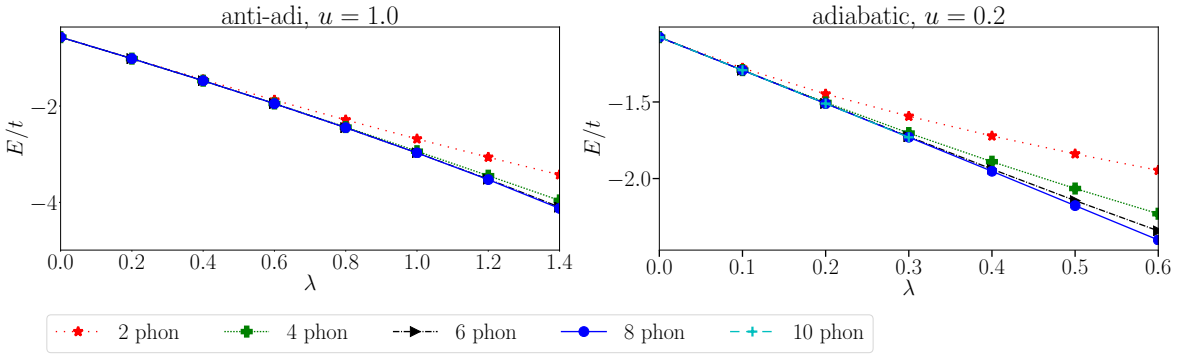

Figure 15.2: Scaling with the number of phononic basis functions per lattice sites for the energy per site E/t. While the results are converged in the anti-adiabatic limit for 8 basis functions, again in the adiabatic limit, no convergence can be reached for a maximal number of basis functions of 10

Both for the energy gap $\Delta c/t$ as well as for the energy per site E/t, we observe similar results as in the DMET calculations: While in the anti-adiabatic limit $\alpha = 5.0$, convergence is reached for a number of phononic basis functions per site of 8, in the adiabatic limit, no convergence can be reached with a maximal number of basis functions of 10. As the position of the gap is predicted quantitatively for the anti-adiabatic and the adiabatic case, both for a number of basis functions of 8, we will conduct all further calculations with this number of basis functions.

15.1.2 Finite size scaling

Unlike in the DMET method, the numerical costs of the DMRG calculations grow polynomial with growing system sizes. This is why, for our extrapolation, we chose to consider system sizes of $N = 24$, $N = 48$ and $N = 96$, as can be seen in Figure. 15.3 We observe that, while Energy gap E/t is

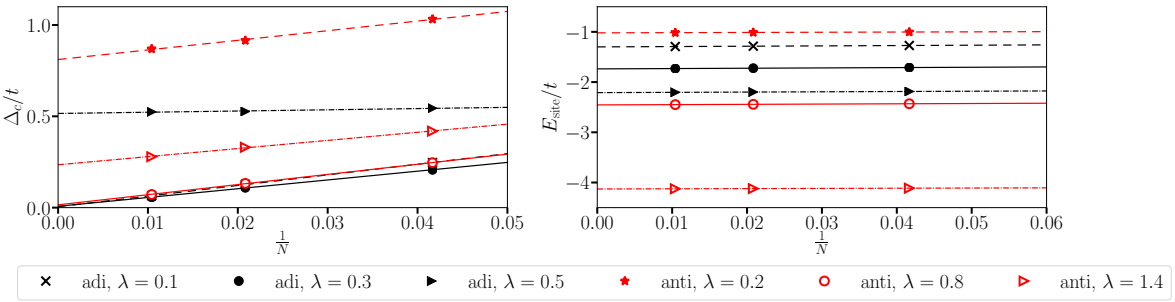

Figure 15.3: Finite size scaling for the energy gap in the DMRG calculation. We show some examples, both for the adiabatic limit ($\lambda = 0.1; 0.3; 0.5$ and $u = 0.2$) as well as for the anti-adiabatic limit ($\lambda = 0.2; 0.8; 1.4$ and $u = 1.0$). The extrapolation is done with system sizes of $N = 24; 48; 96$. The scaling is again linear, making it possible remove finite size effects. Also for the DMRG calculation, we observe that the values do not differ for the different system sizes, which leads us to conclude that for this observable, the finite size effects are already negligible for system sizes ≥ 24.

already converged with respect for a total system size of $N = 24$ lattice sites, hence no extrapolation is needed, this is not the case for the energy gap $\Delta c/t$. In all the DMRG plots shown in the main text, we consider DMRG data that are extrapolated with respect to the total system size.

15.2 Remaining finite size extrapolation for the DMET data

In the main text, in order to keep the discussion short, we only considered selected observables for which showed the extrapolation and the discussion of convergence for the DMET calculations. Here, we also discuss the remaining observables.

15.2.1 Phonon basis functions per site: Double occupancy

Beside the energy gap, also the double occupancy is an important observable that is considered in the discussion of the Hubbard-Holstein phase diagram.

We see that the convergence with respect to the total number of phononic basis functions per site is analogous to the energy gap. While for the anti-adiabatic limit $\alpha = 5.0$, the results are converged for a number of basis functions of 8, in the adiabatic limit $\alpha = 0.5$, not even a number of basis functions of 12 is sufficient to converge the behaviour deep in the Peierls phase although the position of the phase transition is predicted correctly.

We choose a number of phononic basis functions of 8 for all DMET calculations.

15.2.2 Scaling with the whole system size: Energy per site

Considering the finite size scaling of the energy per site E/t with the total system size, we observe no dependence of this observable on the considered system sizes of $N = 408; 816; 1632$. We therefore conclude that the energy per site is already converged for total system size of $N = 408$.

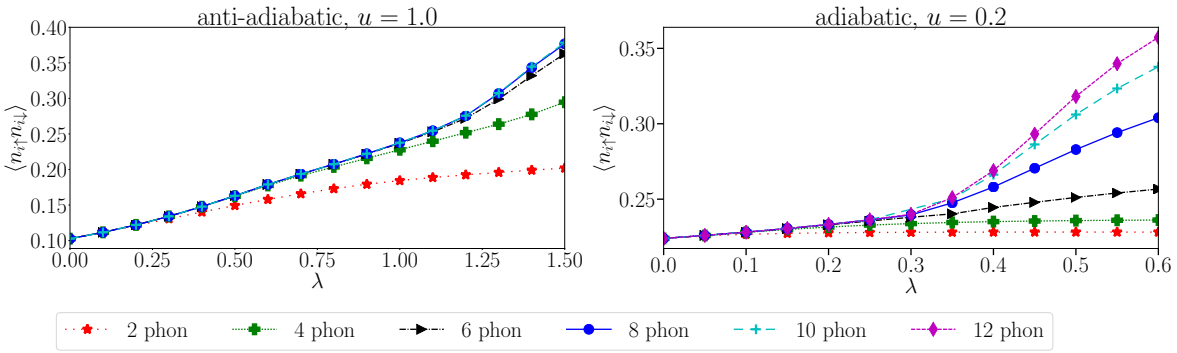

Figure 15.4: Scaling of the double occupancy $\langle n_{\uparrow i} n_{\downarrow i} \rangle$ in the adiabatic $\alpha = 0.5$, $u = 0.2$ and in the anti-adiabatic limit $\alpha = 5.0$, $u = 1.0$. In the anti-adiabatic regime, the results are converged for 8 phononic basis functions per site while in the Peierls phase of the adiabatic regime, not even 12 basis functions are sufficient.

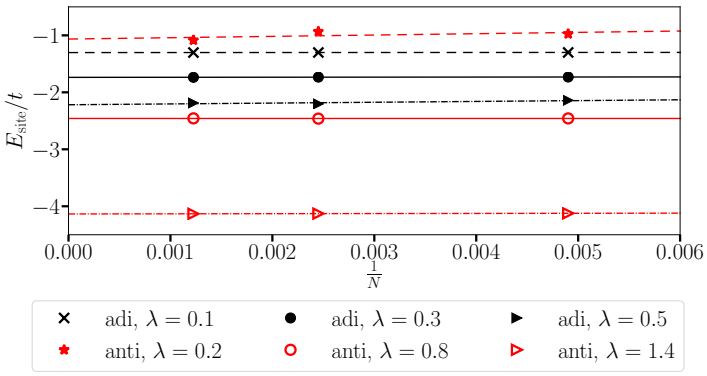

Figure 15.5: Finite size scaling for the energy per site in the DMET calculation. We show some examples, both for the adiabatic limit ($\lambda = 0.15; 0.35; 0.55$ and $u = 0.2$) as well as for the anti-adiabatic limit ($\lambda = 0.25; 0.85; 1.45$ and $u = 1.0$). The extrapolation is done with system sizes of $N = 408; 816; 1632$. The scaling is linear, making it possible to remove finite size effects. We also observe that the values do not differ for the different system sizes, which leads us to conclude that for this observable, the finite size effects are already negligible for system sizes ≥ 408.

15.2.3 Scaling with the impurity size: anti-adiabatic limit

In the main text, we showed the scaling with the number of impurity lattice sites in the DMET calculation only for the adiabatic limit. In the anti-adiabatic limit, we observe similar results: While the results are already converged for an impurity size of $N_{\text{imp}} = 6$ in the Mott phase, $\lambda \leq 0.75$ and also the position of the gap is not changing anymore, the size of the gap in the Peierls phase is not converged. The same situation can be observed for the double occupancy $\langle n_{i\uparrow} n_{i\downarrow} \rangle$.

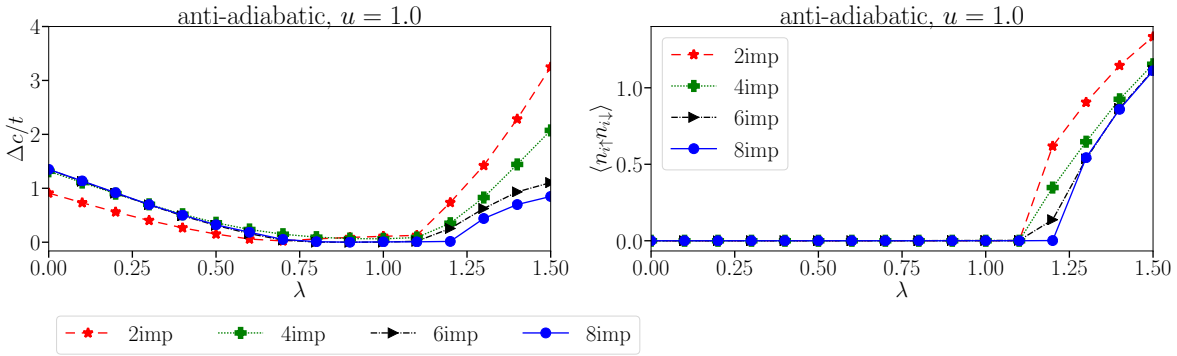

Figure 15.6: Finite size scaling of the impurity for the energy gap $\Delta c/t$ (left hand side) and the double occupancy $\langle n_{i\uparrow} n_{i\downarrow} \rangle$ (right hand side) in the DMET calculation: we plot the dependence energy gap $\Delta c/t$ on the electron-phonon coupling strengths λ for different impurity sizes, going from $N_{\text{imp}} = 2$ to $N_{\text{imp}} = 8$ in steps of 2. While both observables seem to decrease with increasing impurity size, the scaling seems to converge for the double occupancy while that is not the case for the energy gap.

Bibliography

[1] A. A. Allocca, Z. M. Raines, J. B. Curtis, and V. M. Galitski. Cavity superconductor-polaritons. *arXiv:1807.06601*, 2018.

[2] J. Bardeen, L. N. Cooper, and J. R. Schrieffer. Theory of superconductivity. *Phys. Rev.*, 108(5):1175–1204, 1957.

[3] J. Bauer and A. C. Hewson. Competition between antiferromagnetic and charge order in the hubbard-holstein model. *Phys Rev B*, 81(23):235113, 2010.

[4] A. D. Becke. Density-functional exchange-energy approximation with correct asymptotic behavior. *Phys Rev A*, 38(6):3098–3100, 1988.

[5] A. D. Becke. Density-functional thermochemistry. iii: The role of exact exchange. *J. Chem. Phys.*, 98(7):5648–5652, 1993.

[6] J. P. Blaizot and G. Ripka. *Quantum Theory of Finite Systems*. The MIT Press, Cambridge, Massachusetts, 1986.

[7] K. Burke. Perspective on density functional theory. *J. Chem. Phys.*, 136(15):150901, 2012.

[8] R. T. Clay and R. P. Hardikar. Intermediate phase of the one dimensional half-filled hubbard-holstein model. *Phys. Rev. Lett.*, 95(9):096401, 2005.

[9] O. Cotleţ, S. Zeytinoğlu, M. Sigrist, E. Demler, and A. Imamoğlu. Superconductivity and other collective phenomena in a hybrid bose-fermi mixture formed by a polariton condensate and an electron system in two dimensions. *Phys. Rev. B*, 93(5):054510, 2016.

[10] J. B. Curtis, Z. M. Raines, A. A. Allocca, M. Hafezi, and V. M. Galitski. Cavity quantum eliashberg enhancement of superconductivity. *arXiv:1805.01482*, 2018.

[11] R. M. Dreizler and E. K. U. Gross. *Density functional theory: an approach to the quantum many-body problem*. Springer, Berlin, 1990.

[12] W. Ehrenberg and R. E. Siday. The refractive index in electron optics and the principles of dynamics. *Proc. Phys. Soc. B*, 16(1):1062, 1949.

[13] H. Fehske, G. Hager, and E. Jeckelmann. Metallicity in the half-filled holstein-hubbard model. *Europhys. Lett*, 84(5):57001, 2008.

[14] E. Fradkin and J. E. Hirsch. Phase diagram of one-dimensional electron-phonon systems. i. the su-schrieffer-heeger model. *Phys. Rev. B*, 27(3):1680–1697, 1983.

[15] K. J. H. Giesbertz and M. Ruggenthaler. One-body reduced density-matrix functional theory in finite basis sets at elevated temperatures. *arXiv:1710.08805*, 2017.

[16] O. V. Gritsenko, R. van Leeuwen, and E. J. Baerends. Molecular kohn-sham exchange-correlation potential from the correlated ab initio electron density. *Phys. Rev. A*, 52(3):1870–1874, 1995.

[17] R. Gross. *Physik IV Vorlesungsskript zur Vorlesung im SS 2003*. Walther-Meissner-Institut, Technische Universität München, 2003.

[18] G. Gruner. *Density Waves In Solids*. CRC Press, 2018.

[19] R. P. Hardikar and R. T. Clay. Phase diagram of the one-dimensional hubbard-holstein model at half and quarter filling. *Phys. Rev. B*, 75(24):245103, 2007.

[20] N. Helbig, J. I. Fuks, M. Casula, M. J. Verstraete, M. A. L. Marques, I. V. Tokatly, and A. Rubio. Density functional theory beyond the linear regime: Validating an adiabatic local density approximation. *Phys. Rev. A*, 83(3):032503, 2011.

[21] N. Helbig, I. V. Tokatly, and A. Rubio. Exact kohn-sham potential of strongly correlated finite systems. *J. Chem. Phys.*, 131(22):224105, 2009.

[22] M. Hohenadler and F. F. Assaad. Excitation spectra and spin gap of the half-filled holstein-hubbard model. *Phys. Rev. B*, 87(7):075149, 2013.

[23] P. Hohenberg and W. Kohn. Inhomogeneous electron gas. *Phys. Rev.*, 136(3):B864–B871, 1964.

[24] C. Hubig, I. P. McCulloch, and U. Schollwöck. Generic construction of efficient matrix product operators. *Phys. Rev. B*, 95(3):035129, 2017.

[25] C. Hubig, I. P. McCulloch, U. Schollwöck, and F. A. Wolf. Strictly single-site dmrg algorithm with subspace expansion. *Phys. Rev. B*, 91(15):155115, 2015.

[26] E. T. Jaynes. *Probability Theory: The logic of science*. Cambridge University Press, 2003.

[27] D. S. Jensen and A. Wasserman. Numerical methods for the inverse problem of density functional theory. *Int. J. Quantum Chem.*, 118(1):e25425, 2017.

[28] S. Johnston, E. A. Nowadnick, Y. F. Kung, B. Moritz, R. T. Scalettar, and T. P. Devereaux. Determinant quantum monte carlo study of the two-dimensional single-band hubbard-holstein model. *Phys. Rev. B*, 87(23):235133, 2013.

[29] A. A. Kananenka, S. V. Kohut, A. P. Gaiduk, I. G. Ryabinkin, and V. N. Staroverov. Efficient construction of exchange and correlation potentials by inverting the kohn–sham equations. *J. Chem. Phys.*, 139(7):074112, 2013.

[30] P. Kapitza. Viscosity of liquid helium below the λ-point. *Nature*, 141(74), 1938.

[31] T. Kennedy and E. H. Lieb. Proof of the peierls instability in one dimension. *Phys. Rev. Lett.*, 59(12):1309–1312, 1987.

[32] M. Kiffner, J. Coulthard, F. Schlawin, A. Ardavan, and D. Jaksch. Manipulating quantum materials with quantum light. *arXiv:1806.06752*, 2018.

[33] P. Knabner and W. Barth. *Lineare Algebra: Grundlagen und Anwendungen*. Springer Berlin Heidelberg, 2018.

[34] G. Knizia and G. K.-L. Chan. Density matrix embedding: A simple alternative to dynamical mean-field theory. *Phys. Rev. Lett.*, 109(18):186404, 2012.

[35] G. Knizia and G. K.-L. Chan. Density matrix embedding: A strong-coupling quantum embedding theory. *J. Chem. Theory Comput.*, 9(3):1428–1432, 2013.

[36] W. Kohn and L. J. Sham. Self-consistent equations including exchange and correlation effects. *Phys. Rev.*, 140(4):A1133–A1138, 1965.

[37] Rolf Landauer. Information is physical. *Phys. Today*, 44(5):23, 1991.

[38] A. Lanzara, P. V. Bogdanov, X. J. Zhou, S. A. Kellar, D. L. Feng, E. D. Lu, T. Yoshida, H. Eisaki, A. Fujimori, K. Kishio, J.-I. Shimoyama, T. Noda, S. Uchida, Z. Hussain, and Z.-X. Shen. Evidence for ubiquitous strong electron–phonon coupling in high-temperature superconductors. *Nature*, 412(6846):510–514, 2001.

[39] F. P. Laussy, A. V. Kavokin, and I. A. Shelykh. Exciton-polariton mediated superconductivity. *Phys. Rev. Lett.*, 104(10):106402, 2010.

[40] C. Lee, W. Yang, and R. G. Parr. Development of the colle-salvetti correlation-energy formula into a functional of the electron density. *Phys. Rev. B*, 37(2):785–789, 1988.

[41] Elliott H. Lieb and F. Y. Wu. Absence of mott transition in an exact solution of the short-range, one-band model in one dimension. *Phys. Rev. Lett.*, 20(25):1445–1448, 1968.

[42] M. Lubasch, J. I . Fuks, H. Appel, A. Rubio, I. Cirac, and M.-C. Bañuls. Systematic construction of density functionals based on matrix product state computations. *New J. Phys.*, 18(8):083039, 2016.

[43] G. Mazza and A. Georges. Superradiant quantum materials. *arXiv:1804.08534*, 2018.

[44] U. Mordovina, T. E. Reinhard, H. Appel, and A. Rubio. Self-consistent density-functional embedding: a systematically improvable approach for density functionals. *In preparation*, 2018.

[45] Y. Murakami, P. Werner, N. Tsuji, and H. Aoki. Ordered phases in the holstein-hubbard model: Interplay of strong coulomb interaction and electron-phonon coupling. *Phys. Rev. B*, 88(12):125126, 2013.

[46] J. A. Nelder and R. Mead. A simplex method for function minimization. *Comput. J.*, 7(4):308–313, 1965.

[47] S. E. B. Nielsen, M. Ruggenthaler, and R. van Leeuwen. Numerical construction of the density-potential mapping. *Eur. Phys. J. B*, 91(10):235, 2018.

[48] E. A. Nowadnick, S. Johnston, B. Moritz, R. T. Scalettar, and T. P. Devereaux. Competition between antiferromagnetic and charge-density-wave order in the half-filled hubbard-holstein model. *Phys. Rev. Lett.*, 109(24):246404, 2012.

[49] H. K. Onnes. The resistance of pure mercury at helium temperatures. *Commun. Phys. Lab. Univ. Leiden*, 12:120, 1911.

[50] R. E. Peierls and R. Peierls. *Quantum Theory of Solids*. Clarendon Press, 1955.

[51] J. P. Perdew, K. Burke, and M. Ernzerhof. Generalized gradient approximation made simple. *Phys. Rev. Lett.*, 77(18):3865–3868, 1996.

[52] K. Pernal and K. J. H. Giesbertz. *Reduced Density Matrix Functional Theory (RDMFT) and Linear Response Time-Dependent RDMFT (TD-RDMFT)*, pages 125–183. Springer International Publishing, 2016.

[53] T. E. Reinhard, U. Mordovina, C. Hubig, J. S. Kretchmer, U. Schollwöck, H. Appel, M. A. Sentef, and A. Rubio. Density-matrix embedding theory study of the one-dimensional hubbard-holstein model. *arXiv:1811.00048*, 2018.

[54] F. Schlawin, A. Cavalleri, and D. Jaksch. Cavity-mediated electron-photon superconductivity. *arXiv:1804.07142*, 2018.

[55] U. Schollwöck. The density-matrix renormalization group in the age of matrix product states. *Ann. Phys.*, 326(1):96–192, 2011.

[56] M. A. Sentef, M. Ruggenthaler, and A. Rubio. Cavity quantum-electrodynamical polaritonically enhanced electron-phonon coupling and its influence on superconductivity. *arXiv:1802.09437*, 2018.

[57] K. M. Shen, F. Ronning, D. H. Lu, W. S. Lee, N. J. C. Ingle, W. Meevasana, F. Baumberger, A. Damascelli, N. P. Armitage, L. L. Miller, Y. Kohsaka, M. Azuma, M. Takano, H. Takagi, and Z.-X. Shen. Missing quasiparticles and the chemical potential puzzle in the doping evolution of the cuprate superconductors. *Phys. Rev. Lett.*, 93(26):267002, 2004.

[58] G. Stefanucci and R. Van Leeuwen. *Nonequilibrium many-body theory of quantum systems: a modern introduction*. Cambridge University Press, 2013.

[59] M. Ruggenthaler T. E. Reinhard, I. Theophilou and A. Rubio. Foundations of density matrix embedding theory revisited: a density matrix functional perspective.

[60] I. Theophilou, F. Buchholz, F. G. Eich, M. Ruggenthaler, and A. Rubio. Kinetic-energy density-functional theory on a lattice. *J. Chem. Theory Comput.*, 14(8):4072–4087, 2018.

[61] R. van Leeuwen and E. J. Baerends. Exchange-correlation potential with correct asymptotic behavior. *Phys. Rev. A*, 49:2421–2431, Apr 1994.

[62] Thomas Vojta. Quantum phase transitions in electronic systems. *Ann. Phys.*, page 38, 2000.

[63] W. von der Linden, E. Berger, and P. Valášek. The hubbard-holstein model. *J. Low Temp. Phys.*, 99(3):517–525, 1995.

[64] K. von Klitzing. The quantized hall effect. *Rev. Mod. Phys.*, 58(3):519–531, 1986.

[65] J. Wang and S.-C. Zhang. Topological states of condensed matter. *Nat. Mat.*, 62:8–21, 2017.

[66] M. Weber and M. Hohenadler. Two-dimensional holstein-hubbard model: Critical temperature, ising universality, and bipolaron liquid. *Phys. Rev. B*, 98(8):085405, 2018.

[67] M. Welborn, T. Tsuchimochi, and T. Van Voorhis. Bootstrap embedding: An internally consistent fragment-based method. *J. Chem. Phys.*, 145(7):074102, 2016.

[68] P. Werner and A. J. Millis. Efficient dynamical mean field simulation of the holstein-hubbard model. *Phys. Rev. Lett.*, 99(14):146404, 2007.

[69] John Archibald Wheeler. Information, physics, quantum: The search for links. In *Proceedings III International Symposium on Foundations of Quantum Mechanics*, pages 354–358. Physics Department, Princeton University, 1989.

[70] S. Wouters, C. A. Jiménez-Hoyos, Q. Sun, and G. K.-L. Chan. A practical guide to density matrix embedding theory in quantum chemistry. *J. Chem. Theory Comput.*, 12(6):2706–2719, 2016.

Acknowledgements

Finishing this thesis would have never been possible without the help of many people that I would like to thank here.

First of all, I wish to thank my supervisors Angel Rubio and Heiko Appel. I am grateful to Angel Rubio for helping me to find the bigger picture and the guiding thread of my thesis. I also benefited much from the possibilities to travel and learn at conferences, summer schools and during my stay in Princeton and from the flexibility to work from other places than Hamburg. I am thankful to Heiko Appel for teaching me to think outside the box, being creative and for always believing in me and finding encouraging words when things did not go according to plan. Thanks to Daniela Pfannkuche for agreeing to be the second referee of my thesis, for showing interest in my work and for her counsel.

I am grateful for the support from Michael Sentef in organizing and writing my first paper. Furthermore, I am highly indebted to Iris Theophilou and Michael Ruggenthaler, who, in endless discussions on the white board, taught me to be precise in my expressions and to think things through to the end. It was a pleasure learning from you and I am grateful for all the time you invested in me. Thank you to all group members for creating an agreeable working environment and for giving me the feeling that I could knock at any door any time with some problem, be it directly related to physics or not.

During the three months I spent in Princeton, I was received very warmly by Garnet Chan and Joshua Kretchmer. Thank you for your kind hospitality and for teaching me a lot about both physics and American culture. Additionally, I thank Claudius Hubig for not only letting me use his DMRG implementation but for also explaining everything related to his code in a calm, friendly and very patient manner (sometimes various times). I profited a lot from the private lectures about the nuts and bolts of computing from Henning Glawe and the high art of *Klönschnack* and from the patience of Enrico Ronca in our numerous fights with EOS and Draco.

Thanks also to the ladies in charge of administrative things: Patricia Rihs, Graciela Sanguino, Ute Ramseger, Julia Quante, Neda Lotfiomran, Kathja Schroeder, Carolin Wodars and Tania Hartin for the help with special treatments, travelling to interesting, but not directly work-related events, and bureaucratic complications.

I am most grateful to my *better half* Uliana Mordovina without whom I might not have started and most definitely would not have finished this thesis. Thanks for all the time spent together, in heated discussions on the white board, rating the dahlias or drinking red wine. A special thanks is owed to Christian Schäfer for listening to the weird noises in our office, for always missing the trash bin, and for endless walks in circles in the park while solving the mysteries of physics and human nature, in short: for not only being the best office colleague ever, but for becoming a good friend.

On a more personal level, I wish to thank Alexandra Göbel, Johannes Kaub and Nele Müller for their encouragement and their updates about whats going on in Hamburg. Ein ganz besonderer Dank geht an meine Eltern und meine Schwester: Ich danke Kordula und Rudolf Reinhard für ihre grenzenlose Unterstützung in allen Bereichen, dafür dass sie mich erden wenn ich es brauche und dafür dass sie stolz auf mich sind auch wenn sie nicht nachvollziehen können, was ich den ganzen Tag eigentlich mache. Ich bin sehr froh dass es meine Schwester Lea Reinhard gibt, die mich von der Arbeit ablenkt und mir immer das Gefühl gibt, dass am Ende alles gut wird. Finally, I wish to thank my partner Philipp Strasberg for always being there for me, for helping me through the rough times of my PhD and for making me laugh even when I was not feeling like it.

Eidesstattliche Versicherung

Hiermit versichere ich an Eides statt, die vorliegende Dissertationsschrift selbst verfasst und keine anderen als die angegebenen Hilfsmittel und Quellen benutzt zu haben.

Die eingereichte schriftliche Fassung entspricht der auf dem elektronischen Speichermedium.

Die Dissertation wurde in der vorgelegten oder einer ähnlichen Form nicht schon einmal in einem früheren Promotionsverfahren angenommen oder als ungenügend beurteilt.

Hamburg, den 20.12.2018

.....
Teresa E. Reinhard